

Monday Morning, November 10, 2014

Advanced Surface Engineering

Room: 302 - Session SE+EM+EN+PS+TF-MoM

New Developments in Atmospheric Pressure Plasma Deposition and Thin Films for Energy Applications

Moderator: Hana Barankova, Uppsala University, Sweden, Michael Stueber, Karlsruhe Institute of Technology

8:40am **SE+EM+EN+PS+TF-MoM2 Real Time Characterization of Polymer Surface Modification by an Atmospheric Pressure Plasma Jet**, *Andrew Knoll, P. Luan, E.A.J. Bartis, C. Hart*, University of Maryland, College Park, *Y. Raitses*, Princeton Plasma Physics Laboratory, *G.S. Oehrlein*, University of Maryland, College Park

Atmospheric pressure plasma jets (APPJ) have been shown to modify surfaces, leading to a variety of potential industrial and medical applications. APPJ treated surfaces are typically evaluated post treatment, but few studies exist showing surface changes in real time. In this study, we characterized both closely-coupled and remote APPJ treatments of a PMMA-based 193 nm photoresist polymer (PR193) using *in situ* ellipsometry to monitor film thickness and refractive index in real time. The kilohertz-driven, two-ring electrode APPJ was fed with low admixtures of O₂ and N₂ to Ar. Voltage and current waveforms were collected to electrically characterize the APPJ and measure power dissipation. In addition, high speed photography of the APPJ was conducted in order to characterize plasma interaction with various controlled environments and with PR193. Ellipsometry shows that PR193 etch rates depend on the feed gas chemistry and treatment time. Etch rates are reduced for Ar/O₂ compared with pure Ar and Ar/N₂. This reduction is correlated to a decrease in plasma density with O₂ addition. It is also shown that the etch rate changes over time initially during APPJ heating and reaches steady state as the temperature stabilizes. When the plasma is brought close enough to the sample, the discharge couples with the surface and arcing to the film occurs. This interaction greatly increases the etch rate and introduces major damage to the polymer, which can be observed by the naked eye. From electrical data and high speed photography we see that the pure Ar discharge exhibits filamentary behavior that is enhanced by O₂ addition and rendered more diffuse by N₂ addition. High speed photography shows that the coupling of the plasma and the environment increases when the environment matches the feed gas chemistry, which causes the plume to extend farther than in open air. While the Ar plume is confined to a single plasma channel, N₂ admixture to Ar branches out into many smaller discharges, similar to a Lichtenberg figure. We also correlate damage seen on the polymer surface with observed arcing. The authors gratefully acknowledge financial support by US Department of Energy (DE-SC0001939).

9:00am **SE+EM+EN+PS+TF-MoM3 Gas-Liquid Mixed Phase Plasma at Atmospheric Pressure**, *Akira Ando, G. Tang, R. Ohno, A. Komuro, K. Takahashi*, Tohoku University, Japan **INVITED**

A gas-liquid mixed phase plasma discharge is investigated using nanosecond high-voltage pulse generator. Non-thermal atmospheric pressure plasmas have recently attracted significant attention due to their good energy efficiency in production of reactive species. Plasma in water can generate many reactive species, such as ozone, hydroxyl radicals and oxygen radicals. These products have strong oxidizing power and is applicable for many applications without any thermal stress.

We have utilized a nanosecond high-voltage pulse to produce a discharge within bubbles introduced into water, where semiconductor opening switching (SOS) diodes are used in the pulse generator.

The reactor for the gas-liquid hybrid plasma consists of two regions, gas and liquid regions, separated by a thin plate with a small holes (1mm in diameter). Several working gases are fed into the reactor from the gas region and bubbles are formed via the separator holes in the water. High-voltage pulse with 10-15kV are applied to a wire electrode situated in the gas phase. A grounded electrode is set into the water. When the high voltage pulse with the duration of 40ns is applied, a streamer-like discharge occurs within the bubbles and the streamer extends along the surface of gas-liquid interface.

The formation process of discharge bubbles were observed with a high-speed CCD images of the discharge. The area of discharge extension depends on the gas species and conductivity. Production rate of reactive species, ozone and hydroxyl radicals in a discharge reactor was also depends on the parameters. As the life time of hydroxyl radicals is very short, the amount is estimated from concentration of hydrogen peroxide

produced in treated water, which is produced by the recombination process of hydroxyl radicals.

In order to evaluate the oxidation power in the gas-liquid mixed plasma, we applied it to water purification, such as decolorization, sterilization and decomposition of persistent organic pollutants (POPs). The sterilization effect in the water is estimated from the survival ratio of bacillus subtilis and it reaches more than 99.5% after 15min treatment. The survival ratio is large in air discharge and the value of pH in water as well as ultraviolet (UV) ray generated by plasma discharge affects the sterilization. SEM images shows the surface of the bacteria were damaged by the treatment.

9:40am **SE+EM+EN+PS+TF-MoM5 Atmospheric Pressure High Power Impulse Plasma Source (AP-HiPIPS) for Plasma Enhanced Chemical Vapor Deposition of Thin Films**, *Vasiliki Poenitzsch, R. Wei, M.A. Miller, K. Coulter*, Southwest Research Institute

Southwest Research Institute is currently developing a High Power Impulse Plasma Source (HiPIPS) that supplies a high flux of energetic reactants to a surface while maintaining a low processing temperature. HiPIPS is a new plasma enhanced chemical vapor deposition technology that combines variable pressure plasma jets with advanced pulsed power technology. Several complementary techniques, including mass spectroscopy, optical emission spectroscopy (OES) and electrical and thermal probes were employed, for measuring and calculating the plasma characteristics in a wide range of the HiPIPS process parameters and conditions. The preliminary HiPIPS experiments have revealed that high peak power (~40 kW) in the pulses can be achieved resulting in a high peak current (~200 A) and increased plasma density (i.e. $n = \text{Ar}: 10^{20} \text{ cm}^{-2} \text{ s}^{-1}$) while maintaining a low average power (35W) and a low substrate processing temperature (50-150 °C). A prototype atmospheric-pressure HiPIPS (AP-HiPIPS) was successfully developed and proof-of-concept AP-HiPIPS diamond-like carbon (DLC) film deposition was demonstrated. Beyond DLC films, HiPIPS plasmas could be applicable to deposition of many classes of films and many types of surface treatments. In contrast to conventional state-of-the-art non-thermal atmospheric pressure plasma jets, typically driven by RF or AC, the power densities and currents during pulse on-time are 2-3 orders of magnitude higher in HiPIPS. Since plasma is created through inelastic electron collision with precursor gas molecules, the increased power and current directly equates to significantly improved ionization and dissociation of precursor gases in HiPIPS. Thus, distinguishing features of HiPIPS as compared to RF or AC APPJs are increased ionization, enhanced molecular gas dissociation, and higher flux of reactive species while maintaining the same low deposition temperatures. In this presentation, an overview of HiPIPS and AP-HiPIPS will be given with a specific focus on plasma characteristics and areas for further development.

10:00am **SE+EM+EN+PS+TF-MoM6 Importance of Argon's Spectral Emission for Plasma Diagnostics at an Atmospheric Open Air Plasma Discharge**, *Vladimir Milosavljevic, J. Lalor, P. Bourke, P.J. Cullen*, Dublin Institute of Technology, Ireland

In recent years, plasma on atmospheric pressure attracts a lot of attention due to their numerous applications in plasma biology, health care, and medicine, as well as surface and materials processing and nanotechnology. Among several atmospheric pressure plasma devices, a dielectric barrier discharge plasma jet (DBDPJ) is the most used, because of its simplicity and a fact that the generated plasma is in surrounding air and not in a confined space. The dynamics of DBDPJ in noble gases reveal that the plasma plumes propagate at a speed several orders of magnitude higher than the gas flow velocity. This is why it is generally accepted that the propagation of the plasma plumes is driven electrically rather than by the gas flow, which imposes in the first place the importance of the plasma diagnostics. Because of the frequent collisions between electrons and neutrals at high pressure, the electrical probe methods are generally less useful for plasmas produced at atmospheric pressure. Therefore, other diagnostic methods are needed and optical emission spectroscopy (OES) has been used as one of the alternative diagnostics because of its simplicity and non-intrusive nature.

Nitrogen dominates the ionic composition of atmospheric discharge and has an impact on the breakdown voltage. Nitrogen acts as a 'sensor gas' and OES diagnostics are applied in assumption that most nitrogen molecular emissions are excited during electron impact of ground state N₂(X). When nitrogen is added/mixed with argon plasma discharges, the argon emission lines are significantly quenched and the resulting plasma spectral emission is changed. Measurements and analysis of neutral argon spectral emission lines give very important information about the plasma properties. In this work the absolute spectral emissions of the atomic and molecular lines associated with argon, oxygen, nitrogen and hydrogen are presented. Wavelength resolved optical emission profiles of argon's spectral lines

shows that the change in electron energy distribution functions (EEDF) has taken place for a low gas flow rate only. After the gas flow rate goes above a certain limit, the EEDF remains constant. At the same time the density of argon metastable atoms are changed with the gas flow rate. Overall, analysis of the spectral intensities assist in the development of optimised plasma processing parameters for treatments such as surface activation or removal of contaminates.

The research leading to these results has received funding from the European Union's Seventh Framework Programme managed by REA Research Executive Agency (FP7/2007-2013) under Grant Agreement number 605125

10:40am **SE+EM+EN+PS+TF-MoM8 Hot 'n Flaky: Thermal Properties of Layered Atomic Structures, Christopher Muratore, University of Dayton, V. Varshney, Air Force Research Laboratory/UTC, J.J. Hu, Air Force Research Laboratory/UDRI, A.A. Voevodin, Air Force Research Laboratory**

INVITED

Synthesis capability for uniform growth of 2D materials over large areas at lower temperatures without sacrificing their unique properties is a critical pre-requisite for seamless integration of next-generation van der Waals heterostructures into novel devices. We have demonstrated, for the first time, vapor phase growth techniques for precisely controlled synthesis of continuous, uniform molecular layers of all MoX_2 and WX_2 transition metal dichalcogenide (TMD) compounds on diverse substrates, including graphene, hexagonal boron nitride, highly oriented pyrolytic graphite (HOPG), SiO_2 , and metal substrates over several square centimeters. Preliminary results show MoX_2 and WX_2 transition metal dichalcogenide materials grown in a novel ultra-high vacuum (UHV) physical vapor deposition (PVD) process demonstrate properties identical or even superior (e.g., electron mobilities $>500 \text{ cm}^2 \text{ V}^{-1} \text{ s}^{-1}$) to exfoliated layers. Growth of bi-layer MoS_2 on few-layer graphene with a 30% lattice mismatch and TMD/TMD heterostructures are shown to demonstrate how natural accommodation of stresses at 2D van der Waals interfaces has the remarkable potential to transform the way materials selection is considered for synthetic heterostructures, as concerns regarding lattice constant matching can be abandoned with preference given to desired properties and performance. Investigations relating to application of these materials in thermoelectric device applications are presented. Thermal conductivity values of TMD thin films were compared to bulk crystals, revealing expected trends with mass, but a >10 fold reduction in thin film thermal conductivity. Phonon scattering lengths at domain boundaries based on computationally derived group velocities were consistent with the observed film microstructure, accounting for the reduction. We also explore thermal anisotropy in MoS_2 films. Measurement results are correlated with MD simulations of thermal transport for perfect and defective MoS_2 crystals, demonstrating the importance of thermal boundary scattering.

Surface Science

Room: 309 - Session SS+AS+EN-MoM

Mechanistic Insights into Surface Reactions: Catalysis, ALD, etc.

Moderator: Falko Netzer, University of Graz, Junseok Lee, National Energy Technology Laboratory

8:20am **SS+AS+EN-MoM1 Electron Trap or Atomic Hydrogen Recombination Catalyst? The Role of Metals in Photocatalysis Revisited, J.-B. Joo, R.J. Dillon, I. Lee, C.J. Bardeen, Francisco Zaera, University of California - Riverside**

INVITED

The production of hydrogen from water with semiconductor photocatalysts is often promoted by the addition of a small amount of a metal to their surfaces. It is commonly believed that the resulting enhancement in catalytic activity is due to a fast transfer of the excited electrons generated by photon absorption from the semiconductor to the metal, a step that prevents de-excitation back to the ground electronic state. Here we provide several pieces of evidence to argue against this mechanism. An alternative explanation is advanced where the metal acts as a catalyst for the recombination of the hydrogen atoms made via the reduction of protons on the surface of the semiconductor instead. New metal@ TiO_2 yolk-shell nanomaterials were conceived to test our hypothesis, and the preparation and characterization of these will be discussed in this presentation as well.

9:00am **SS+AS+EN-MoM3 Atomically Resolved Observation of Defects Catalysing Phase Transitions in an Adsorbate System, M. Cordin, B.A.J. Lechner, S. Duerrbeck, A. Menzel, Erminald Bertel, University of Innsbruck, Austria, J. Redinger, Vienna University of Technology, Austria, C. Franchini, University of Vienna, Austria**

First order phase transitions exhibit a nucleation barrier. Normally, the barrier is lowered by heterogeneous nucleation at interfaces or extrinsic defects. Homogeneous nucleation, in contrast, is strongly activated and results in a significant hysteresis. Molecular dynamics calculations have suggested that an important step in homogeneous nucleation involves the formation and subsequent separation of defect pairs^{1,2}.

Here we report a $(2 \times 1) \rightarrow c(2 \times 2)$ order-order phase transition in a two-dimensional (2D) adsorbate system ($\text{Br}/\text{Pt}(110)$ at 0.5 monolayer coverage) as a function of temperature³. Although an order-order phase transition is first-order according to Landau rules, the present system exhibits strong fluctuations within a wide temperature range (50K-250K). At 50 K the fluctuations are sluggish enough to allow atomically resolved observation of the phase conversion mechanism by temperature-variable Scanning Tunneling Microscopy. The transition is heralded by local density fluctuations in the adsorbate. The density variation consists of a compression (soliton) and a dilution (anti-soliton). At the transition temperature the two defect moieties are able to separate and travel independently through the system, thereby converting one phase into the other. Away from the transition temperature, separation of the defect pair would create the "wrong" phase, thus increasing the free energy of the system. This is equivalent to an effective attractive interaction between soliton and anti-soliton, in close analogy to the string interaction in spin systems⁴. The one-to-one correspondence can be made transparent by introducing a pseudo-spin variable, i.e. an occupation number ± 1 assigned to every bonding site. The defect-pair separation mechanism partially circumvents the nucleation barrier and thus promotes fluctuations, particularly in low-dimensional systems.

Defect-pair separation as a key step in phase transitions is a concept which arose from the analysis of molecular dynamics calculations. To our knowledge, the present study represents the first direct experimental observation with atomic resolution of such a mechanism. Furthermore, it illustrates the important role of the string interaction in suppressing fluctuations, which is very efficient in 3D systems, weaker in 2D systems and totally absent in 1D.

¹ K. Mochizuki, M. Matsumoto, and I. Ohmine, *Nature* **498**, 350 (2013).

² M. Forsblom and G. Grimvall, *Nat Mater* **4**, 388 (2005).

³ M. Cordin, B. A. J. Lechner, S. Duerrbeck, et al., *Sci. Rep.* **4** (2014).

⁴ T. Giamarchi, *Quantum Physics in One Dimension* (Oxford University Press, New York, 2004).

9:20am **SS+AS+EN-MoM4 The Co-adsorption of Water and ammonia on Pt(111), B.A.J. Lechner, Lawrence Berkeley National Laboratory, Y. Kim, H. Kang, Seoul National University, Korea, Miquel Salmeron, Lawrence Berkeley National Laboratory**

Water (H_2O) and ammonia (NH_3) are arguably the most important inorganic molecules in the chemical industry. Both have the ability to form hydrogen bonds and mix readily in the liquid form. However, upon adsorption onto a metal surface, the molecules can form fewer yet more directional hydrogen bonds. To investigate the interaction between these two species at the molecular level we present a scanning tunneling microscopy (STM) study of the co-adsorption of water and ammonia on Pt(111), a substrate which bonds both molecules strongly but does not promote their decomposition.

Prior investigations have suggested the formation of the ammonium ion, NH_4^+ , upon adsorption of ammonia onto a water monolayer on Ru(0001) [1], implying that the two molecules react readily when adsorbed on transition metal surfaces. Furthermore, a theoretical study of the co-adsorption of ammonia and water on Cu(110) proposed an intimately mixed layer of ammonia and water as the energetically most favorable structure [2].

Here, we present the first microscopic investigation of co-adsorbed water and ammonia species. Upon adsorption at 4 K, ammonia and water form disordered structures, yet as the temperature is increased the two species segregate on the substrate. Indeed, at temperatures above 77 K, ammonia invariably prefers to bond to the Pt surface and only adsorbs on a water film once the monolayer is complete and no active sites remain on the substrate. When adsorbed on the water layer, we find that ammonia bonds to the water molecules that are lifted off the substrate due to a lattice mismatch of the water monolayer and the Pt(111) geometry, which we believe is due to their ability to provide a hydrogen atom for the hydrogen bond more readily than the molecules bonded more strongly to the substrate.

[1] Y. Kim, E. Moon, S. Shin, H. Kang, *Angew. Chem. Int. Ed.* **51**, 12806 (2012).

9:40am **SS+AS+EN-MoM5 Thermal Decomposition of Ethylene on Ru(001)**, *Yuan Ren, I. Waluyo, M. Trenary*, University of Illinois at Chicago

Ruthenium is an important catalyst in the Fischer-Tropsch process which deals with the conversion of syngas (CO and H₂) into hydrocarbons. One of the most important aspects in the Fischer-Tropsch reaction is the chain growth from a C₁ species to longer chain hydrocarbons. It is, therefore, important to study the chemistry of various C_nH_y hydrocarbon fragments on transition metal surfaces as building blocks in the chain growth mechanism. Ethylidyne (CCH₃) is an interesting hydrocarbon fragment that has been studied on many surfaces as the decomposition product of ethylene. Although the formation of ethylidyne on Ru(001) from the dehydrogenation of ethylene has been studied using high resolution electron energy loss spectroscopy (HREELS) and reflection absorption infrared spectroscopy (RAIRS) in the past, there is a lack of agreement in the literature about the mechanism of ethylene decomposition.

In this study, reflection absorption infrared spectroscopy (RAIRS) and temperature programmed desorption (TPD) were used to characterize and identify the surface intermediates formed in the thermal decomposition of ethylene (C₂H₄) on Ru(001). Ethylene is found to adsorb to the surface in a di-σ bonded complex at 95 K and dehydrogenates to form ethylidyne (CCH₃) above 150 K. Upon further annealing the crystal to above 300 K, ethylidyne dehydrogenates to ethynyl (CCH). Annealing to higher than 450 K causes ethynyl to decompose to methylidyne (CH). The characterization of surface intermediates provides us with more insights into the thermal decomposition of ethylene on Ru(001), which is essential to reveal the reaction mechanism.

10:00am **SS+AS+EN-MoM6 Kinetics of Alkyl Species on Pt(111)**, *Yifeng Song, I.A. Harrison*, University of Virginia
Kinetics of Alkyl Species on Pt(111)

Yifeng Song and Ian Harrison

University of Virginia

Charlottesville, VA 22904

A heated effusive molecular beam was used to dose hot alkanes on to a relatively cold Pt(111) surface to overcome the initial activation barrier for dissociative chemisorption and to trap reactive intermediate species on the surface for subsequent spectroscopic and kinetic studies. Both reflection absorption infrared spectroscopy (RAIRS) and temperature programmed reaction (TPR) techniques were employed, in a complimentary way, to investigate the kinetics of alkyl fragments. Particular attention was paid to methylidyne (-CH) decomposition kinetics, which have been proposed to be potentially rate-limiting in catalytic steam reforming of methane according to recent DFT calculations. Comparison between reforming kinetics of single crystal surfaces and nanocatalysts are made. Elementary steps including the cleavage and formation of C-H and C-C bonds within other C₁, C₂ and C₃ reactive intermediates were also studied. The experimental findings, together with some theoretical work, provide molecularly resolved information relevant to catalytic reforming of light alkanes.

10:40am **SS+AS+EN-MoM8 C₂ Hydrogenation at Ambient Pressure on Pt(111)**, *Joel Krooswyk, M. Trenary*, University of Illinois at Chicago

Carbon has been shown to be the decomposition product from catalytic reactions involving hydrocarbons adsorbed on metal catalysts. Its presence reduces the amount of active surface sites available during a reaction. The decomposition products from adsorbed acetylene and ethylene on Pt(111) are C₂ and C₁ species, respectively. A previous UHV study showed that C₂H₂ adsorbed on Pt(111) at 750 K immediately decomposes to mostly C₂ species. H₂ was then coadsorbed with C₂ at 85 K and annealed to 400 K, which produced ethylidyne (CCH₃), ethynyl (CCH), and methylidyne (CH) species. None of the species were hydrogenated to ethylene or ethane, and after annealing to 750 K, a percentage of the carbon on the surface could be rehydrogenated after cooling the crystal to 300 K and coadsorbing H₂.

In this study, the hydrogenation of C₂ species in 1×10⁻² to 1 Torr of H₂ was monitored with RAIRS. The species was created on Pt(111) with C₂H₂ adsorption at 750 K as done previously and the crystal was cooled to 300 K. The crystal was then annealed in an ambient pressure of H₂. The C₂ species are hydrogenated to ethylidyne at 400 K and then to ethane at approximately 450-500 K. This reaction is shown to be dependent on the pressure of H₂. The results show that ethylidyne will be hydrogenated at 450 and 500 K at 1.0 and 1×10⁻² Torr H₂, respectively. To show that the C₂ species are fully hydrogenated and desorbed as ethane, which indicates that the surface is clean, CO was leaked into the cell with H₂. We observe after the 500 K anneal that the peak assigned to the CO species is similar in intensity to one from CO adsorbed on a clean surface. This indicates that there are no C₂ species remaining on the surface. Also, the peak positions of

the terminal and bridge sites are shifted, which indicates that there is a high coverage of H atoms adsorbed on the surface.

11:00am **SS+AS+EN-MoM9 Reaction Kinetics and Mechanism between Nitrate Radicals and Functionalized Organic Surfaces**, *Yafen Zhang, J.R. Morris*, Virginia Tech

Interfacial reactions of nitrate radicals (NO₃) with organic surfaces play an important role in atmospheric chemistry. To gain insight into the kinetic and mechanistic details, reactions between gas-phase nitrate radicals and model organic surfaces have been investigated. The experimental approach employs *in situ* reflection-absorption infrared spectroscopy (RAIRS) to monitor bond rupture and formation while a well-characterized effusive flux of NO₃ impinges on the organic surface. Model surfaces are created by the spontaneous adsorption of either vinyl-terminated alkanethiols (HS(CH₂)₁₆CHCH₂) or hydroxyl-terminated alkanethiols (HS(CH₂)₁₆OH) onto a polycrystalline gold substrate. The H₂C=CH-terminated self-assembled monolayers (SAMs) provide a well-defined surface with the double bond positioned precisely at the gas-surface interface. The surface reaction kinetics obtained from RAIRS revealed that the consumption rate of the terminal vinyl groups is nearly identical to the formation rate of a surface-bound nitrate species and implies that the mechanism is one of direct addition to the vinyl group rather than hydrogen abstraction. Upon nitrate radical collisions with the surface, the initial reaction probability for consumption of carbon-carbon double bonds was determined to be (2.3 ± 0.5) × 10⁻³. This rate is approximately two orders of magnitude greater than the rate of ozone reactions on the same surface, which suggests that oxidation of surface-bound vinyl groups by nighttime nitrate radicals may play an important role in atmospheric chemistry despite their relatively low concentration. In addition to studies involving the H₂C=CH-terminated SAMs, we have probed the reaction dynamics of NO₃ on HO-terminated SAMs. These experiments have revealed that the polarity of the terminal group has a large effect on the interfacial reaction rates. For the HO-terminated SAMs, the initial reaction probability was determined to be (5.5 ± 0.6) × 10⁻³ and the reaction mechanism appears to involve efficient hydrogen abstraction at the methylene group adjacent to hydroxyl terminus.

11:20am **SS+AS+EN-MoM10 Oxide Growth Kinetics at SiO₂/Si(001) Interfaces Induced by Rapid Temperature Raising**, *Shuichi Ogawa, J. Tang*, Tohoku University, Japan, *A. Yoshigoe*, JAEA, Japan, *K. Nishimoto*, Tohoku University, Japan, *S. Ishizuka*, Akita Nat. Col. Technol., Japan, *Y. Teraoka*, JAEA, Japan, *Y. Takakuwa*, Tohoku University, Japan

Thermal oxidation of Si is widely used in the fabrication of electric devices and MEMS. In the recent process, rapid thermal annealing (RTA) is used in a thermal oxidation process. In the RTA process, the temperature changes during the oxidation, but the temperature changing effects in the oxidation rate have not been cleared yet. In this study, the dependence of interface oxidation kinetics on the temperature was investigated by real-time RHEED combined with AES to measure the oxide growth rate. Based on the activation energy and pre-exponential factor of the interface oxidation at SiO₂/Si(001) interface, the rate-limiting reaction of the interface oxidation is discussed.

The oxidation experiments were performed with an apparatus equipped with facilities of RHEED combined with AES (Tohoku Univ.), and chemical bonding states including not only suboxide components but also strained Si atoms were investigated XPS at BL23SU, SPring-8. The clean Si(001) surfaces were oxidized by dry O₂ gas at initial temperature T₁. When the clean surfaces were completely oxidized, the temperature was raised from T₁ to T₂. T₁ was changed between room temperature (RT) and 561 °C.

When temperature was raised from T₁ to T₂, the interface oxidation is enhanced. The initial oxidation rate after rising temperature k₂ is discussed in this study. The k₂ strongly correlates to the difference of T₁ and T₂. The Arrhenius equations between k₂ and T₂ are obtained in various T₁. As the result, activation energy is obtained as 0.27 eV in good agreement with the previous experimental result[1] and theoretical study[2]. In addition, it is found that activation energy is independent from T₁. On the other hand, pre-exponential factor decreases with increasing T₁, decreasing by about one order when T₁ increases from RT to 561 °C. In the XPS results, the Si⁴⁺ component increases and suboxide components and strained Si components (Si^α and Si^β)[3] decrease with temperature elevation from 300 to 600 °C.

Based on these results, we propose the reaction between point defects (emitted Si atoms and its vacancies) generated by the oxidation-induced strain and O₂ molecules as the rate-limiting reaction of the interface oxidation.

[1] H. Watanabe et al., Phys. Rev. Lett. **80** (1998) 345.

[2] H. Kageshima et al, Jpn. J. Appl. Phys. **45** (2006) 7672.

[3] S. Ogawa et al., Jpn. J. Appl. Phys. **52** (2013) 110128.

11:40am **SS+AS+EN-MoM11 Electron Beam Induced Surface Reactions of Adsorbed π -allyl Ruthenium Tricarbonyl Bromide: Towards the Design of Precursors Specifically for Electron Beam Induced Deposition.** *Julie Spencer*, Johns Hopkins University, *R.G. Thorman*, University of Iceland, *M.S. Barclay*, Johns Hopkins University, *J.A. Brannaka*, University of Florida, *O. Ingólfsson*, University of Iceland, *L. McElwee-White*, University of Florida, *D.H. Fairbrother*, Johns Hopkins University

This surface science study focuses on elucidating the electron stimulated elementary reactions involved in Electron Beam Induced Deposition (EBID) of π -allyl ruthenium tricarbonyl bromide (π -C₃H₅Ru(CO)₃Br), an organometallic precursor synthesized specifically to test its suitability as an EBID precursor. EBID is a minimally invasive, resistless lithographic process which uses the electron stimulated decomposition of volatile organometallics under low vacuum conditions to fabricate and prototype three-dimensional metallic nanostructures. To date, EBID nanostructures has used precursors designed for thermal processes, such as chemical vapor deposition (CVD). However, precursors that yield pure metal deposits in CVD often create EBID deposits with high levels of organic contamination which severely limits the range of potential applications for EBID nanostructures, highlighting the need to better understand how the structure of organometallics influences their electron stimulated reactions. To address this knowledge gap we have conducted ultra-high vacuum (UHV) surface science studies to probe the effects of 500eV electrons on nanometer scale films of organometallics adsorbed on inert substrates at low temperatures using X-ray Photoelectron Spectrometry and Mass spectrometry. Recently, we have collaborated with synthetic organometallic chemists to study organometallic complexes not designed for CVD to test specific hypotheses about how the EBID process occurs; the first example of this new collaboration is π -allyl ruthenium tricarbonyl bromide (π -C₃H₅Ru(CO)₃Br). Experimental results indicate that electron stimulated decomposition of π -C₃H₅Ru(CO)₃Br causes the central Ru atom to become reduced and in the process causes the vast majority of the carbonyl ligands to be ejected into the gas phase, with no loss of Br or the carbon atoms in the π -allyl ligand. A parallel study of π -C₃H₅Ru(CO)₃Cl indicated that the identity of the halogen does not affect the decomposition process. However, although halogen atoms are not labile in the initial decomposition step, they can be removed by a slower electron stimulated desorption process at higher electron fluxes more representative of those encountered in typical EBID experiments which are conducted in electron microscopes. Collectively, these results suggest that organometallic precursors whose ligand architecture contains a combination of carbonyl and halogen ligands could be used to create EBID deposits with higher metal contents than are currently possible. To test this hypothesis we will also present results on the behavior of cis-dicarbonyldichloro platinum(II), *cis*-PtCl₂(CO)₂.

Surface Science

Room: 315 - Session SS+EN-MoM

Photocatalysis and Photochemistry at Surfaces

Moderator: Andrew Gellman, Carnegie Mellon University, Bruce Koel, Princeton University

8:20am **SS+EN-MoM1 Reaction Chemistry at Surfaces of Hematite-Based Photoelectrocatalysts.** *P. Zhao*, *C. Kronawitter*, *Bruce Koel*, Princeton University

Hematite (α -Fe₂O₃)-based photoanodes are promising materials for photoelectrochemical hydrogen generation. We report on fundamental studies of surface structure and reaction chemistry associated with the heterogeneous oxidation of water on such materials by applying a classical surface science approach. We have characterized the structure and properties of Ni-doped and mixed-oxide hematite surfaces formed by vapor deposition under controlled conditions utilizing a range of techniques for surface analysis. The structure of Ni-modified thin films of α -Fe₂O₃ model catalysts with different morphology and geometry was characterized by LEED and STM. Then, water adsorption and reaction were studied by TPD, XPS, UPS, and vibrational spectroscopy by HREELS, characterizing the influence of Ni-modification on thermal and photochemical reaction mechanisms. Ni doping is found to be associated with a new termination for the α -Fe₂O₃(0001) film. Water TPD shows that Ni doping induces new surface chemistry, as revealed by a new, higher temperature OH recombination desorption peak, which is due to more stable surface-bound OH groups as identified by UPS. These surface-science type experiments were combined with photoelectrochemical water oxidation measurements on photoanodes prepared by thin-film and nano-materials synthesis to elucidate new information on the surface phases of hematite-based

photoanodes and about their specific stability and reactivity toward photoelectrochemical water splitting.

This work was supported by the Addy/ISN North American Low Carbon Emission Energy Self-Sufficiency Fund of the Andlinger Center for Energy and the Environment (ACEE) and by the Grand Challenges Program at Princeton University.

8:40am **SS+EN-MoM2 Infrared Reflection-Absorption Spectroscopy Study of Adsorption and Photo-Decomposition of Formic Acid on Reduced and Defective Rutile TiO₂ (110) Surfaces.** *Andreas Mattsson*, *L. Österlund*, Uppsala University, Sweden

Adsorption and photo-decomposition of formic acid on rutile TiO₂(110) have been investigated with infrared reflection-absorption spectroscopy (IRRAS) employing p- and s-polarized light along the [001] and [1-10] crystal directions. The single crystal surfaces were prepared either by sputtering and annealing in ultra-high vacuum (UHV) to obtain a reduced surface (r-TiO₂), or by sputtering alone to create a rough, highly defective surface (sp-TiO₂). Results are compared with corresponding measurements in synthetic air on rutile nanocrystals performed. IRRAS spectra obtained on r-TiO₂ and rutile nanocrystals are very similar (Fig. S1), and show that in both cases formic acid dissociates and is predominately adsorbed as a bridging bidentate formate species,¹ demonstrating that the adsorption structure on the nanocrystals is determined by interactions with majority (110) surfaces. In contrast, the IRRAS spectra on sp-TiO₂ are different (Fig. S1), with only minor spectral features associated with (110) surfaces, which can be explained by changed adsorption geometry due to bonding to low-coordinated Ti³⁺ atoms. IRRAS measurements in UHV on thin nanoporous rutile films, made by reactive DC sputtering, were performed to compare the adsorption geometry of formate with that for single crystal surfaces and nanoparticles. The UV-induced rate of formate photo-decomposition is about 30 times higher on rutile nanocrystals in synthetic air compared with sp-TiO₂ under UHV conditions, and even larger than on r-TiO₂.² These differences are explained by the lack of oxygen and limited hydroxyl coverage under UHV conditions (thus quenching electron scavenging by adsorbed O₂ and lowering OH radical formation), and by strong bonding of formate on (110) surfaces which lowers the reactivity on r-TiO₂ further. Our results suggest that surface reaction studies of formic acid conducted at elevated pressures on rutile nanocrystals can be accurately modelled with single crystal studies conducted in UHV.

¹ A. Mattsson, S.-L. Hu, K. Hermansson, L. Österlund, Journal of Chemical Physics 140 (2014) 034705

² L. Österlund, Solid State Phenomena 162 (2010) 203-219

9:00am **SS+EN-MoM3 Molecular Beam Epitaxy of Highly Mismatched GaN Alloys with GaAs, GaSb and GaBi for Potential Water Splitting and Other Solar Energy Conversion Applications.** *Sergei Novikov*, University of Nottingham, UK, *K.M. Yu*, Lawrence Berkeley National Laboratory, *W.L. Sarney*, US Army Research Laboratory, *Z. Liliental-Weber*, Lawrence Berkeley National Laboratory, *R.W. Martin*, University of Strathclyde, UK, *S.P. Svensson*, US Army Research Laboratory, *W. Walukiewicz*, Lawrence Berkeley National Laboratory, *C.T. Foxon*, University of Nottingham, UK **INVITED**

We have grown GaN layers alloyed with GaAs, GaSb and GaBi compounds using plasma-assisted molecular beam epitaxy (PA-MBE) and extensively characterized their structural, optical and electrical properties.

Electronic band structures of these so-called highly mismatched alloys (HMAs) are described by the band anticrossing (BAC) model which predicts that the alloys should exhibit a wide range of direct energy gaps. We have shown previously that the energy gap of GaN_{1-x}As_x alloys varies from 0.7eV to 3.4eV. An even larger modification of the band structures is anticipated for more extremely mismatched GaN_{1-x}Sb_x and GaN_{1-x}Bi_x alloys. The large band gap range and controllable conduction and valence band edge positions makes the HMAs promising materials for efficient solar energy conversion devices. For example, these HMAs may be suitable for solar water splitting applications for hydrogen production. As efficient photoelectrodes, the bandgap of the semiconductor must be >2 eV to induce electrochemical decomposition of water but still small enough to absorb a significant portion of the solar spectrum. In addition the band edges must also straddle the H₂O redox potentials.

At dilute doping levels, substitutions of As, Sb and Bi into the N sublattice results in formation of localized energy levels above the valence band in GaN. Our measurements on GaN doped with As and Sb have demonstrated that the As and the Sb impurity levels lie at about 0.7eV and 1.2eV above the valence band edge of GaN, respectively.

The BAC model predicts that at a higher concentration of the group V elements the interaction of the impurity levels with the extended states of the valence band leads to formation of an impurity-derived, fully occupied narrow band that plays a role of the new valence band edge. This results in

an abrupt upward shift of the valence band edge and a reduction of the optical gap of the HMAs. We have achieved the enhanced incorporation of As, Sb and Bi by growing the layers at extremely low temperatures (down to about 100°C). Although the layers become amorphous for high As, Sb and Bi content, the measured composition dependence of the optical absorption edge are consistent with the predictions of the BAC model, indicating that the amorphous HMAs samples have a short-range order resembling random crystalline alloys. The large band gap range and controllable positions of the conduction and valence bands make these HMAs promising materials for efficient solar energy conversion devices.

9:40am **SS+EN-MoM5 Photochemistry of Acetone on Reduced Rutile TiO₂(110)**, *Nikolay Petrik, M.A. Henderson, G.A. Kimmel*, Pacific Northwest National Laboratory

TiO₂ is an important photocatalyst with many practical applications. However, fundamental understanding of thermal and non-thermal reactions on TiO₂ surfaces is still lacking. We have investigated the ultraviolet (UV) photon-stimulated reactions acetone and oxygen adsorbed on reduced rutile TiO₂(110). Previous research suggests that a thermal reaction between acetone and chemisorbed oxygen forms acetone diolate – a photochemically active product.¹ During UV irradiation, a methyl radical is ejected leaving acetate on the surface. Using infrared reflection absorption spectroscopy, we have identified the acetone diolate, which degrades during UV irradiation forming a new product. We have also measured the angular distribution of the photodesorbing methyl radicals, which is consistent with their ejection from the acetone diolate. Specifically, a peak in the distribution near ~60° to the surface normal is detected in the plane perpendicular to the BBO rows. However, we have also observed a second channel for photo-ejection of methyl radical for larger acetone:O₂ ratios. It manifests itself with a photodesorption peak normal to the surface and slower signal decay kinetics. These studies provide new insights into mechanisms responsible for the photochemistry of small molecules on TiO₂ and other oxide surfaces. This work was supported by the US Department of Energy, Office of Basic Energy Sciences, Division of Chemical Sciences, Geosciences & Biosciences. The work was performed using EMSL, a national scientific user facility sponsored by the Department of Energy's Office of Biological and Environmental Research and located at Pacific Northwest National Laboratory (PNNL). PNNL is a multiprogram national laboratory operated for DOE by Battelle under Contract DE-AC05-76RL01830.

(1) Henderson, M. A. Relationship of O₂ Photodesorption in Photooxidation of Acetone on TiO₂. *J. Phys. Chem. C*, 2008, 112, 11433-11440.

10:00am **SS+EN-MoM6 STM Spectroscopic Studies of TMAA Photocatalysis on TiO₂**, *Denis Potapenko, Z. Li, R.M. Osgood*, Columbia University

Titanium oxide is a versatile photocatalytic material and it has been the subject of much research throughout the last two decades. Scanning Tunneling Microscopy (STM) allows explorations on the single molecule basis thus providing important insight into the physical phenomena involved in photocatalysis. Our experiments examine the tip-induced chemistry of tri-methyl acetic acid (TMAA) molecules adsorbed on TiO₂ rutile(110) surface; this system was chosen as a model for light-driven catalysis since it is easily imaged with STM and since this system has been the subject of many earlier studies of photo and thermal chemistry. In the present work we combine three methods of initiation of surface chemistry: a) excitation of charge carriers in bulk TiO₂ with monochromated light from a UV-vis lamp, b) injection of the charge carriers from the STM tip directly into an adsorbed molecule, and c) injection of hot carriers into the substrate from the STM tip. In the latter case the surface reactions are initiated in the vicinity of the injection point by the electrical charges diffusing in the bulk of TiO₂, thus giving a unique insight into the charge dynamics. We show that there is a threshold energy for a hot hole below the edge of the TiO₂ valence band that is required for TMAA photo-decomposition.

11:00am **SS+EN-MoM9 Photoluminescence Response of p-GaInP₂ Photocathodes to Vapor and Solution Ambients**, *James Young*, University of Colorado, Boulder, *H. Doscher, T.G. Deutsch, J.A. Turner*, National Renewable Energy Laboratory, *S.M. George*, University of Colorado, Boulder

III-V photoelectrochemical (PEC) devices have achieved high solar-to-hydrogen water splitting efficiencies but corrosion greatly limits their operating lifetime. A dynamic three-phase semiconductor-electrolyte-hydrogen (oxygen) system exists at a photocathode (photoanode) surface during operation. Understanding the interaction of water, hydrogen, and oxygen with III-V surfaces is critical to optimizing device performance and applying corrosion-resistant surface modifications. In this work, we use photoluminescence (PL) to probe the surface response of p-type GaInP₂ to several gas and solution ambients *in-situ*. X-ray photoelectron spectroscopy

and photoelectrochemical techniques are used to characterize surface changes *ex-situ*. Pretreating p-GaInP₂ with sulfuric acid removes surface oxide and doubles p-GaInP₂ band-to-band PL yield when measured in air. Measurements in vacuum show that PL of pretreated samples increases reversibly with adsorption isotherm dependence on water vapor at partial pressures below 2 Torr while samples without the pretreatment show no PL response to water vapor. A comparison of water to other vapor phase ambients suggests that PL response increases with the dipole strength and involves dissociative adsorption. In oxygen ambient, the PL decays irreversibly which we attribute to photo-oxidation of the p-GaInP₂ surface. We will also present results from measurements in hydrogen ambient and PL measurements and monitoring in electrolyte solutions with a discussion of their relevance to PEC device performance and usefulness in characterizing corrosion resistant surface modifications.

Monday Afternoon, November 10, 2014

Energy Frontiers Focus Topic

Room: 315 - Session EN+EM+MN+NS+TR-MoA

Energy Harvesting with Nanostructures

Moderator: Phillip Christopher, University of California - Riverside

2:00pm EN+EM+MN+NS+TR-MoA1 **Optical Engineering for Colloidal Quantum Dot Photovoltaics**, *Susanna Thon*, Johns Hopkins University **INVITED**

The next generation of photovoltaics seeks to improve both efficiency and cost through the use of flexible platforms and new materials. Colloidal quantum dots (CQDs), semiconductor nanoparticles synthesized from solution, are a particularly attractive material for solar energy. The bandgap of films composed of arrays of CQDs can be tuned via the quantum confinement effect for tailored spectral utilization. The performance of CQD solar cells is currently limited by an absorption-extraction compromise, whereby photon absorption lengths in the near infrared regime exceed minority carrier diffusion lengths. I will review several photonic and optical engineering schemes aimed at overcoming this compromise. These include nanophotonic and geometric light trapping techniques, as well as jointly-tuned plasmonic-excitonic photovoltaics. Additionally, I will discuss how nanoscale engineering of CQDs and related materials can lead to emergent optical properties for building color-tuned optoelectronic films.

2:40pm EN+EM+MN+NS+TR-MoA3 **Energy Transfer from Nanocrystal Quantum Dots to Si Nanomembranes Monitored via Wavelength Dependent Photocurrent Response**, *Weina Peng, S. Sampat, S. Rupich, B. Anand, H. Nguyen, D. Taylor, Y. Gartstein, Y.J. Chabal, A. Malko*, University of Texas at Dallas

We report the observation of wavelength dependent photocurrent in thin silicon nanomembranes (75 nm) coupled to colloidal CdSe/ZnS nanocrystal quantum dots (NQDs). The measurement was performed on back-gated, FET-type thin Si structures, which are functionalized with self-assembled monolayer (SAM) of ester termination groups to prevent surface oxidation and the formation of surface defect states. A thin film of nanocrystals is drop casted on the surface and an increase of photocurrent, up to several hundred nA, are recorded as a function of excitation wavelength on NQD/SAM/Si devices vs. plain SAM/Si structures. Quantitative analysis of photocurrent vs. NQD absorption spectrum allows us to ascribe the observed photocurrents to the photoexcited NQD excitons transferred to the underlying Si substrate via non-radiative and radiative energy-transfer mechanisms¹.

¹H. M. Nguyen, O. Seitz, W. N. Peng, Y. N. Gartstein, Y. J. Chabal, and A. V. Malko, *ACS Nano* **6**, 5574 (2012).

3:40pm EN+EM+MN+NS+TR-MoA6 **Triboelectric Nanogenerator - A New Energy Technology**, *ZhongLin Wang*, Georgia Institute of Technology **INVITED**

Triboelectrification is an effect that is known to each and every one probably ever since the ancient Greek time, but it is usually taken as a negative effect and is avoided in many technologies. We have recently invented a triboelectric nanogenerator (TEG) that is used to convert mechanical energy into electricity by a conjunction of triboelectrification and electrostatic induction. As for this power generation unit, in the inner circuit, a potential is created by the triboelectric effect due to the charge transfer between two thin organic/inorganic films that exhibit opposite tribo-polarity; in the outer circuit, electrons are driven to flow between two electrodes attached on the back sides of the films in order to balance the potential. Ever since the first report of the TENG in January 2012, the output power density of TENG has been improved for five orders of magnitude within 12 months. The area power density reaches 500 W/m², volume density reaches 490 kW/m³, and a conversion efficiency of ~50% has been demonstrated. The TENG can be applied to harvest all kind mechanical energy that is available but wasted in our daily life, such as human motion, walking, vibration, mechanical triggering, rotating tire, wind, flowing water and more. Alternatively, TENG can also be used as a self-powered sensor for actively detecting the static and dynamic processes arising from mechanical agitation using the voltage and current output signals of the TENG, respectively, with potential applications for touch pad and smart skin technologies. The TENG is possible not only for self-powered portable electronics, but also as a new energy technology with a potential of contributing to the world energy in the near future.

[1] Z.L. Wang "Triboelectric Nanogenerators as New Energy Technology for Self-Powered Systems and as Active Mechanical and Chemical Sensors", *ACS Nano* **7** (2013) 9533-9557.

[2] G. Zhu, J. Chen, T. Zhang, Q. Jing, Z. L. Wang* "Radial-arrayed rotary electrification for high-performance triboelectric generator", *Nature Communication*, **5** (2014) 3456.

4:20pm EN+EM+MN+NS+TR-MoA8 **Conflicting Roles of Charge Traps in ETA Solar Cells: The CREM Point of View**, *Hagai Cohen*, Weizmann Institute of Science, Israel

The characterization of multi-interfacial devices commonly encounters critical difficulties due to the limited access of standard electrical probes to selected inner domains. In this respect, the XPS (x-ray photoelectron spectroscopy) based CREM (chemically resolved electrical measurements) [1] is a technique proposing particularly useful capabilities. Demonstration of internal junction fields evaluation has already been provided, as well as the direct measurement of layer-specific photovoltages in ETA (extremely thin absorber) solar cells.[2] However, the complex dynamics realized during charge separation in such cells has not yet been investigated thoroughly by CREM.

The present work focuses on this issue, showing conflicting roles of charge trap states and, specifically, their different expression under controllably varied conditions. Comparison with complementary characterization techniques is further discussed, demonstrating the unique insight provided by CREM for their interpretation.

References

1. H. Cohen, *Appl. Phys. Lett.* **85**, 1271 (2004).

2. Y. Itzhaik, G. Hodes, H. Cohen, *J. Phys. Chem. Lett.* **2**, 2872 (2011).

4:40pm EN+EM+MN+NS+TR-MoA9 **Understanding Morphological and Structural Effect on Organic Photovoltaic Devices from Plasmonic Particles using Advanced Characterization Techniques**, *Nuradhika Herath, V. Lauter, J. Browning*, Oak Ridge National Laboratory

Organic electronics have been under intense scientific interest in recent years because of their attractive properties such as low cost fabrication processes, ability to performance under low light, and flexibility. Major achievements are based on use of new conjugated polymer and small molecules in bulk heterojunction (BHJ) devices to increase the inner donor acceptor interfaces of fully functional devices such as organic photovoltaics (OPVs) and organic light emitting devices (OLEDs). Many strategies have been introduced to enhance the power conversion efficiency (PCE) of organic electronics. Among them, one of the most promising solutions to enhance the absorption and device efficiencies of OPVs is incorporation of various metal nanoparticles (NPs). Metallic NPs enhanced the efficiency of the devices through local surface plasmonic responses (LSPR). This phenomenon reduced the recombination level of geminate excitons and increases the exciton dissociations, which enhanced the photocurrent and fill factors of devices. However, metallic NPs blended within the active layer can act as polaron traps detracting the device performances. In this study, we investigate layer and interfacial structure of small molecule (SM), *p*-DTS(FBTTh₂)₂ and fullerene, PC₇₀BM system incorporated with silver (Ag) NPs, using neutron reflectometry (NR), X-ray reflectometry and Atomic Force Microscopy (AFM). We present detailed composition changes with Ag NPs concentrations along the film depth to understand morphological and dynamical effects of BHJ devices incorporated with plasmonic particles. To complement and enhance the findings from NR, we report optical properties of the samples using UV-Visible absorption and Photoluminescence spectroscopy. Our findings provide unique information and clear insights into dynamics of plasmonic organic solar cells and their future applications for further enhancement of PCE.

This research was conducted at Spallation Neutron Source and at the Center for Nanophase Materials Sciences, which is sponsored at ORNL by the Scientific User Facilities Division, Office of Basic Energy Sciences, U.S. Department of Energy.

5:00pm EN+EM+MN+NS+TR-MoA10 **Doped TiO₂ Based Core-Shell Structures for High Efficiency Hybrid Solar Cells**, *Jonas Weickert, J. Dorman, M. Noebels, M. Putnik, T. Pfadler*, University of Konstanz, Germany, *A. Wisnet, C. Scheu*, LMU Munich, Germany, *L. Schmidt-Mende*, University of Konstanz, Germany

Hybrid solar cells, with an inorganic/organic interface for charge separation, have been extensively investigated in the past decade in order to replace the expensive Si based technology with an inexpensive alternative. Typically, these devices incorporate a mesoporous TiO₂ film which is decorated with dye molecules and filled with a hole transport polymer, for example P3HT,

to conduct the electrons and holes, respectively. Recently, we have shown that the efficiency of nanowire based hybrid solar cells can be increased from ~1.8 % to 2.5 % through the formation of a Sn-doped TiO₂/TiO₂ core-shell device created via a hydrothermal growth and subsequent TiCl₄ treatment. However, this surface treatment presents difficulties in creating a crystalline conformal coating, limiting the control over the extent of coating and the crystallinity, directly affecting the charge injection from the polymer into the TiO₂ array. In this work, we directly deposit a controllable TiO₂ film through atomic layer deposition to conformally coat the nanowire arrays with various thicknesses. By changing the thickness and TiO₂ crystallinity, we are able to engineer the energy levels at the TiO₂-dye-P3HT interface due to the magnitude and position of the Fermi levels of the core and shell material, influencing the rate of charge injection and recombination. Furthermore, the crystallinity of the shell layer directly affects the amount of dye that can be absorbed on the surface of the nanostructures with a reduction in light absorption by roughly 30% from anatase to rutile TiO₂. Finally, a detailed mechanism will be proposed for the device performances based on the energy level alignment between the pinned Fermi-level TiO₂ structure and the HOMO of the P3HT resulting in a shifting open circuit voltage based on the crystal phases. Additionally, the core-shell structures are characterized with photovoltage decay and impedance spectroscopy measurements to study the charge transport and recombination across these various interfaces.

5:20pm EN+EM+MN+NS+TR-MoA11 Stack Numbers Dependence of the Activation Energies for Carrier Escape from and Recombination in Strain-Balanced InGaAs/GaAsP MQW, Atsuhiko Fukuyama, T. Ikari, K. Nishioka, T. Aihara, H. Suzuki, University of Miyazaki, Japan, H. Fujii, M. Sugiyama, Y. Nakano, The University of Tokyo, Japan

Fabrication of multiple quantum well (MQWs) in an absorption layer can extend the absorption region toward a longer wavelength and enhance the short-circuit current in the solar cells. However, MQWs function as recombination centers, leading to degradation in both open-circuit voltage and fill factor. We have already reported that the increase in stack number of QW causes the degradation of carrier collection efficiency [1]. In this study, we investigate the effects of stacks number on temperature dependences of the photoluminescence (PL), photothermal (PPT) and the surface photovoltage (SPV) signals. Although the photoexcited carriers in the barrier should relax by the radiative recombination (PL), carriers can thermally escape (SPV) or non-radiatively recombine (PPT) at the same time. Therefore, the latter two methodologies give us new insights for the carrier recombination and drift through the QW.

The present strain-balanced InGaAs/GaAsP MQWs absorption layer was composed of a 7.0-nm-thick In_{0.25}Ga_{0.75}As well and a 10.8-nm-thick GaAs_{0.66}P_{0.34} barrier. All layers were grown on an *n*-type GaAs substrate using metal-organic vapor phase epitaxy. We prepared different samples with MQW stack numbers of 10, 20, 30, and 40 in the *i*-region.

All PPT and SPV spectra showed three distinctive peaks followed by a step like function. They were decomposed into inter-subband transitions expressed by the two dimensional density of states for the QW and exciton peaks [2]. Although the PL intensity decreases with increasing the temperature, signals for PPT and SPV increases. We suppose two activation energies for the process: one is that for the carrier escape from the QW and another is for the non-radiative recombination in the QW. The three rate equations were built for PL, PPT and SPV and the temperature dependences are numerically fitted to estimate the two activation energies. As a result, we have estimated the activation energy for carrier escaping from the QW is constant as 70 meV for all samples with different stacks number. This is the same as the calculated barrier height. However, the activation energy for the non-radiative recombination increases from 6 to 49 meV for the sample with 10 and 40 stacks. This means that radiative recombination increases with increasing the stack number. The carriers thermally escape from the QW again relax into next well and may contribute to increase the radiative recombination.

[1] H. Fujii et al., Jpn. J. Appl. Phys. **51**, 10ND04 (2012).

[2] M. Kondow, A. Fukuyama, and T. Ikari et al., Appl. Phys. Express **2**, 041003 (2009).

Nanometer-scale Science and Technology

Room: 304 - Session NS+EN-MoA

Nanophotonics and Plasmonics

Moderator: WeiDavid Wei, University of Florida

2:00pm NS+EN-MoA1 Sculpting the Flow of Light at the Nanoscale, Harry Atwater, California Institute of Technology INVITED

Understanding the fundamental properties of plasmonic and dielectric materials in resonant subwavelength structures has fueled an explosion of interest in metamaterials and nanophotonic devices. In this seminar, we explore new directions for plasmonics by examining the relationship between plasmons and the electrochemical potential of the electron gas, and we discuss opportunities to observe quantum coherent states in plasmonic structures. Usually plasmons are described in a classical electromagnetic theory context, yet plasmons are fundamentally quantum excitations. Moreover, the carrier density and optical properties of plasmonic materials are typically fixed at the time of fabrication. Field effect tuning of the electrochemical potential in graphene nanoresonators enables the plasmon and phonon dispersion to be measured. Electrochemical and carrier density modulation in metals yields tunable resonances in metal nanostructures and reveals the plasmoelectric effect, a newly-discovered photoelectrochemical potential. By tuning the permittivity and index to near-zero values, expands the length scale over which coherent quantum emitter phenomena (e.g., concurrence, superradiance) can be observed in epsilon-near-zero media. Finally, we demonstrate entanglement or coherent superposition states of single plasmons using two plasmon-quantum interference in chip-based plasmon waveguide directional couplers.

Web resources:

<http://www.lmi.caltech.edu/>

<http://daedalus.caltech.edu/>

2:40pm NS+EN-MoA3 Patterning of Plasmonic Structures for Chiroptical Spectroscopy, Oded Rabin, A.P. Lawson, P.C. McAvoy, I.D. Mayergoyz, University of Maryland, College Park

Fabrication of truly chiral nanostructures is a challenging process, often requiring multiple cycles of patterning, deposition and planarization. Planar and three dimensional plasmonic nanostructures were fabricated through focused ion beam (FIB) milling, electron beam lithography (EBL) patterning, and a combination thereof, achieving truly chiral nanoscale patterns in a single deposition step. Using computational modeling tools, the plasmon resonance spectra of the structures were predicted. We have combined our computational results and novel fabrication methods to achieve chiral plasmonic nanostructures with useful resonances in the visible and near infrared ranges of the EM spectrum. These substrates are promising for the selective manipulation of circularly polarized radiation at nanometer length scales.

3:00pm NS+EN-MoA4 Hot Electron Generation Enhanced by Carrier Multiplication Probed with a Graphene/TiO₂ Nanodiode, YoungKeun Lee, KAIST, Republic of Korea, H.K. Choi, ETRI, Republic of Korea, H. Lee, KAIST, Republic of Korea, J.S. Choi, ETRI, Republic of Korea, E. Hwang, Sungkyunkwan University, Republic of Korea, J.Y. Park, KAIST, Republic of Korea

Graphene has attracted intensive attention for viable applications such as energy conversion and optoelectronic devices. When photons hit the graphene, the photon energy can be transferred to hot carriers above the Fermi level from the valence band of the graphene before the photon energy is lost as heat. The efficiency of the conversion depends on the interaction of photons with electrons/holes in the system. In graphene without a bandgap, the process of energy relaxation consists of the Auger process (impact ionization), which leads to carrier multiplication. Here, we fabricated a graphene/TiO₂ nanodiode to investigate carrier multiplication by experimental detection and theoretical confirmation of hot electron amplification. Our findings indicate that carrier multiplication of the graphene based on the strong electron-electron interaction is highly efficient, compared with Au/TiO₂ at a given photon energy. Multiple generations of hot electrons can induce photocurrent, which suggests the possibility of feasible applications such as photovoltaics and photodetectors.

3:40pm NS+EN-MoA6 Doping Induced 1D Plasmons in Ag Monolayer Stripes on Si(557), Timo Lichtenstein, U. Krieg, C. Teegenkamp, H. Pfniür, Leibniz Universität Hannover, Germany

An efficient way to transfer energy, e.g. light, into an electronic system is by excitation of plasmons. Due to their flat and almost linear dispersion, allowing extreme confinement in a broad frequency range, and their natural function as wave guides 1D plasmons are particularly interesting.

As we show here for the system Ag adsorbed on Si(557), the interaction between adsorbate layers of transition metal atoms and strongly anisotropic surfaces can lead to various quasi-one-dimensional (1D) signatures, which, however, are not all necessarily metallic. Using low energy electron diffraction in combination with scanning tunneling microscopy and electron energy loss spectroscopy, we correlate the structure, determined by SPALEED and STM, with the properties of low dimensional collective excitations, as measured with momentum and energy resolving electron loss spectroscopy. Semiconducting structures with double periodicity along the chains are formed Ag coverages below 0.3 monolayers (ML). At higher coverages, the formation of wires with $(\sqrt{3}\times\sqrt{3})$ order sets in. Only these wires turn out to be metallic, as is evident from the appearance of plasmonic losses, which show 1D dispersion only along the wires. This 1D property even persists up to one monolayer, where a densely packed array of metallic $(\sqrt{3}\times\sqrt{3})$ stripes is formed. We show evidence that the metallic property is induced by an extrinsic doping process of excess Ag (or other) atoms localized at the step edges, which can be reversibly removed and added. With this system we were able to explicitly show that the 1D plasmon frequency depends on the electron density proportional to $\sqrt{n_e}$ also in the 1D case, and that the confinement of the electrons on the wires is also dependent on doping concentration.

4:00pm NS+EN-MoA7 Surface Plasmon-Mediated Gold Nanoparticle Deposition via Two Different Mechanisms, *Jingjing Qiu, W.D. Wei,** University of Florida

Utilizing intrinsic surface properties to direct and control nanostructure growth on a large-scale surface is fundamentally interesting and holds great technological promise. We have developed a novel "bottom-up" approach to fabricating sub-15 nm Au nanoparticles on a nanostructured Ag surface via a chemical solution deposition by using localized surface plasmon resonance (SPR) excitation. Nanoparticle sizes were tunable between 3 to 10 nm by adjusting the deposition time utilizing the photothermal effects on a nanostructured Ag film surface. In addition, Au nanoparticles can be selectively deposited at the tip of a Ag bowtie nanostructure with the enhanced electric field.

4:20pm NS+EN-MoA8 Enhanced Light-Matter Interactions in Nanoparticle Arrays, *Teri Odom*, Northwestern University **INVITED**

Metal nanostructures concentrate optical fields into highly confined, nanoscale volumes that can be exploited in a wide range of applications. This talk will describe new ways to design arrays of strongly coupled nanoparticles and plasmonic hetero-oligomers that can exhibit extraordinary properties such as plasmon lasing and enhanced gas sensing. First, we will describe a new type of nanocavity based on arrays of metal nanoparticles. These structures support lattice plasmon modes that can be amplified and that can result in room-temperature lasing with directional beam emission. Second, we will focus on nanoparticle assemblies composed of more than one type of material. Hetero-oligomers composed of strong and weak plasmonic materials (Au-Pd dimers and trimers) showed unusual wavelength shifts when subjected to hydrogen gas. We performed detailed modeling to understand the near-field coupling responsible for these amplified light-matter interactions.

5:00pm NS+EN-MoA10 Plasmon-induced Current Enhancement at Nano-sized Metal-Oxide Interfaces, *Jiechang Hou, D.A. Bonnell,** University of Pennsylvania

Nano-sized metal-oxide interfaces possess unique physical properties and offers new access to novel functionalities. We have shown that at the nanoscale the electronic properties of Au/SrTiO₃ interfaces are size and atomic structure dependent [1]. This size dependence of interface properties has consequences to related behavior, such as resistive switching [2]. Earlier we have shown that plasmon induced hot electrons can be extracted from Au nanoparticles into molecular devices [3]. Here we use Au nano-antennas/SrTiO₃ interfaces as a facile model system to study this phenomenon. The study combines nanofabrication, optical spectroscopies, field simulation and advanced scanning probe microscopy. The dependences of photocurrent on power density and temperature are quantified, and the mechanism of photocurrent enhancement is discussed. We believe that this study can improve the understanding of the mechanism of plasmon-induced current enhancement and facilitate the modern device design.

References:

- [1] J. Hou, S. S. Nonnenmann, W. Qin, D. A. Bonnell, *Appl. Phys. Lett.* **103**, 252106, 2013.
- [2] J. Hou, S. S. Nonnenmann, W. Qin, D. A. Bonnell, *Adv. Funct. Mater.* (2014). doi: 10.1002/adfm.201304121.

* NSTD Student Award Finalist

[3] D. Conklin, S. Nanayakkara, T. Park, M. F. Lagarde, J. T. Stecher, X. Chen, M. J. Therien, D. A. Bonnell, *ACS Nano*, **7**, 4479 (2013).

5:20pm NS+EN-MoA11 Extreme Tunability of Metal-Dielectric Multilayered Structures using Al-doped ZnO Grown by Atomic Layer Deposition, *Jonathan Skuza, R.M. Mundle, K.C. Santiago,* Norfolk State University, *D.L. Lepkowski,* Louisiana State University, *A.K. Pradhan,* Norfolk State University

Plasmonic metamaterials have been a burgeoning area of research in recent years, where surface plasmon polaritons (SPPs) can manipulate light on the nanoscale. Typically, noble metals (e.g. Ag, Au) have been the key materials in this field of research, but suffer drawbacks (e.g. high loss) especially in the mid- and near-infrared (NIR) spectral ranges. Recently, wide bandgap semiconductors, such as Al-doped ZnO (AZO), have been shown to hold great potential in surpassing the tunability and flexibility of traditional noble metals in nanoplasmonic applications. Generally, these transparent conducting oxides have been extremely important for various optoelectronic applications due to the coexistence of high conductivity and high transparency, which can be tuned through doping. Recent studies have shown that these wide bandgap semiconductors, in particular AZO, are also efficient nanoplasmonic materials in the NIR due to their metallic behavior, strong confinement of SPPs, and low loss. AZO has been studied extensively using a multitude of deposition techniques, especially atomic layer deposition (ALD), which is particularly useful to grow uniform and conformal films with a high degree of thickness control on complex three-dimensional topographies because it is based on a binary sequence of self-limiting surface chemical reactions. Furthermore, the doping concentration can be precisely controlled by adjusting the ALD cycle ratios of the host and dopant materials, thus making ALD a unique and powerful method to deposit AZO into high aspect ratio structures for nanoplasmonic applications. Recently, it has been shown that ALD-grown AZO offers extreme tunability that can be utilized for many applications, including plasmonic components for epsilon-near-zero metamaterials. This extreme tunability is exploited here in metal-dielectric multilayered structures in order to manipulate and control light in subwavelength volumes for various optical applications.

Surface Science

Room: 309 - Session SS+EN-MoA

Metals, Alloys and Oxides: Structure, Reactivity & Catalysis

Moderator: Jason Weaver, University of Florida

2:00pm SS+EN-MoA1 High Throughput Discovery and Optimisation of Metal Alloy Electrocatalysts, *Brian Hayden,* University of Southampton **INVITED**

High-throughput synthesis and screening methodologies provide a powerful tool for the optimisation of alloy electrocatalysts. Libraries of thin film metal alloys have been synthesised using MBE sources to produce compositional gradient thin films in masked fields on micro-fabricated electrochemical screening chips. Examples will be given of ternary metal alloy catalysts designed as alternatives to platinum for the oxygen reduction reaction at the cathode in PEM Fuel Cells. The combination of ab-initio theory and high throughput synthesis and electrocatalyst screening is also shown to provide a powerful combination in the search for alternative catalysts to platinum for hydrogen oxidation at the anode. The approach has also been extended to the development of PdCu and PdSn alloys for the electro-reduction of nitrate, alloys which exhibit strong compositional dependencies which can be related to the redox behaviour of the surfaces. A full structural characterisation allows a direct comparison of catalytic activity to not only composition but also to the structure and phase of the alloy. In addition to measuring the total activity of the electrocatalysts, a secondary screen has been developed adapting the Differential Electrochemical Mass Spectroscopy (DEMS) method to assess the specificity of the reaction to produce the desired gas phase product.

2:40pm SS+EN-MoA3 Methanol Oxidation on Pt-Re Surfaces: Ambient Pressure XPS and Reactor Studies, *A.S. Duke, R.P. Galhenage, K. Xie,* University of South Carolina, *S.A. Tenney, P. Sutter,* Brookhaven National Laboratory, *Donna Chen,* University of South Carolina

Methanol oxidation has been investigated on Pt-Re bimetallic surfaces in order to understand how the addition of Re promotes activity on Pt in alcohol reforming and other oxidation reactions. Pt-Re alloy surfaces were prepared by depositing Re on Pt(111) or polycrystalline Pt foils and annealing to 1000 K. Scanning tunneling microscopy studies demonstrate that the deposited Re islands diffuse into the Pt(111) surface upon

annealing, and low energy ion scattering studies indicate that the top monolayer consists mainly of Pt. XPS investigations were carried out at the X1A1 beamline at the National Synchrotron Light Source under methanol oxidation conditions of 200 mtorr O_2 /100 mtorr methanol between 300 and 550 K, and gaseous products were monitored using a mass spectrometer. Methanol oxidation was studied on clean Pt(111), the Pt-Re alloy and Re films grown on Pt before and after surface oxidation at 450 K. The main products on all surfaces were CO_2 and H_2O with formaldehyde, CO and H_2 as minor products. On the unoxidized surfaces, the selectivity toward H_2 and CO production increased above 500 K. Deposition of atomic carbon during reaction was suppressed on the Pt-Re alloy surfaces as compared to pure Pt, and the oxidized Pt-Re alloy was found to reach maximum activity at the lowest temperatures. The Re films were unstable under methanol oxidation conditions at temperatures above 450 K due to the sublimation of Re oxides, but the Re in the Pt-Re alloy remained on the surface under the same conditions. Activity studies in a flow reactor coupled to the ultrahigh vacuum chamber showed that methanol oxidation activity increases with surface oxidation; unoxidized Pt and Pt-Re surfaces initially exhibit minimal activity until the surface becomes oxidized under reaction conditions.

3:00pm **SS+EN-MoA4 Ångstrom-resolved Real-Time Dissection of Electrochemically Active Noble-Metal Interfaces during Oxidation and Reduction**, *B.R. Shrestha, T. Baimpos, S. Raman, Markus Valtiner*, Max Planck Institut für Eisenforschung GmbH, Germany

Electrochemical metal-oxide/liquid interfaces are critically important for a variety of technological applications and materials for energy storage, harvesting and conversion. Yet, a real-time Ångstrom-resolved visualization of dynamic processes at electrified metal-oxide/liquid interfaces has not been feasible. Here we present a unique direct and real-time atomistic experimental view into dynamic processes at electrochemically active metal interfaces using white light interferometry in an electrochemical surface forces apparatus. This method allows to simultaneously decipher both sides of an electrochemical interface - the solution side and the metal side - in real-time under dynamically evolving reactive conditions, which are typically found in technological systems *in operando*. Quantitative *in situ* analysis of the electrochemical oxidation and reduction of noble metal surfaces shows that the Å-thick oxide films formed on Au and Pt are reflecting high-*ik* materials, *i.e.* they are metallic or highly doped semiconductors, while Pd forms a transparent low-*ik* oxide during dynamic change of applied electrochemical potentials. In contrast, under potentiostatic growth conditions all electrochemically grown noble metal oxides are transparent, with thicknesses ranging from 2-10 Å. On the solution side the data simultaneously reveals hitherto unknown strong electrochemical depletion forces, which are due to a temporary charge imbalance in the electric double layer caused by the consumption or generation of charged species. The real time capability of our approach shows significant time lags between electron transfer, oxide reduction/oxidation and solution side equilibration during a progressing electrode process. Comparing the kinetics of solution side and metal side reactions provide detailed experimental evidence that noble metal oxide reduction initiates via hydrogen loading and subsequently proceeds via a dissolution/re-deposition mechanism. The presented approach may have important implications for designing emerging materials utilizing electrified interfaces such as fuel cells, batteries or super-capacitors.

3:40pm **SS+EN-MoA6 Catalytic Dehydration of 2-propanol on Size Selected $(WO_3)_n$ and $(MoO_3)_n$ Metal Oxide Clusters**, *Xin Tang*, Johns Hopkins University, *D. Bumüller, G. Gantefoer*, Universität Konstanz, Germany, *D.H. Fairbrother, K.H. Bowen*, Johns Hopkins University

Metal oxide nanoparticles and clusters are widely used as redox and acid/base catalysts in heterogeneous catalysis. The catalytic activity of the size selected metal oxide clusters $(WO_3)_n$ and $(MoO_3)_n$ ($n = 1, 2, 3, 5, 30$) were studied as a function of their size. The 2-propanol dehydration reaction was conducted on both two cluster catalysts. Temperature programmed reaction (TPR) was utilized to characterize the catalytic activity of the deposited cluster catalysts. The cluster size, supporting substrates, and the chemical compositions of the clusters were found to play an important role in determining the catalytic activity of the metal oxide clusters. For tungsten oxide clusters on the annealed oxide films, the catalytic activity of the clusters was found to be linear correlated to the size of the cluster. In addition, lower catalytic activity was observed for $(WO_3)_1$ monomer supported on the HOPG surface compared to the annealed oxide support. Meanwhile, molybdenum oxide clusters exhibited low catalytic activity toward 2-propanol dehydration reactions.

4:00pm **SS+EN-MoA7 Growth and Characterization of Ultrathin ZnO Layers on Au(111) – STM Study of Growth Mode and Adsorption of Water**, *Junseok Lee, X. Deng, D.C. Sorescu*, National Energy Technology Laboratory

Zinc oxide is an important material in the low-temperature synthesis of methanol. In this study, the growth mode of ZnO ultrathin films has been studied on the Au(111) surface using scanning tunneling microscopy (STM). The ultrathin ZnO layers have been found to grow by forming islands on Au(111). Different growth conditions during reactive deposition resulted in ZnO islands whose thickness ranging from one to four layers. The STM results and the density functional theory (DFT) calculation have been used to model the observed phenomena. STM results indicate that the brightness of the Moire pattern of the ZnO layer on Au(111) surface is significantly modulated by the adsorption of water molecule at the positive tip bias. Various water adsorption sites have been identified in the STM results after annealing the sample to various temperatures that correspond to temperature programmed desorption (TPD) peaks. The DFT calculation results provide the most stable configurations of water molecules at each adsorption site.

4:20pm **SS+EN-MoA8 In Situ Imaging of the Dynamic Interaction of the Oxide with the Atomic Steps During the Oxide Growth on NiAl(100)**, *Hailang Qin*, SUNY Binghamton, *X. Chen*, Biola University, *P. Sutter*, Brookhaven National Laboratory, *G.W. Zhou*, SUNY Binghamton

Ultrathin oxide films on metal supports represent a unique combination of materials systems with potential applications ranging from heterogeneous catalysis to electronic devices. In particular, the oxidation of NiAl alloys has received extensive interest for its ability to form a well-ordered Al_2O_3 film. Here we study the dynamic interaction of the atomic steps with the oxide stripes during their growth on single-crystal NiAl(100) at high temperature. With in-situ low-energy electron microscopy (LEEM) imaging and theoretical modeling, it is shown that the oxygen surface diffusion is the main mechanism controlling the oxide growth kinetics while the migration and shape evolution of the substrate steps follows the fluid-like Hele-Shaw flow governed by the attachment/detachment of Al atoms at step edges. When the oxide stripe encounters a series of step edges, the step edges are "pushed" along with the oxide stripe growth and bent towards the growth direction of the stripe. However, the growing oxide stripes do not cross over the substrate steps; instead, they stay on the same terrace even after encountering a number of step edges. Such a process is reversible during the oxide decomposition. The scanning tunneling microscopy (STM) images of the oxide stripes and the atomic steps after the interaction further confirm that the oxide stripes stay on the same terrace after encountering multiple substrate steps, instead of crossing the step edges.

4:40pm **SS+EN-MoA9 Subsurface Oxygen on Ni(111) and Ag(111)**, *Daniel Killelea, J. Derouin, R. Farber*, Loyola University Chicago

Subsurface oxygen atoms are enigmatic sources of energetic reagents in the heterogeneously catalyzed partial oxidation of small hydrocarbons on metal surfaces. Subsurface oxygen atoms are absorbed in the selvedge of a metal, and may emerge to the surface at elevated temperatures to react with adsorbed molecules. Furthermore, when subsurface atoms emerge from beneath adsorbed molecules new reaction geometries are enabled that are otherwise inaccessible between reactants co-adsorbed to a surface. Although believed to be important reactive intermediaries, a systematic study of their fundamental chemistry has yet to be undertaken. To address this, we have selected two model systems for study; oxygen on Ni(111) and Ag(111). These are two systems that will provide basic details of subsurface absorption and reactivity, and further provide guidance for utilization of these species to selectively control chemistry. Subsurface atoms are key components of catalytic processes, but it remains unclear how they enhance reactions. The surface-subsurface dynamics will be elucidated using scanning tunneling microscopy (STM) to image the surfaces with and without subsurface O atoms. We will use the images to determine the presence of a bias for particular surfaces sites for the absorption / emergence processes and further study any structural or electronic effects of the subsurface O atoms on the host metal surface. To complement STM images, temperature programmed desorption and Auger electron spectroscopy will identify adsorbates and provide thermodynamic information. Our results will show mechanisms for subsurface migration and we will also probe the energetics of subsurface incorporation. Taken together, this new information seeks to narrow the gap our understanding between model and actual catalytic systems and enable chemists to accurately gauge the role of subsurface species in the transformation of plentiful feedstock into energy-rich chemicals over metal catalysts.

5:00pm **SS+EN-MoA10 Direct Imaging of the Amphoteric Nature of Rutile (110) Surfaces in Solution**, *Dapeng Jing, A. Song, M.A. Hines*, Cornell University

High-profile applications of nanocrystalline TiO₂, such as next-generation solar cells and self-cleaning surfaces, have triggered extensive studies on the structure and chemical reactivity of rutile surfaces. But are UHV-prepared clean surfaces a good representation of technologically relevant surfaces? In this study, we show that a simple aqueous procedure produces near-ideal hydrocarbon-free rutile (110) surfaces characterized by well-defined terraces and nearly straight, single-layer-high steps without high-temperature annealing. The structure of rutile surfaces after water exposure is very different from that observed on UHV-prepared clean surfaces. In particular, the O vacancies that dominate the reactivity of surfaces in UHV are not present, as evidenced by both XPS spectra and STM images. This water-induced “healing” of O vacancies is consistent with chemical intuition. The step structures, too, are quite different. In addition, the amphoteric nature of the surface is directly observed in STM. Depending on the pH of the solution, a low density of protrusions decorate either the Ti rows or the bridging oxygen atoms, consistent with pH dependent protonation/deprotonation of the basic/acidic sites on the surface. No evidence of the corresponding counterions is observed.

5:20pm **SS+EN-MoA11 Water Splitting Kinetics at MgO(100) Terrace Sites**, *John Newberg*, University of Delaware

Understanding the surface chemistry of water with metal oxide interfaces has important implications in energy and environmental research. In order to understand surface kinetics and thermodynamics under environmental conditions, in situ molecular level studies are needed to assess adsorbate chemistry and coverage under conditions where adsorption and desorption occur concomitantly. In this talk we will outline a proposed precursor kinetic model to describe recently published ambient pressure XPS (APXPS) results for MgO(100) terrace hydroxylation observed under adsorption-desorption conditions. By combining APXPS with computational studies, mechanistic details for water dissociation on MgO(100) terrace sites are put forth.

Tuesday Morning, November 11, 2014

Energy Frontiers Focus Topic

Room: 315 - Session EN+AS+EM+SE-TuM

Fuel Formation and Thermal Transport

Moderator: Michael Filler, Georgia Institute of Technology

8:00am EN+AS+EM+SE-TuM1 **Unraveling Thermodynamic and Kinetic Factors in Solar-Thermochemical Fuel Production**, *Sossina Haile*, California Institute of Technology **INVITED**

Perhaps the greatest challenge facing our planet is sustainable energy. Given the vast solar energy resource base available to modern society, key to addressing this challenge is the conversion of solar energy into a storable form suitable for on-demand utilization. So emerges the concept of 'Solar Fuels.' Amongst many approaches currently pursued to generate solar fuels, thermochemical dissociation of water splitting is particularly attractive. It provides the benefits of full utilization of the solar spectrum and inherent temporal separation of hydrogen and oxygen gases. In recognition of these advantages, numerous multi-step cycles have been considered over the past several decades. Recently, two-step cycles making use of *non-stoichiometric* oxides have received attention because of the simplicity of their implementation. The approach relies on the large oxygen nonstoichiometry change that the material undergoes in response to variations in oxygen partial pressure (pO_2) and temperature (T). Specifically, upon exposure to high temperatures ceria undergoes reduction without change in crystalline phase to release oxygen. On cooling in the presence of H_2O (or CO_2), the oxide is reoxidized, releasing H_2 (or CO). The success of the method relies not only on favorable thermodynamics but also on facile kinetics, both in terms of surface reaction rates and bulk diffusion coefficient. Accordingly, we have undertaken a comprehensive study of ceria and its doped derivatives to assess both the equilibrium redox behavior by thermogravimetric methods and the kinetic response by conductivity relaxation methods. We find, for example, that introduction of Zr strongly increases the absolute non-stoichiometry of ceria, but at a penalty in terms of the sensitivity of the nonstoichiometry to changes in environmental conditions and in terms of bulk diffusivity. In another example, we find that the relaxation behavior of Sm-doped ceria is substantially more rapid than that of both undoped and Zr-doped ceria, a result that is tentatively assigned to differences in species mobilities. The implications of these fundamental differences in material properties for thermochemical fuel production are discussed.

8:40am EN+AS+EM+SE-TuM3 **Controlling Catalysis on Metal Nanoparticles by Direct Photoexcitation of Adsorbate-Metal Bonds**, *M.J. Kale, T. Avanesian*, University of California, Riverside, *H. Xin, J. Yan*, SLAC National Accelerator Laboratory, *Phillip Christopher*, University of California, Riverside **INVITED**

Heterogeneous photocatalysis is typically assumed to occur via photon absorption by a solid-state photocatalyst (only the photocatalyst electronic states are involved in photon absorption) followed by charge carrier diffusion through the photocatalyst bulk and subsequent transfer to adsorbates. This process of energetic charge carrier generation and transfer results in wavelength dependent quantum efficiencies that strictly follow the absorption spectrum of the solid-state photocatalysts, regardless of the chemical transformation. The substrate (photocatalyst) mediated photo-absorption process inhibits approaches to control reaction selectivity by matching photon excitation wavelengths to bond specific electronic transitions, as typically done in molecular systems.

Here, we show that strong chemisorption bonds formed between CO and Pt metal surfaces can be activated with visible photons to drive catalysis through direct, resonant photoexcitation of hybridized Pt-CO states. This is enabled as the dominant photoexcitation mechanism (over substrate mediated photoexcitation) driving catalysis by using sub-5-nanometer Pt nanoparticle catalysts, where high surface area to volume ratios force photon absorption onto surface metal atoms. The direct photoexcitation process is observed to be significantly more efficient for driving photocatalysis than the indirect photoexcitation process when the energy of exciting photons is resonant with adsorbate specific electronic transitions involving hybridized metal-adsorbate states. It is also demonstrated that resonant photoexcitation of Pt-CO bonds on sub-5-nanometer Pt nanoparticles by visible light significantly enhances selectivity towards CO_2 , over H_2O production, in the selective oxidation of CO by O_2 in an H_2 rich stream (also known as preferential CO oxidation). These results open new avenues to control catalytic reaction selectivity on sub 5-nm catalytic particles by resonant photoexcitation of adsorbate-specific electronic transitions involving hybridized metal and adsorbate states. It is expected

that the development of insights into resonant electronic transitions between hybridized metal-adsorbate states should allow rational control of catalytic selectivity that cannot be achieved exclusively with thermal energy input.

9:20am EN+AS+EM+SE-TuM5 **Atomistic Insights as the the pH Dependence of the Onset Potential of the Oxygen Evolution Reaction on Hematite**, *Anders Hellman*, Chalmers University, Sweden

Hematite ($\alpha-Fe_2O_3$) is an extensively investigated semiconductor for photoelectrochemical water oxidation, and recent research has shed light on many of the atomic processes involved. However, a controversy about the nature and role of surface states in the water oxidation reaction remains. Here first-principles calculations are used to investigate surface states present in hematite under photoelectrochemical conditions. Most specifically a model describing how the onset potential for oxygen evolution reaction on hematite depend on the pH of the electrolyte is put-forth. The predictions of this model are confirmed to a high extent by measurements of the onset potential on hematite based model photoanodes. In particular, a linear dependence of the onset potential on the pH was observed, with a 49 mV / pH slope. Detailed photoelectrochemical characterization confirmed that the oxygen evolution reaction takes place via the same surface states irrespective of the pH. Moreover, the photovoltage and flat band potential of the hematite were also found to be pH independent. These results provide a framework for a deeper understanding of the OER when taking place on semiconductors (like hematite) via surface states

9:40am EN+AS+EM+SE-TuM6 **Rational Design of Pt₃Ni Alloy Surface Structures for Oxygen Reduction**, *Liang Cao, T. Mueller*, Johns Hopkins University

A cluster expansion approach based on ab-initio calculations has been used to investigate the relationship between surface structures of Pt₃Ni(111) alloy catalysts and their catalytic activity. With this approach, we build a direct bridge between the atomic structure and catalytic properties of Pt-Ni alloy system at a variety of compositions and chemical environments. The equilibrium near-surface structures are presented as a function of O_2 partial pressure and the chemical potential difference between Ni and Pt. We discuss the relative importance of strain, ligand, and ensemble effects in determining catalytic activity, and demonstrate how ensemble effects can be leveraged to rationally design alloy surfaces with optimal ORR activity by searching for surfaces with targeted oxygen binding energy.

11:00am EN+AS+EM+SE-TuM10 **Molecular and Mesoscale Design for Organic and Hybrid Thermoelectrics**, *Rachel Segalman*, University of California, Santa Barbara **INVITED**

Thermoelectric materials for energy generation have several advantages over conventional power cycles including lack of moving parts, silent operation, miniaturizability, and CO_2 free conversion of heat to electricity. Excellent thermoelectric efficiency requires a combination of high thermopower (S , V/K), high electrical conductivity (σ , S/cm), and low thermal conductivity (κ , W/mK). To date the best materials available have been inorganic compounds with relatively low earth abundance and highly complex, vacuum processing routes (and hence greater expense), such as Bi_2Te_3 . Molecular materials and hybrid organic-inorganics bring the promise of solution processible, mechanically durable devices. While highly conductive polymers are now common place, they generally demonstrate low thermopower. Our work on molecular scale junctions that nanostructuring of organics allows them to act as thermionic filters between inorganic junctions which can lead to enhanced thermoelectric properties. We have taken inspiration from this fundamental understanding to design material systems in which we combine a high electrical conductivity, low thermal conductivity polymer with a nanoparticle that contributes high thermopower. Additionally, the work functions of the two materials are well-aligned which introduces the possibility of thermionic filtering at the interface and an additional boost to the power factor. The combination of these effects results in a new hybrid, solution processible material with a thermoelectric figure of merit within an order of magnitude of the Bi_2Te_3 . In this talk, I will discuss both the use of thermoelectric measurements to gain insight to molecular junctions and how this insight translates to design principles for polymer and hybrid thermoelectrics.

11:40am EN+AS+EM+SE-TuM12 **Advances in Solid-State Energy Harvesting from Asymmetric Thermoelectric Devices**, *B. Cook, Jay Lewis*, RTI International

The amount of thermal energy rejected as waste heat from industrial processes in the United States has been estimated at 32 quadrillion BTU per year, with an associated emission of 1,680 million metric tons of carbon

dioxide. The ability to cost-effectively convert a portion of this thermal energy into useful electrical energy could improve energy efficiency, reduce operating costs, and decrease CO₂ emissions. Waste heat is typically categorized by temperature as high-grade (650°C and above), medium-grade (232°C to 650°C, and low-grade (232°C and below). In order to improve the thermal-to-electrical conversion efficiency of medium-grade waste heat, RTI has combined two different materials to form a high figure-of-merit, hybrid thermoelectric (TE) device. Recently-developed enhanced “TAGS-85”, or e-TAGS, was employed as the p-leg, while the n leg was comprised of improved half-Heusler (HH) material. This hybrid material pair provides a high ZT, lead-free TE material solution for waste heat recovery for use in vehicle or industrial platforms. The improved HH material employs two novel techniques to reduce thermal conductivity: (1) high-energy milling, and (2) addition of coherent inclusions. Single n/p-couples were produced that achieved a 9.2% thermal to electric power conversion efficiency for T_{hot} = 559°C and ΔT = 523K. This is a significant efficiency improvement at a lower hot side temperature with the hybrid e-TAGS/HH single couple over the performance of a conventional, all HH couple. By optimizing the cross sectional areas of the pellets for equal heat flow, the resulting asymmetric couple achieved a conversion efficiency of 10.5% at T_{hot} = 537°C and ΔT = 497°C. A 49-couple hybrid module using HH materials paired with e-TAGS and operated with T_{hot} up to 600°C reached a maximum efficiency of 10%. The improved module efficiency is believed to be due to both improved materials and optimized cross-sectional area ratios between the n- and p- elements. We will also discuss additional advances in thermal to electric power conversion using multi-stage modules.

12:00pm **EN+AS+EM+SE-TuM13 The Effect of Particle Size and Surface Termination of n-Si on Thermal and Electrical Conductivity**, *Thomas Lopez, L. Mangolini*, University of California - Riverside, *S. Bux, J.P. Fleurial*, California Institute of Technology

A discussion of synthesis and characterization of bulk nanocrystalline silicon with grain sizes of around 20 nm and thermal conductivities as small as 100 mW/cmK at room temperature, will be presented. Nanostructured materials have great potential for thermoelectric applications because of the reduction in thermal conductivity due to phonon scattering at grain boundaries [1] and silicon is a well-understood, cheap, earth-abundant material. Other silicon nanostructures, such as nanowires [2], are being investigated as viable thermoelectric materials. We have used, for the first time, the combination of a non-thermal plasma process for the synthesis of silicon nanocrystals with hot pressing to produce bulk nanostructured silicon samples. The non-thermal plasma synthetic route has been proposed for the production of photo-luminescent silicon quantum dots with narrow size distribution (3 +/- 0.5 nm) [3]. The same reactor has been scaled up to produce silicon nanocrystals at a rate of hundreds of milligrams per hour. Silicon powder with sizes between 5 nm and 15 nm has been produced using either silane (SiH₄) or silicon tetrachloride (SiCl₄), which are low-cost silicon precursors. Results have shown surface termination of the non-thermal plasma synthesized particle, i.e. H or Cl, play a role in densification kinetics. Hot pressing is a high pressure, high temperature process that allows for the production of samples with bulk like densities while limiting grain growth. In this study we have produced bulk (12 mm diameter, 2-4 mm in thickness) samples of nanocrystalline silicon with relative densities exceeding 95%. Characterization by XRD and TEM confirms that grain sizes are around 30 nm. The effects of surface termination of nano-silicon on grain growth and grain boundary conditions will be extensively discussed.

1. Dresselhaus, M.S., et al., *Advanced Materials*, 2007. 19(8): p. 1043-1053.
2. Hochbaum, A.I., et al., *Nature*, 2008. 451(7175): p. 163-U5.
3. Mangolini, L., et al., *Nano Letters*, 2005. 5(4): p. 655-659.

Surface Science

Room: 309 - Session SS+AS+EN-TuM

Synthesis, Structure and Characterization of Oxides

Moderator: Andrew Gellman, Carnegie Mellon University

8:00am **SS+AS+EN-TuM1 Coexisting Accessible Surface Phases on BaTiO₃ (001)**, *Erie Morales, J.M. Martinez*, University of Pennsylvania, *W.A. Saiti*, University of Pittsburgh, *A.M. Rappe, D.A. Bonnell*, University of Pennsylvania

Novel ferroelectric BaTiO₃ applications ranging from sensors to nanogenerators require a detailed understanding of atomic interactions at surfaces. Single crystals provides a platform that allows the exploitation of surface physical and chemical properties that can be readily transferred to

other ABO₃ perovskite structures. The processes that result in the atomic and electronic structures of surfaces in tandem with details of surface reactivity are necessary steps towards an understanding of BaTiO₃. Here we demonstrate that two surface reconstruction phases can coexist on a surface and explain the stability of the surface with a quantitative comparison of thermodynamic and kinetic considerations. Specifically, scanning tunneling microscopy (STM) and scanning tunneling spectroscopy (STS) of atomically resolved c(2x2) and c(4x4) reconstructions on BaTiO₃ (100) are compared with density functional theory models to determine the structures of the phases. First principles calculations are also used to examine the thermodynamic stability of the phases and the reaction pathways to both the stable and meta stable structures. We also show the atomic structures of 1 D interfaces between the phases. The ferroelectric properties of BaTiO₃ lead to polarization dependent surface reactions and recent results based on poling at atomic level and will be discussed.

8:20am **SS+AS+EN-TuM2 Oxidation and Chemical Reactivity of TbO_x Thin Films on Pt(111)**, *W. Cartas, R. Rai, A. Sathe*, University of Florida, *A. Schaefer*, University of Bremen, Germany, *Jason Weaver*, University of Florida

Rare earth oxides (REOs) exhibit favorable catalytic performance for a diverse set of chemical transformations, including both partial and complete oxidation reactions. In this talk, I will discuss our recent investigations of the growth, oxidation and chemical reactivity of TbO_x(111) thin films on Pt(111), and make comparisons with results for Sm₂O₃(111) films grown on the same substrate. Bulk terbium and samarium represent examples of REOs that are reducible vs. effectively irreducible, respectively. From low energy electron diffraction and scanning tunneling microscopy, we find that samarium and terbium grow as high quality thin films on Pt(111) during deposition in ultrahigh vacuum. Both oxides develop in the Ln₂O₃ stoichiometry and adopt an oxygen-deficient fluorite structure wherein the metal cations form a hexagonal lattice in registry with the Pt(111) substrate, while oxygen vacancies are randomly distributed within the films. We find that plasma-generated O-atom beams are highly effective in transforming the Tb₂O₃(111) films to higher Tb oxides. Based on results of X-ray photoelectron spectroscopy and O₂ temperature programmed desorption (TPD), we show that exposure to O-atom beams completely oxidizes the Tb₂O₃(111) films to TbO₂ at 300 K, for film thicknesses up to at least seven layers. Heating to ~1000 K in UHV restores the films to the Tb₂O₃(111) stoichiometry, and produces O₂ desorption in two distinct TPD features centered at ~370 K and 660 K which we attribute to oxygen release from lattice sites located in the surface vs. bulk layers, respectively. We also find that O-atom adsorption at 90 K produces a weakly-bound state of oxygen on the TbO_x films which desorbs between ~100 and 270 K. This state of oxygen may correspond to a form of chemisorbed oxygen on the TbO_x film. Consistent with this interpretation, TPD experiments performed after oxidizing a Tb₂¹⁸O₃ film with ¹⁶O-atoms demonstrate that oxygen desorption below about 500 K originates only from the oxygen that is “added” to the Tb₂O₃ film, while all isotopic combinations of O₂ desorb from the bulk above 500 K. Lastly, I will present results which show that the oxidized TbO_x films exhibit high activity and selectivity for the dehydrogenation of methanol to formaldehyde, whereas the initial Tb₂O₃ films have limited reactivity toward methanol.

8:40am **SS+AS+EN-TuM3 Structure/Function Relationships on Cerium Oxide: Reactions on Single Crystal Films and Shape-Selected Nanocrystals**, *David Mullins*, Oak Ridge National Laboratory **INVITED**

Cerium oxide is a principal component in many heterogeneous catalytic processes. One of its key characteristics is the ability to provide or remove oxygen in chemical reactions. Recent work has demonstrated how the reactivity and selectivity of various molecules are dramatically altered on different crystallographic faces of cerium oxide. The structure and composition of different faces determine the number of coordination vacancies (CV) surrounding surface atoms, the availability of adsorption sites, the spacing between adsorption sites and the ability to remove O from the surface. The Ce cation sites are less accessible and have fewer coordination vacancies (CV) on CeO₂(111) than on CeO₂(100). Even though the Ce is in the second layer on CeO₂(100), molecules can adsorb in the open bridge sites between two Ce cations. While there have been numerous studies of the adsorption and reaction of various molecules on CeO₂(111) only recently have comparable experiments been conducted on CeO₂(100).

To investigate the role of surface orientation on reactivity, CeO₂ films with different orientations were grown by two different methods. CeO₂(100) films were grown ex situ by pulsed laser deposition on Nb-doped SrTiO₃(100). CeO₂(111) films were grown in situ by thermal deposition of Ce metal onto Ru(0001) in an oxygen atmosphere. The chemical reactivity was characterized by the adsorption and decomposition of various molecules such as CO₂, H₂O, alcohols, aldehydes and organic acids. In general the CeO₂(100) surface was found to be more active, i.e. molecules

adsorbed more readily and reacted to form new products, especially on a fully oxidized substrate. However the CeO₂(100) surface was less selective with a greater propensity to produce CO, CO₂ and water as products. Experiments are underway to determine if CeO₂(110), where the Ce adsorption sites are in the top layer and have 2 CV but the O has only 1 CV, will produce an active yet more selective catalyst.

It is possible to synthesize high surface area shape-selected nanoparticles (octahedra and cubes), i.e. powders that expose a single, well-defined surface. Experiments have shown similarities between the single crystal surfaces and shape-selected nanoparticles, e.g. CeO₂(111)/octahedra are less active than CeO₂(100)/cubes. However there have also been significant differences in selectivity and the types of products formed. Possible explanations for the differences on the single crystal surfaces vs. the nanoshapes will be considered.

Research sponsored by the US Department of Energy, Office of Science, Basic Energy Sciences, Chemical Sciences, Geosciences, and Biosciences Division.

9:20am **SS+AS+EN-TuM5 Ceria on Cu(110): Formation of Nanostripe Strain Defects**, *L. Ma, N. Doudin, S. Surnev, Falko Netzer*, Karl-Franzens University, Austria

The growth morphology and atomic geometry of ceria nanostructures on Cu(110) have been investigated by STM, LEED and XPS. Ceria grows epitaxially in a two-dimensional (2-D) hexagonal layer, which is associated with a CeO₂(111)-type trilayer structure forming a (3x11) coincidence lattice. An important experimental parameter is the oxygen pressure during growth: it influences the stoichiometry of the ceria overlayer as well as the Cu surface oxide phase, which coexists with the ceria for coverages below the full monolayer. For oxygen pressures in excess of 10⁻⁷ mbar, stoichiometric CeO₂ and coexisting Cu-c(6x2) surface oxide are formed, whereas for lower oxygen pressures, in the 10⁻⁸ mbar range, slightly substoichiometric ceria (CeO_{1.9}) and a Cu-(2x1) surface oxide are observed. The ceria overlayer grows essentially 2-D, but displays a peculiar nanostripe pattern, with varying periodicities ranging from 4-8 nm and a corrugation amplitude of 0.2-0.3 nm. This nanostripe pattern is due to a topographic modulation of the overlayer caused by the frustration of overlayer-substrate bonding as a result of the epitaxial mismatch at the ceria-Cu interface. Detailed STM investigation reveals a distortion of the ceria lattice in the transition region between dark (low) and bright (high) stripes, which gives rise to periodic regions of anisotropic lattice strain - so-called "lattice strain defects". It is speculated that these lattice strain defects may support particular chemical reactivity.

Work supported by the ERC Advanced Grant "SEPON" and by the COST Action CM1104

9:40am **SS+AS+EN-TuM6 Design Rules for Stabilizing Polar Metal Oxide Surfaces: Adsorption of O₂ on Zn-rich Polar ZnO(0001)**, *Ming Li, P. Gorai, E. Ertekin, E.G. Seebauer*, University of Illinois at Urbana-Champaign

For oxide semiconductors with appreciable ionic character, under-coordination of the surface atoms leads to thermodynamic instability that is typically restored by reconstruction, faceting, or extensive surface defect creation. Developing design rules for stabilizing polar metal oxide surfaces that avoid these phenomena could offer novel protocols for applications such as improved nanostructure growth and design of photocatalytic heterostructures. The present work describes calculations by density functional theory for Zn-rich polar ZnO(0001) which demonstrate that stabilization via chemisorbed O₂ together with vacancy formation is energetically as favorable as stabilization by vacancies alone. The stabilization mechanism including adsorption is so effective that it promotes O₂ adsorption to an extent that is not possible on non-polar ZnO. Experimental evidence for such stabilization behavior is presented based on measurements of O₂ adsorption on polar ZnO(0001) via the optical modulation technique of photoreflectance. The measured isotherms yield a sizable adsorption enthalpy of adsorption near 1.8eV, confirming a strong interaction with the polar surface.

11:00am **SS+AS+EN-TuM10 The Growth of Catalytic Thin Films on a Polar Substrate: Cr₂O₃ on ZnO (0001) and ZnO (000-1)**, *Xiaodong Zhu*, Yale University

Zinc oxide is a wurtzite-structured polar crystal with dramatic polarization direction-dependent surface chemistry. Meanwhile, chromium III oxide is a non-polar material catalytically active for a number of industrial chemical reactions, most notably dehydrogenation. Therefore, the Cr₂O₃/ZnO system has been chosen to demonstrate how the polarization direction of a substrate can be exploited to tailor the surface properties of catalytically active non-polar thin films. Photoelectron spectroscopy and electron diffraction have been performed to determine the growth mode as well as the film quality. The growth is 2D; however, the films appear initially disordered on both

positive and negatively poled substrates. On both substrates the order was observed to improve with thickness. Small band offsets between Cr₂O₃ and oppositely poled substrates were observed that were consistent with charge compensation at the Cr₂O₃/ZnO interface. No obvious change in the oxidation state of the chromium was seen and so it is assumed that the charge compensation at the interface only involves Zn and/or O. The offset between the Cr peaks on positively and negatively poled substrates was obvious at the initial growth stages but then decayed with film thickness, suggesting that the compensating charges at the interface may migrate to the film surface. Valence band spectra were analyzed to characterize the bonding at the interface. The surface chemical behavior of Cr₂O₃ on the two zinc oxide surfaces is being characterized to determine how significantly the polar interface impacts the surface properties of thin supported layers.

11:40am **SS+AS+EN-TuM12 Chemical Characterization of Elements in Oxides using X-ray Satellite Lines**, *Terrence Jach*, National Institute of Standards and Technology (NIST)

X-ray satellite lines come about in x-ray fluorescence spectroscopy as a result of shake-off events in the excitation process. The ratio of their intensities has been shown to be a sensitive function of their oxidation states. We are able to observe the K satellite lines in the x-ray spectra of oxides and glasses, excited by the beam of an electron microscope and detected by a high resolution x-ray microcalorimeter detector. The results show surprising departures from the expected states of some metal elements that we expect to be fully oxidized. The satellite ratio is a way of determining the chemical environment of insulators without charging or ultra-high vacuum.

12:00pm **SS+AS+EN-TuM13 In Situ XPS and NRA Studies of Hydrogen Diffusion in TiO₂ Single Crystals**, *Vaithiyalingam Shuthanandan, M.I. Nandasiri, S.A. Thevuthasan, M.A. Henderson, S. Manandhar*, Pacific Northwest National Laboratory

The intrinsic point defects associated with oxygen vacancies and Ti³⁺ ions play a crucial role in the usage of titanium dioxide (TiO₂) in various technological applications including catalysis and photochemistry. It is well known that the interactions between H atoms and surface oxygen in TiO₂ lead to the formation of Ti³⁺ ions at elevated temperatures. However the Ti³⁺ ion formation and accumulation as a function of elevated temperatures in UHV conditions during hydrogen diffusion in TiO₂ is not well understood. In this study, we have used ion implantation method to incorporate hydrogen in single crystal TiO₂ (110) samples and investigated the behavior of point defects in both pure and hydrogen implanted TiO₂ as a function of elevated temperatures using Rutherford backscattering spectrometry (RBS), nuclear reaction analysis (NRA), x-ray photoelectron spectroscopy (XPS) and ultra violet photoemission spectroscopy (UPS). TiO₂ single crystals were implanted with 40 keV hydrogen ions at room temperature with ion fluences of 1x10¹⁵, 1x10¹⁶ and 1x10¹⁷ atoms/cm². Samples were isochronally annealed in vacuum for 30 minutes at each temperature up to 1100K and hydrogen and Ti³⁺ defects were quantified. Hydrogen depth profile measurements obtained from 1x10¹⁷ atoms/cm² implanted sample reveal that hydrogen diffused towards the surface at lower temperatures and it slowly diffuses out from the samples at higher temperatures. XPS and UPS measurements from the hydrogen implanted samples show significantly higher Ti³⁺ defects in comparison to pure TiO₂ at these temperatures under UHV conditions. These defects reach a maximum around 880 K in which almost all hydrogen was removed from the sample. When the implanted sample further annealed to high temperatures, the amount of Ti³⁺ in hydrogen implanted samples started to decrease and reaches the values from the pure TiO₂ samples around 1100K.

Tuesday Afternoon, November 11, 2014

Energy Frontiers Focus Topic

Room: 315 - Session EN+EM+NS-TuA

Charge Storage Materials and Devices

Moderator: Susanna Thon, Johns Hopkins University

2:20pm EN+EM+NS-TuA1 **Spatiotemporal Investigation of Li-Air Battery under Operating Condition: Understanding the Cathodic and Anodic Electrochemical Processes and their Interdependence**, *Di-Jia Liu*, Argonne National Laboratory **INVITED**

Li-O₂ battery has generated a great deal of interests due to its high theoretical energy storage capacity for vehicular application. Many studies were carried out in attempt to understand the fundamental chemical processes inside of Li-O₂ battery. The reports so far have been segmented into the investigation on the individual regions of the battery, cathode, anode and separator, mostly at the post mortem state due to the limitation of the characterization methods used.

We adopted a holistic approach in studying electrochemical processes and mechanism of the Li-O₂ battery using operando methods. Particularly, we introduced the microfocussed synchrotron X-ray diffraction (μ -XRD) and tomographic (μ -CT) techniques for the spatiotemporal study on the phase and structural changes in Li-O₂ battery. These tools offered some unique capabilities to probe battery properties under the actual discharge-charging condition. For example, the μ -XRD has a spatial resolution at the micron scale of with a complete side penetration to the battery, rendering it feasible to study battery's composition layer-by-layer without the interruption of battery operation. In this presentation, we will discuss our recent investigation of the Li-O₂ batteries under cycling condition in real time using the cells fabricated with the most representative design and materials. We were able not only to reveal individually the changes at anode, cathode and separator, but also to provide a comprehensive view between the regional chemical processes and their interdependence to the overall battery performance during the multiple discharge-charge cycles. More importantly, the finding of this study provides new insights on the catalytic process inside of Li-O₂ cell and calls for new design and materials which could lead to high capacity and longer battery life.

The work performed at Argonne is supported by DOE under Contract No. DE-AC02-06CH11357 by UChicago Argonne, LLC.

3:00pm EN+EM+NS-TuA3 **Insights into Ionic vs. Electronic Transport in Nanostructured Battery Electrodes Enabled by Microfabrication and Spatially Resolved XPS**, *Alexander Pearse, E. Gillette, S.B. Lee, G.W. Rubloff*, University of Maryland, College Park

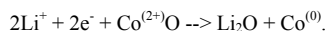
Nanostructured battery electrodes provide a design opportunity to achieve high power at high energy density, using thin active storage layers whose short ion diffusion pathways assure fast transport throughout the layers. However, this must be coupled with fast electron transport through current collectors to all regions of the ion storage layers, posing a design challenge in balancing and optimizing both charge transport components. Spatial inhomogeneity in the utilization of active material due to electronic or ionic transport limitations may lead to decreases in performance, but characterizing this effect with bulk electrochemical measurements is difficult. We address this challenge with a new state-of-charge (SOC) measurement scheme utilizing a patterned ultra-thin film battery electrode and spatially resolved XPS, and focus on the case of limited electronic transport by examining SOC as a function of distance from the current collector.

We fabricate electrode test structures by evaporating metallic strips as current collectors on an electrically insulating substrate. A patterned thin film of active material (V₂O₅) is then deposited using atomic layer deposition (ALD) and mechanical masking so that only a small fraction of the active material is in contact with the current collector. The use of ALD allows for an ultrathin (\leq 30nm) pinhole-free film. We discharge these electrodes in a liquid electrolyte under different rates and conditions and directly measure the state of charge as a function of distance from the current collector using small spot XPS, achieving a lateral resolution of better than 20 μ m. We find that a rate-dependent SOC gradient develops in the electrodes, with the SOC decreasing with distance from the current collector. Unlike microspot Raman or XRD, XPS provides a direct quantitative measurement of the SOC through the concentration of inserted ions and/or reduced vanadium ions. Additionally, in the ultrathin films relevant to nanostructured storage, XPS becomes a "quasi-bulk" measurement, because the escape depth of photoelectrons becomes a significant fraction of the film thickness. We also explore the depth dependence of the SOC using angle resolved XPS and ion beam depth

profiling. We compare our observations with simulations using COMSOL Multiphysics, and attempt to resolve discrepancies between the two. We believe this approach can provide design guidance for heterogeneous nanostructures applied to electrical energy storage, and we anticipate it to be broadly applicable to other electrode materials and active ions.

3:20pm EN+EM+NS-TuA4 **The Lithium-Induced Conversion Reaction of CoO Thin Film Battery Materials in Ultra-High Vacuum as Studied by ARXPS and STM**, *Ryan Thorpe, S. Rangan, A. Howansky, R.A. Bartynski*, Rutgers, the State University of New Jersey

Li-ion conversion batteries can store 2-3 times more charge than intercalation batteries by utilizing the full range of oxidation states of their constituent divalent or trivalent transition metal compounds during discharge. A prototypical conversion compound is CoO, which follows the reaction



Cobalt oxide and other transition metal oxides are attractive for use as Li-ion anodes in portable electronics due to their high charge storage capacity and moderate voltage versus Li^{+/}Li⁰. However, the cycling stability of conversion electrodes is poor, and capacity losses have thus far prevented their implementation.

In order to understand phase progression during the conversion reaction of CoO, high-purity CoO thin films grown in UHV were sequentially exposed to atomic lithium. The electronic structure of the pristine films and of the products of lithiation was studied using x-ray photoemission spectroscopy (XPS), UV photoemission spectroscopy, and inverse photoemission spectroscopy. The crystal structure and film reorganization were probed in parallel with transmission electron microscopy (TEM) and scanning tunneling microscopy.

The amount of CoO reduction for a given Li dose was observed to be highly dependent upon the temperature at which lithiation was performed. At 150°C, Li mobility in the active material was sufficient to allow full reduction of the CoO film as confirmed by XPS. Consistent with electrochemically lithiated CoO electrodes, precipitation of Co nanoparticles in a Li₂O matrix was observed in TEM images. However, at room temperature, the Li-rich overlayers that formed on the CoO film after initial lithiations inhibited further Li diffusion. This could be due to the intrinsically poor kinetic properties of Li₂O or to the formation of Li₂O₂ and/or LiOH passivating films.

The reactivity of CoO films was also found to depend on the orientation of the film. CoO(100) films exhibited a higher degree of conversion for a given Li exposure than polycrystalline films. STM and angle-resolved XPS of these films have been used to investigate the differences between these two film morphologies upon exposure to Li.

4:20pm EN+EM+NS-TuA7 **Controlled Cathode/Catalyst Architectures for Li-O₂ Batteries**, *Malakhi Noked, M.A. Schroeder, A.J. Pearse, C. Liu, A.C. Kozen, S.B. Lee, G.W. Rubloff*, University of Maryland, College Park

Electrochemical power sources based on metal anodes have specific energy density much higher than conventional Li ion batteries, due to the high energy density of the metal anode (3842mAh/g¹ for Li). Rechargeable Li-O₂ batteries consume oxygen from the surrounding environment during discharge to form Li oxides on the cathode scaffold, using reactions

- (1) [anode] $\text{Li(s)} \leftrightarrow \text{Li}^+ + \text{e}^-$
- (2) [cathode] $\text{Li}^+ + \frac{1}{2} \text{O}_2(\text{g}) + \text{e}^- \leftrightarrow \frac{1}{2} \text{Li}_2\text{O}_2(\text{s}), \sim 2.959 \text{ V vs Li/Li}^+$
- (3) [cathode] $\text{Li}^+ + \text{e}^- + \frac{1}{4} \text{O}_2(\text{g}) \leftrightarrow \frac{1}{2} \text{Li}_2\text{O}(\text{s}), \sim 2.913 \text{ V vs Li/Li}^+$

The cathode reaction requires large over-potentials for charging due to the mass transfer resistance of reagents to the active sites on its surface, decreasing the round trip efficiency, making recharge of the Li-O₂ cell difficult. To overcome these problems, the cathode needs good electrical conductivity and a porous structure that enables facile diffusion of oxygen and can accommodate the reduced oxygen species in the pores.

Two significant challenges exist in the use of the traditional activated carbon material as the cathode of the Li-O₂ system. First, in the presence of Li₂O₂ the carbon electrode becomes relatively unstable even at low voltages (\sim 3V). Second, cathode structures must be porous to accommodate a substantial amount of Li-peroxide (Li₂O₂) without blocking ion transport channels in the cathode. While a few studies have been reported on the effect of catalyst on the onset potentials for the oxygen evolution reaction (OER) and oxygen reduction reaction (ORR) in the Li-O₂ cell, the results were inconclusive due to the lack of systematic study in a single system and conditions.

We report here results from a model cathode system which enable determination of the effects of various catalysts on the OER/ORR reactions in the non-aqueous Li-O₂ cell. Mesoporous CNT sponge is used as the model cathode material, decorated with catalyst nanoparticles by nucleation-controlled atomic layer deposition (ALD) of Ru, RuO₂, MnO₂, and Pt catalyst components whose loading and composition are controlled by manipulating the ALD conditions. Using a custom Li-O₂ battery cell, we have studied the effect of different catalysts on the voltage of the OER and ORR, and on the cycling performances of the cell. We demonstrate a Li-O₂ cell that sustains >3000 mAhg⁻¹ over more than 15 cycles at current density of 200 mA g⁻¹. To our knowledge, this is the first comparison of a variety of catalysts with a well-defined morphology (controlled by ALD and monitored by TEM), and under the same electrochemical conditions.

4:40pm EN+EM+NS-TuA8 Vertically Aligned Carbon Nanotubes on Ni Foam as a 3D Li-O₂ Battery Cathode, Marshall Schroeder, M. Noked, A.J. Pearse, A.C. Kozen, S.B. Lee, G.W. Rubloff, University of Maryland, College Park

The Li-O₂ battery system is one of the prime candidates for next generation energy storage. Like other metal-O₂ systems, this technology is known for its impressive theoretical specific energy due to use of metallic anodes and because the cathode active material (oxygen) is not stored in the battery, but is available in the cell environment. A typical cell consists of a pure lithium metal anode, an organic electrolyte (in this study), and a porous positive electrode (usually made of carbon or oxides) which acts as a reaction scaffold for oxygen reduction to Li₂O₂ or Li₂O during discharge. Despite remarkable scientific challenges within every component of the cell, the positive electrode is particularly complicated by its role in the oxygen evolution (OER) and reduction (ORR) reactions, leading to strict requirements for electrode architecture and physicochemical stability for optimal performance. We present herein one of the first experimental realizations of a controlled macroscale 3D carbon nanotube architecture with a practical carbon loading of 1mg/cm² in an attempt to satisfy these requirements.

The O₂ cathode highlighted in this work features a macroporous nickel foam current collector coated with dense forests of vertically aligned carbon nanotubes (VACNT). This freestanding, hierarchically porous system is the first to feature VACNT robustly and electrically connected to a 3D current collector without a binder, and without requiring delamination of the CNT from the growth substrate. Grown via LPCVD with an Fe catalyst on a thin ALD interlayer, the micron-length VACNT provide a very promising electrode material due to their high electrical conductivity, physicochemical stability, and a high surface area architecture that is conducive to ionic mobility and storage of the reduced oxygen discharge product. As a result, this structure exhibits significant capacity (>2Ah/g-carbon) at high ORR voltages (>2.76V) without requiring a catalyst.

Electrochemical performance results as a scaffold for oxygen reduction in various non-aqueous electrolytes will be presented with SEM/TEM/XPS of pristine/discharged electrodes.

5:00pm EN+EM+NS-TuA9 Solid Micro-supercapacitor using Directed Self-Assembly of Tobacco Mosaic Virus and RuO₂, Markus Gnerlich, E.I. Tolstaya, J. Culver, D. Ketchum, R. Ghodssi, University of Maryland, College Park

The 3D micro-supercapacitor reported here utilizes a novel bottom-up assembly method that combines genetically modified Tobacco mosaic virus (TMV-1Cys) with deposition of RuO₂ on multi-metallic microelectrodes. The nanostructured RuO₂ coating is selectively deposited on the electrodes due their unique composition, which is a significant advantage for microfabrication process integration. Test results show electrode capacitance as high as 18 mF/cm² in 1.0M H₂SO₄ electrolyte and 7.2 mF/cm² in solid Nafion electrolyte.

The device fabrication involves the photolithographic patterning of titanium nitride (TiN) microelectrodes with Au cap on top of polyimide micropillars supported by a silicon wafer. A schematic cross section of the device is shown in Figure 1 and a photograph of the fabricated chip in Figure 2. The complexity of the self-assembly process in multiple chemically reactive solutions required the development of a special kind of micro-electrode. The TiN functions as a chemically resistant current collector, the Au cap as an adhesion layer for the TMV-1cys, and the Ni pad as a sacrificial material during the RuO₂ deposition process. After microfabrication, each chip is submerged in TMV-1Cys solution for 24 hours and then transferred to a 0.5% solution of RuO₄. A nanostructured coating of RuO₂ forms on all exposed electrode areas as the Ni is sacrificed in a galvanic displacement reaction. EDX spectral imaging of the constituent elements on the electrode demonstrates selective RuO₂ coating (Figure 3), and SEM images of the electrodes before and after TMV/RuO₂ coating shows the TMV-1Cys/RuO₂ nanostructures (Figure 4).

Cyclic voltammetry (CV) was performed from 0-800mV versus Ag/AgCl at 10 mV/s in 1.0M H₂SO₄ electrolyte. Figure 5 shows the CV curves, and Figure 6 shows the associated capacity fading, which was insignificant after 100 cycles for electrodes annealed at 150°C. Separately prepared chips were coated with Nafion dispersion and tested in a controlled humidity environment. The measured capacitance drops from 18 to 7.2 mF/cm² per electrode due to ionic conductivity limitations, but 80% capacity is retained after 12,000 cycles (Figure 7). Associated rate capability (Figures 8-9) shows 60% capacity is retained when comparing 3 uA/cm² to 3000 uA/cm², and the low leakage current of only 5 nA (Figure 10) enables use in a wide variety of energy storage applications.

The primary challenge of nanomaterials is often integration into microfabrication processes. The RuO₂ electrode developed here is optimized for compatibility with standard microfabrication steps by using a novel bottom-up assembly approach for manufacturing micro-supercapacitors.

5:20pm EN+EM+NS-TuA10 Characterization of Tobacco Mosaic Virus-templated Ni/NiO Electrodes for Solid Flexible Supercapacitors, Sangwook Chu, K.D. Gerasopoulos, M. Gnerlich, J. Culver, R. Ghodssi, University of Maryland, College Park

Characterization of nickel oxide supercapacitor electrodes utilizing *Tobacco mosaic virus* (TMV) nanotemplates is presented. NiO was formed on Ni coated TMV nanotemplates by annealing at high temperatures (Figure 1). The resulting electrode showed excellent electrochemical performance with remarkable cycle stability. The TMV/Ni/NiO nanostructured electrodes were also integrated with a solid electrolyte to demonstrate their potential application as solid flexible supercapacitors.

NiO supercapacitor electrodes have been prepared in literature using various methods, and it has been found that the crystallinity of the NiO is critical for its electrochemical charge capacity [1]. The NiO electrode presented in this work was thermally grown on Ni coated TMVs. Gold electrodes (0.5cm²) were immersed in TMV solution for virus self-assembly followed by electroless deposition of Ni uniformly coating the TMV nanostructure [2]. TMV/Ni electrodes were annealed in a furnace at three different temperatures (200°C, 300°C, and 400°C) and the NiO formation on TMV/Ni surface was characterized by XPS (Figure 2). The results indicate that thermal growth of NiO layer on TMV/Ni electrodes starts at temperatures higher than 300°C, in good agreement with previously reported results.

Electrochemical testing was performed in aqueous 2M KOH electrolyte in a three-electrode configuration. The electrodes annealed at 300°C showed the highest areal capacitance (148mF/cm²) measured by a galvanostatic (2mA/cm²) charge/discharge test shown in Figure 3a. The redox charge storage mechanism was confirmed by cyclic voltammetry (CV) with good rate capability up to 100mV/s (Figure 3b). Excellent cycle stability was measured with little degradation over 500 cycles as shown in Figure 4. This is attributed to the conformal layers of Ni/NiO over the TMV nanostructure, and the stabilizing effect of KOH on NiO. The continuous electrical contact between the Ni and NiO layers ensures an optimized current collector configuration.

A PVA-KOH-H₂O polymer was prepared to study the performance of the nanostructured electrodes with a solid electrolyte. Polymer electrolyte solution was poured onto the nanostructured NiO electrodes and the Pt foil was assembled on top as an anode. The polymer electrolyte film formed after 24hours was flexible and strong enough to support both electrodes. Figure 5 shows CV curves measured with the assembled cell, verifying proper operation of the nanostructures in both liquid and solid electrolytes. The successful integration of TMV/Ni/NiO electrodes with polymer electrolytes highlights the potential of this approach to develop flexible solid-state supercapacitor devices.

5:40pm EN+EM+NS-TuA11 Charged Particles Micro-Penning-Malmberg Trap: An Approach to Store High Densities with Substantially Lower End Barrier Potentials, Alireza Narimannezhad, J. Jennings, C. Minnal, M.H. Weber, K.G. Lynn, Washington State University
Among devices that have been used to store antimatter, Penning-Malmberg trap has become the device of choice because of its simplicity and versatility. However, the challenge involved in these traps is when the number of particles increases inside the trap to the densities of energy harvesting interest, the confining fields rise to unpractical values. One of the authors has proposed a design of microtube arrays with much lower end barrier potentials. The microtraps are designed for non-neutral plasma storage such as positrons. Here, we present fabrication, simulation studies, and trapping milestones so far. The fabrication involved advanced MEMS techniques including photolithography, deep reactive ion etching of silicon wafers, sidewalls smoothing, gold sputtering, wafers aligning, and thermo-compression gold bonding. Alignment of less than 2 microns was achieved using a micro-machined jig and precision ground sapphire rods.

Simulation using a WARP Particle-In-Cell code showed that density of $1.6 \times 10^{11} \text{cm}^{-3}$ is achievable with the new trap design while the end barrier potentials are several orders of magnitude smaller compared to the conventional traps. However, positron losses occur in experimentation by both trap imperfections such as misalignment of wafers, asymmetries, and physical imperfections on the surface, and also field misalignment and perturbations. The loss rates were also compared to the results from simulation in order to study and distinguish each effect. This project will open the door to a wide range of new and exciting research areas. The size of these traps along with the low confining potentials is a big step to make them portable. It could be used as a source of energy or in propulsion system where alternate sources are not feasible.

Thin Film

Room: 307 - Session TF+EN+PS-TuA

ALD for Energy

Moderator: Erwin Kessels, Eindhoven University of Technology, Netherlands

2:20pm **TF+EN+PS-TuA1 Li-Based ALD Solid Electrolytes for Beyond-Li-Ion Batteries, Alexander Kozen***, A.J. Pearse, M.A. Schroeder, C. Liu, M. Noked, C.F. Lin, G.W. Rubloff, University of Maryland, College Park

Solid Li-based inorganic electrolytes offer profound advantages for energy storage in 3-D solid state batteries: (1) enhanced safety, since they are not flammable like organic liquid electrolytes; and (2) high power and energy density since the solid electrolyte can support interdigitated nanostructured electrodes, avoiding binders, separators, and much larger spacing (tens of mm's) between fully separated electrodes. The quality of thin solid electrolytes – even in planar form – is currently a major obstacle to solid state batteries[1] restricting electrolyte thickness to $>100 \text{ nm}$ to control electronic leakage, consequently slowing ion transport across the electrolyte and impeding interdigitated 3-D nanostructure designs that offer high power and energy. Furthermore, the ion-conducting, electron-insulating properties of solid electrolytes are promising for their use as passivation or protective layers on metal anodes (Li, Na, Mg) and on cathodes in proposed “beyond-Li-ion” battery configurations such as Li-O₂ and Li-S.

Atomic layer deposition (ALD) is well suited to the challenge of solid electrolytes, providing ultrathin, high quality films with exceptional 3-D conformality on the nanoscale. We have developed ALD processes for Li₂O, Li₃PO₄, and LiPON from LiO^tBu, H₂O, and N₂, exploiting spectroscopic ellipsometry, downstream mass spectrometry, and XPS surface analysis, all *in-situ*. Post-ALD XPS reveals for the first time carbon-free electrolytes and their intrinsic surface chemistry. E.g., ALD Li₂O grown at 250C is reversibly transformed to LiOH upon exposure to H₂O, but transforms back upon annealing. LiOH is completely and irreversibly converted to Li₂CO₃ by CO₂ exposure. These kinds of observations are essential to developing process sequences for fabricating 3-D solid batteries.

We then demonstrate the impact of this solid electrolyte synthesis in several examples. For solid state batteries, we employ the electrolytes in planar and nanostructured battery configurations to determine their Li diffusivity and electrochemical performance. For beyond-Li-ion configurations with organic electrolytes, we show the use of ALD Li₂O at controlled mass loading in high aspect ratio Li-O₂ cathodes to elucidate the Li-O₂ charging chemistry, and we demonstrate the use of the ALD solid electrolytes in passivating Li anodes in Li-S batteries.

[1] D. Ruzmetov, V. P. Oleshko, P. M. Haney, H. J. Lezec, K. Karki, K. H. Baloch, A. K. Agrawal, A. V. Davydov, S. Krylyuk, Y. Liu, J. Huang, M. Tanase, J. Cumings, and A. A. Talin, “Electrolyte Stability Determines Scaling Limits for Solid-State 3D Li Ion Batteries,” *Nano Lett*, vol. 12, no. 1, pp. 505–511, Jan. 2012.

2:40pm **TF+EN+PS-TuA2 Engineering Lithium-Containing Ionic Conductive Thin Films by Atomic Layer Deposition for Lithium-ion Battery Applications, Jea Cho, T. Seegmiller, J. Lau, L. Smith, J. Hur, B. Dunn, J.P. Chang**, University of California at Los Angeles

Lithium (Li)-ion batteries have drawn much attention for their outstanding performance in portable electronics applications. These batteries have the potential to function as miniaturized power sources for microelectromechanical (MEMS) devices through the fabrication of 3-dimensional configurations. To fabricate a fully functional 3D Li-ion

microbattery, however, an ultra-thin and highly conformal electrolyte layer is required to coat the 3D electrodes. The solid oxide Li-ion conductor, lithium aluminosilicate (Li_xAl₃Si₂O, LASO), synthesized by atomic layer deposition (ALD) is a promising electrolyte material for 3D battery applications owing its adequate ionic conductivity as well as improved electrode stability.

The self-limiting characteristic of ALD allows for precise control of thickness and composition of complex oxides and results in a highly conformal and pinhole-free coating even on highly complex structures such as high aspect ratio 3D electrodes. The metal precursors, lithium t-butoxide (LTB), trimethylaluminum (TMA), tris(tert-butoxy)silanol (TTBS), and tetraethylorthosilicate (TEOS) were used to form Li_xAl₃Si₂O via ALD. *In-situ* FTIR was implemented to study the incubation time and growth mechanisms for each oxide deposited on the other to improve the controllability of the films. *In-situ* FTIR studies revealed that the growth mechanism of silicon oxide is strongly affected by the underlying oxide layer, exhibiting different surface reaction mechanisms during the incubation stage.

Li-ion conductivities and the activation energy for conduction of as-deposited LASO/LAO/LSO films were determined for different lithium contents and film thickness. The LASO ALD coating on 3D carbon array posts were confirmed to be conformal and uniform using transmission electron microscopy (TEM) imaging. A Li-ion half-cell consisting of LASO coated on 3D carbon array electrode showed reversible electrochemical behavior. Lithiation cycling tests of thin LASO/LAO/LSO films were found to be functions of both composition and thickness. The reversibility and kinetics of insertion as well as the effect on the cycling stability from the direct deposition of LASO/LAO/LSO on potential anode materials, SiNWs were also investigated using *in-situ* TEM observations during lithiation.

3:00pm **TF+EN+PS-TuA3 Applications of ALD for Li ion Batteries and Low Temperature Fuel Cells, Xueliang (Andy) Sun**, University of Western Ontario **INVITED**

Atomic layer deposition (ALD) is a novel and unique coating technique with many applications in energy storage and conversion [1]. In this talk, I will present our recent work on exploring the applications of atomic layer deposition (ALD) in both fuel cells and Li ion batteries [2-7].

In the first part, we will report on use of ALD for Pt catalysts used in low temperature fuel cells. In particular, atomic Pt or clusters prepared by ALD show ten times higher methanol oxidation properties compared with ETK commercially-used catalysts [2].

In the second part, we will focus on employing ALD as a surface-modification method to enhance the performance of LIBs. Different materials for surface-modification (such as Al₂O₃, ZrO₂, TiO₂ and AlPO₄) [3,4] were first developed by ALD. Then systemic studies were carried out by using those materials to modify the anode (Li₄Ti₅O₁₂, SnO₂) [5] and the cathode (commercial LiCoO₂, NMC) [6]. The effects of different coating materials on the LIB performance of the anode and cathode were investigated in details. In addition, the potential application of ALD as a powerful technique for preparing solid-state electrolyte will be demonstrated [7]. We will discuss further development of ALD for fuel cells and Li ion batteries.

Reference:

- [1] X. Meng, X.-Q. Yang, X. Sun. *Adv. Mater.* 2012, 24, 3589-3615.
- [2] S. Sun, G. Zhang, N. Gauquelin, N. Chen, J. Zhou, S. Yang, W. Chen, X. Meng, D. Geng, M. Banis, R. Li, S. Ye, S. Knights, G. Botton, T.-K. Sham, X. Sun, *Scientific Reports* 3 (2013) 1775.
- [3] J. Liu, X. Meng, Y. Hu, D. Geng, M.N. Banis, M. Cai, R. Li, X. Sun. *Carbon* 2013, 52, 74-82.
- [4] J. Liu, Y. Tang, B. Xiao, T.K. Sham, R. Li, X. Sun. *RSC Adv.* 2013, 3, 4492-4495.
- [5] X. Li, X. Meng, J. Liu, D. Geng, Y. Zhang, M. Banis, Y. Li, R. Li, X. Sun, M. Cai, M. Verbrugge, *Adv. Funct. Mater.* 22 (2012) 1647-1654.
- [6] X. Li, J. Liu, M. Banis, A. Lushington, R. Li, M. Cai, X. Sun, *Energy Environ. Sci.* 7 (2) (2014) 768-778
- [7] J. Liu, M. Banis, X. Li, A. Lushington, M. Cai, R. Li, T.-K. Sham, X. Sun, *J. Phys. Chem. C* 117(2013) 20260-20267

* TFD James Harper Award Finalist

4:20pm **TF+EN+PS-TuA7 ALD for a High Performance “All-in-One” Nanopore Battery**, Chanyuan Liu, X. Chen, E. Gillette, A.J. Pearse, A.C. Kozen, M.A. Schroeder, K. Gregorczyk, S.B. Lee, G.W. Rubloff, University of Maryland, College Park

A self-aligned nanostructured battery fully confined within a single nanopore presents a powerful platform to determine the performance and cyclability limits of nanostructured storage devices. We have created and evaluated such structures, comprised of nanotubular electrodes and electrolyte confined within anodic aluminium oxide (AAO) nanopores as “all-in-one” nanopore batteries. The nanoelectrodes include metal (Ru or Pt) nanotube current collectors with crystalline V_2O_5 storage material on top of them, penetrating part way into the AAO nanopores to form a symmetric full storage cell, with anode and cathode separated by an electrolyte region.

The unprecedented thickness and conformality control of atomic layer deposition (ALD) and the highly self-aligned nanoporous structure of anodic aluminum oxide (AAO) are essential to enable fabrication of precision, self-aligned, regular nanopore batteries, which display exceptional power-energy performance and cyclability when tested as massively parallel devices (~ 2 billion/cm²), each with $\sim 1 \mu\text{m}^3$ volume (~ 1 fL).

To realize these “all-in-one” nanopore batteries, we focused on the precise control of Ru and Pt thin film conformality inside very high aspect ratio (300:1) AAO nanopores by thermal ALD process. 7.5nm thick Ru and Pt are optimized to be 15 μm deep at both sides of 50 μm long AAO pores in order to provide fast electron transport to overlying V_2O_5 at both anode and cathode sides, while keeping them spatially and electrically isolated. Active storage layers of 23nm thick crystalline V_2O_5 were deposited inside the metal nanotubes to form core-shell nanotubular structures at low temperature (170°C) using O_3 as the oxidant, with $\langle 001 \rangle$ direction perpendicular to tube surface and RMS roughness ~ 4 nm. Then the V_2O_5 was prelithiated at one end to serve as anode while pristine V_2O_5 without Li at the other end served as cathode, enabling the battery to be cycled between 0.2V and 1.8V and to achieve full theoretical Faradaic capacity of the V_2O_5 . Capacity retention of this full cell at high power (relative to 1C rates) is 95% at 5C and 46% at 150C rates (i.e., 24 sec charge/discharge time). At 5C rate (12 min charge-discharge cycle), 81.3% capacity remains after 1000 cycles. These performance metrics are exceptional, exceeding those of most prototypes reported in the literature. These results demonstrate the promise of ultrasmall, self-aligned/regular, densely packed nanobattery structures as a building block for high performance energy storage systems.

4:40pm **TF+EN+PS-TuA8 Pseudocapacitive Manganese Oxide Grown by Atomic Layer Deposition**, Matthias Young, C.D. Hare, A.S. Cavanagh, C.B. Musgrave, S.M. George, University of Colorado, Boulder

Pseudocapacitive supercapacitors are a class of energy storage materials that are midway between lithium ion batteries and capacitors in terms of both power and energy densities. Manganese oxide is a well-known pseudocapacitive material with particular appeal due to its earth abundance and low cost. In previous work, we have demonstrated that MnO ALD produced using bis(ethylcyclopentadienyl)manganese ($\text{Mn}(\text{CpEt})_2$) and water can be electrochemically oxidized to produce pseudocapacitive MnO_2 in aqueous electrolytes. However, recent results have shown that the electrochemical oxidation of MnO ALD films results in partial dissolution and delamination. To avoid these problems, we have worked to grow pseudocapacitive MnO_2 by ALD that requires no post-processing. We have grown manganese oxide ALD films using ozone as the coreactant with $\text{Mn}(\text{CpEt})_2$. We have also used intermediate ozone doses during $\text{Mn}(\text{CpEt})_2$ and water exposures during ALD growth. The use of ozone results in more oxidized manganese oxide films. Another issue is that the alpha- MnO_2 crystal structure of MnO_2 which exhibits high pseudocapacitance contains open channels that are only stable in the presence of cations such as Na^+ or K^+ . Consequently, directing the ALD growth toward alpha- MnO_2 pseudocapacitive crystal structures requires the incorporation of an alkali metal into the MnO_2 ALD films.

5:00pm **TF+EN+PS-TuA9 Excellent Chemical Passivation of p^+ and n^+ Surfaces of Silicon Solar Cells by Atomic Layer Deposition of Al_2O_3 and $\text{SiO}_2/\text{Al}_2\text{O}_3$ Stacks**, Bas van de Loo, H.C.M. Knoops, Eindhoven University of Technology, Netherlands, G. Dingemans, ASM, Netherlands, I.G. Romijn, ECN Solar Energy, Netherlands, W.M.M. Kessels, Eindhoven University of Technology, Netherlands

Thin films of Al_2O_3 provide excellent passivation of heavily p -doped (p^+) silicon surfaces and are therefore often applied in silicon solar cells to reach high efficiencies. The high level of passivation by Al_2O_3 can be attributed to its low interface defect density and high negative fixed charge density Q_f . However, the negative fixed charge density of Al_2O_3 can be detrimental for the passivation of n^+ surfaces [1]. Furthermore, in advanced cell architectures such as interdigitated back-contact (IBC) solar cells, both n^+ and p^+ surfaces are adjacent and are preferably passivated simultaneously. To this end, we systematically study the surface passivation by $\text{SiO}_2/\text{Al}_2\text{O}_3$

stacks prepared by atomic layer deposition (ALD), which exhibit excellent chemical passivation while the effective fixed charge density can be tuned to zero by carefully tuning the SiO_2 thickness.

Al_2O_3 and $\text{SiO}_2/\text{Al}_2\text{O}_3$ film stacks with varying ALD SiO_2 thickness (0-12 nm) were prepared by plasma-enhanced ALD at 200°C, with $\text{H}_2\text{Si}(\text{N}(\text{C}_2\text{H}_5)_2)_2$ and $\text{Al}(\text{CH}_3)_3$ as metal-organic precursors and O_2 plasma as oxidant. Moreover, a SiO_2 ALD process using ozone was developed as this oxidant is more suitable for batch ALD. The relevant process parameters for surface passivation, such as ozone exposure time, were identified. The passivation of n^+ and p^+ doped surfaces was studied in detail, and results were compared with industrial passivation schemes, including PE-CVD SiN_x and similar $\text{SiO}_2/\text{Al}_2\text{O}_3$ stacks from a high-volume manufacturing ALD batch reactor.

A superior level of passivation of n^+ surfaces ($R_{\text{sheet}} = 100 \Omega/\text{sq}$) was obtained by $\text{SiO}_2/\text{Al}_2\text{O}_3$ stacks as compared to single layer Al_2O_3 , significantly reducing the recombination current density (J_0) from (81 ± 10) to $(50 \pm 3) \text{ fA}/\text{cm}^2$. On p^+ surfaces ($R_{\text{sheet}} = 60 \text{ Ohm}/\text{sq}$), J_0 increases with increasing SiO_2 thickness. The results can be explained by an excellent level of chemical passivation, combined with a strongly reduced negative fixed charge density when increasing the SiO_2 thickness. To fully exploit the virtues of ALD, the concept of using $\text{SiO}_2/\text{Al}_2\text{O}_3$ stacks for the passivation of both the n^+ and p^+ doped surfaces in a single deposition run was demonstrated on (completed) n -type bifacial solar cells, reaching conversion efficiencies $>19\%$. The results are promising for IBC solar cells, where n^+ and p^+ surfaces are adjacent and care must be to achieve a low surface recombination, high shunt resistance and industrial feasibility.

[1] B. Hoex *et al.*, *Phys. status solidi - Rapid Res. Lett.*, vol. 6, no. 1, pp. 4–6, (2012).

5:20pm **TF+EN+PS-TuA10 Opportunities for Transparent Conductive Oxides Prepared by ALD for Silicon Heterojunction Solar Cells**, Bart Macco, S. Smit, Y. Wu, D. Vanhemel, W.M.M. Kessels, Eindhoven University of Technology, Netherlands

In silicon heterojunction (SHJ) solar cells, transparent conductive oxides (TCOs) serve as the top window layer which provides lateral charge transport to the metal contacts whilst maintaining a high optical transparency. Commonly-employed TCO materials include Sn-doped indium oxide ($\text{In}_2\text{O}_3:\text{Sn}$), Al-doped zinc oxide ($\text{ZnO}:\text{Al}$) and more recently also H-doped indium oxide ($\text{In}_2\text{O}_3:\text{H}$)¹, which are typically deposited by sputtering. In this work, atomic layer deposition (ALD) is explored as an alternative deposition technique for the abovementioned materials. Three salient features of the ALD process will be addressed. Firstly, the applicability of these ALD TCOs is evaluated in terms of their optoelectronic performance. It is shown that through controlled ALD doping cycles the carrier density can be accurately tuned and a low resistivity ($<0.5 \text{ m}\Omega\text{cm}$) required for SHJ solar cells can be obtained. Secondly, it is shown that a thermal ALD process does not induce damage to the underlying a-Si:H passivation layers found in a SHJ solar cell. This is a distinct advantage over the conventional sputtering technique, in which plasma-related (UV, ions) damage is known to reduce the passivation level of the a-Si:H layers.² This perk of ALD is put to use in bilayers of ALD $\text{ZnO}:\text{Al}$ /sputtered $\text{In}_2\text{O}_3:\text{Sn}$, where a thin ALD TCO layer ($<15 \text{ nm}$) can be very effectively protect the a-Si:H layers from sputter damage. TEM and *in-situ* spectroscopic ellipsometry measurements show that the protective properties are strongly correlated with the TCO surface coverage, as the initial ALD TCO growth on the a-Si:H layer suffers from a nucleation delay and associated island-like growth.³ Finally, the accurate control over the doping (profile) of the TCO offered by ALD opens up ways to optimize the band alignment of a SHJ solar cell. At the interface of the TCO and the p -type a-Si:H, a high doping of the TCO is unfavorable for the band alignment and results in a reduced fill-factor.³ On the other hand, the conductivity requirement of the TCO sets a lower bound to the doping level. In this respect, graded doping of the TCO by ALD allows for effective decoupling of the conductivity requirements of the TCO with the optimization of the interface contact formation.

¹ Barraud *et al.*, *Solar Energy Materials and Solar Cells*, **115**, 151–156 (2013)

² Demareux *et al.*, *Applied Physics Letters*, **101**, 171604 (2012)

³ Macco *et al.*, *Applied Physics Letters* (submitted)

5:40pm **TF+EN+PS-TuA11 Study of the Surface Passivation Mechanism of c -Si by Al_2O_3 using *In Situ* infrared spectroscopy**, R.P. Chaukulkar, Colorado School of Mines, W. Nemeth, A. Dameron, P. Stradins, National Renewable Energy Laboratory, Sumit Agarwal, Colorado School of Mines

The quality of Si surface passivation plays an integral role in the performance of c -Si-based solar cells. Recently, Al_2O_3 films grown by atomic layer deposition (ALD) have been shown to be an effective

passivant for *c*-Si surfaces with surface recombination velocities (S_{eff}) that are <5 cm/s. The chemical passivation of the *c*-Si surface via Al₂O₃ is achieved by a reduction in the defect density at the interface, while field-effect passivation is attributed to the fixed negative charge associated with the Al₂O₃ films. However, a post-deposition annealing step is required to achieve this high level of passivation. We have investigated the mechanism of chemical passivation during the annealing step using *in situ* attenuated total reflection Fourier transform infrared (ATR-FTIR) spectroscopy. Specifically, we have studied the role of residual H- and O-atom migration from the ALD Al₂O₃ films to the *c*-Si/Al₂O₃ interface. Using Al(CH₃)₃ and O₃ as the ALD precursors, Al₂O₃ films were deposited directly onto high-lifetime float-zone *c*-Si internal reflection crystals (IRCs) followed by thermal annealing at 400 °C in different atmospheres. Specifically, we have used D-terminated *c*-Si IRCs to differentiate the residual H atoms that may migrate from ALD Al₂O₃ films versus the residual D atoms present at the Al₂O₃/*c*-Si interface after ALD. Within the sensitivity of the ATR-FTIR spectroscopy setup of $\sim 10^{12}$ cm⁻² for Si-H bonds, we do not detect any migration of H from Al₂O₃ to the *c*-Si interface. Therefore, we conclude that the migration of O, and the subsequent restructuring of the interface during the annealing step, primarily contributes towards the chemical passivation of the Al₂O₃/*c*-Si interface. The ATR-FTIR spectroscopy measurements are complemented by the minority carrier lifetime, interface defect density, and built-in charge density measurements on SiO₂/Al₂O₃ stacks on *c*-Si, which enable us to isolate chemical passivation from field-effect passivation. The stacks were annealed in different atmospheres to better understand the role of O versus H atoms in the chemical passivation mechanism.

We gratefully acknowledge the support from the NCPV Fellowship Program and U.S. Department of Energy, Office of Energy Efficiency and Renewable Energy, under Contract No. DE-AC36-08-GO28308 with the National Renewable Energy Laboratory.

6:00pm TF+EN+PS-TuA12 Low Temperature Plasma-assisted Atomic Layer Deposition of TiO₂ Blocking Layers for Flexible Hybrid Mesoscopic Solar Cells, V. Zardetto, Eindhoven University of Technology, Netherlands, F. di Giacomo, T.M. Brown, A. di Carlo, A. D'Epifanio, S. Licoccia, University of Rome "Tor Vergata", Italy, W.M.M. Kessels, Mariadriana Creatore, Eindhoven University of Technology, Netherlands

Atomic Layer Deposition (ALD) is widely acknowledged in the field of *c*-Si and thin film PV technologies, for the fabrication of ultra-thin, uniform and conformal layers.[1] Thermal ALD has been applied also in the case of more challenging interfaces, e.g. dye-sensitized solar cells (DSCs) and the novel hybrid organo-lead-halide perovskite solar cells. Particularly, TiO₂ blocking layers have been developed on glass/TCO substrates with the aim of decreasing the charge recombination processes at the interface between the ITO and the mediator. Recently, we have explored the benefit of plasma-assisted ALD (PA-ALD) in terms of low temperature processing applied to flexible DSCs for the development of highly transparent Pt counterelectrodes on ITO/PEN. [2] In this work, we further explore PA-ALD for the deposition of ultra-thin, highly compact TiO₂ blocking layers on ITO-polymer substrates for DSCs and perovskite solar cells. The layers were prepared in a remote plasma reactor (FlexAL™) at 150 °C using an heteroleptic alkylamido precursor Ti(Cp^{Me})(NMe₂)₃ alternated with an O₂ plasma. For DSCs with an iodide-based electrolyte, the introduction of the blocking layer is essential at low light intensity, in order to increase the indoor performance of the cell. It is found that the presence of ultra-thin (6 nm) TiO₂ layers slightly affects the performance of the cell under sun simulator, whereas it definitely improves the generated power (+40%) under low level illumination (300 lux). The blocking behaviour of the PA-ALD deposited TiO₂ towards the tri-iodide reduction has been investigated by electrochemical impedance spectroscopy and Tafel plot analysis. We pinpointed that an increase in the TiO₂ layer thickness above 6 nm leads to a decrease of the recombination processes at the TCO/electrolyte interface, as well as to a dramatic reduction of the electron collection at the TCO, accompanied by a decrease in cell performance. For mesostructured perovskite (CH₃NH₃PbI₂Cl- based) solar cells, the application of a TiO₂ blocking layer is essential for the performance of the device, due the higher current exchange at the interface TCO-hole transport material, i.e. Spiro-OMeTAD, typically used in this architecture. The application of a 11 nm-thick TiO₂ layer resulted in an efficiency of 7.4%. In conclusion, ALD is a valid approach for controlling electrochemical charge-transfer processes in mesoscopic solar cells.

[1] J.A. van Delft, D. Garcia-Alonso, W. M. M. Kessels, *Semicond. Sci. Technol.*, 27, 74002 (2012)

[2] D. Garcia-Alonso, V. Zardetto, A.J.M. Mackus, F. De Rossi, M.A. Verheijen, T.M. Brown, W.M.M. Kessels, M. Creatore, *Adv. En. Mater.* 4, 1300831 (2014)

Tuesday Evening Poster Sessions

Energy Frontiers Focus Topic
Room: Hall D - Session EN-TuP

Energy Frontiers Poster Session

EN-TuP2 Mini-band Formation in a Strain-balanced InGaAs/GaAsP MQW Solar Cell Structure Investigated by a Photoreflectance and a Surface Photovoltage Spectroscopy, *Tetsuo Ikari, A. Fukuyama, K. Nishioka, T. Aihara, H. Kuradome*, University of Miyazaki, Japan, *K. Toprasertpong, M. Sugiyama, Y. Nakano*, University of Tokyo, Japan

Embedding of multi quantum well (MQW) structures in an absorption layer of GaAs solar cell is a promising idea for developing higher efficient solar cell devices. Extension of the absorbing region to longer wavelength side enhances the short-circuit current. When the mini-band forms between the QW, further developing of the conversion efficiency would be expected in term of a carrier tunneling without recombination of the photo excited carriers. However, recombination at the QW interface still leads to the degradation of the efficiency. Therefore, we fabricated a strain-balanced InGaAs/GaAsP layer in the intrinsic region of the GaAs *p-i-n* solar cell [1]. The mini-band formation for the samples with different thickness of the barrier region from 5.3 to 1.9 nm was studied by using a photoreflectance (PR) and a surface photovoltage (SPV) spectroscopy at room temperature.

The energies at the Brillouin zone edges were detected from the Kramers-Kronig analysis of the PR spectra for estimating the mini-band width as a function of barrier thickness. When the mini-band formed, the ratio of carriers escaped thermally from each QW may change. SPV spectra were, then, measured to know the carrier escaping rate and how this component affects the absorption spectra of the solar cell structures.

The observed PR spectra for the sample with thinnest barrier width of 1.9 nm show two critical energies at 1.274 and 1.312 eV. The energy difference of these critical energies was around 0.038 eV and this energy difference reduces from 0.020 to 0.009 eV for the samples with barrier thickness of 2.7 and 3.6 nm, respectively. Supposing that such energy difference shows the mini-band width, the reduction of the energy with increasing the thickness of the barrier can be understood. The theoretical estimation using a Kronig-Penny model calculation for the width suggests that the mini-band width in the QW is 70 and 0 meV for e1 and topmost hh1 sub-bands. Therefore, the observed mini-band width is smaller than expected. The reason is not clear at present. For the SPV spectra, two broad peaks were observed at 1.29 and 1.32 eV. The energy difference also decreases with increasing the thickness of the barriers. Smaller critical energies for SPV may be explained that these signals detect the maxima energy of the joint-density of states which is larger than the band edge energies. Since the carrier escaping from the QW and radiative and non-radiative recombination rates may be strongly temperature dependent, estimation of the relevant activation energies for carrier escaping from these measurements were useful for further discussion.

[1] M. Sugiyama, *et al.*, *J. Cryst. Growth* 315 (2011) 1.

EN-TuP5 Cu(In,Ga)Se₂ Absorber Layer Deposited by Radiofrequency Magnetron Sputtering, *Romain Meunier, M.-P. Besland, P.Y. Jouan, A. Lafond*, Université de Nantes, France, *P.Y. Thoulon, M. Ricci*, Crosslux Company, France

In the last decades, the deposition of CIGSe thin films by sputtering has seldom been investigated. Besides, the sputtering of a single quaternary CIGSe target would be a real advantage for industrial development. Indeed, sputtering technique exhibits a good compatibility with industrial up-scaling and limits selenium use with respect to toxicity issues. In 1992, Hernandez *et al.*¹ early published on CIGSe layers deposited by sputtering of a single quaternary CIGSe target.

The improvement of plasma discharges at lower working pressures in the last years had allowed news possibilities for CIGS thin films deposited by sputtering. In 2010, Frantz *et al.*² succeeded to obtain a CIGSe solar cell with an efficiency of 8.9%.

At IMN laboratory, a dedicated chamber has been home-designed for CIGSe thin films deposition using one step sputtering. CIGSe thin films were deposited on SLG/Mo substrates by radio-frequency magnetron sputtering at ambient temperature. The deposition parameters like pressure or power density have been investigated. Then, CIGS thin films have been annealed at various temperatures in a furnace under Ar flow. The evolution of chemical composition and structural properties of CIGS thin films as-deposited and annealed will be presented.

References

1. Hernández Rojas, J. L. *et al.* *Appl. Phys. Lett.* 60, 1875–1877 (1992)

2. Frantz, J. A. *et al.* *Thin Solid Films* 519, 7763–7765 (2010).

EN-TuP6 Developments in Power Efficient Dissociation of CO₂ using Non-Equilibrium Plasma Activation, *Waldo Bongers, A.P.H. Goede, M.F. Graswinckel, S. Welzel*, Dutch Institute for Fundamental Energy Research, The Netherlands, *M. Leins, J. Kopecki, A. Schulz, M. Walker*, Universität Stuttgart, Germany, *M.C.M. van de Sanden*, Dutch Institute for Fundamental Energy Research, The Netherlands

In the framework of an emerging Solar Fuel program the first and essential CO₂ dissociation step of CO₂ into CO and O₂ has been studied. The focus was thereby on high energy efficiency of the process using non-thermal (non-equilibrium) microwave plasmas without the use of rare materials. The plasma was generated by tangentially injecting CO₂ gas in a quartz tube placed inside a low loss 915 MHz TM₀₁₀ circular waveguide mode cavity. Powers were used up to 10 kW. The feed gas expanded supersonically after the cavity to quench the plasma and prevent vibrational-translational relaxation losses. These experiments resulted in power efficient conversion (more than 50%) of large CO₂ flows (up to 75 standard liter per minute) with 11% conversion yield. The product formation was measured downstream the plasma at the expansion in a calibrated mass spectrometer.

The research at the plasma Solar Fuels facilities of DIFFER concentrates on optimization of power efficient selective vibrational CO dissociation. This can be achieved by means of several novel methods: like tuning the optimal kinetic energy range of the electrons by controlling the reduced electric field in the microwave cavity or make use of the relaxation time difference of translational and vibrational modes of CO controlled by modulating the microwave field. First results were obtained with a 2.45 GHz 1kW microwave plasma source. The source consists of a quartz tube with a tangential gas injection system placed inside a circular TEM mode coaxial cavity coupled to a TE₁₀ rectangular waveguide mode cavity. The configuration of the coaxial cavity allows control of the electric field. With an input of 7 standard liter per minute of CO₂ energy efficiencies 15% to 36% were obtained (based on CO₂ depletion) in the pressure range from 1Bar (atmospheric) till 0.2 Bar. An update on these new research developments will be shown.

EN-TuP8 GLAD & SAD-GLAD Nanorod Array Catalyst Electrodes for Polymer Electrolyte Membrane Fuel Cells, *Fatma Yurtsever, M. Begum, M. Yurukcu, M.F. Cansizoglu, A.U. Shaikh*, University of Arkansas at Little Rock, *W.J. Khudhayer*, University of Babylon, Iraq, *N. Kariuki, D.J. Myers*, Argonne National Laboratory, *T. Karabacak*, University of Arkansas at Little Rock

Polymer electrolyte membrane (PEM) fuel cell technology is one of the promising alternative

energy systems for an environmentally friendly, sustainable energy economy. However, PEM

fuel cells require an expensive platinum catalyst which raises the cost of the fuel cell. In this

study we investigated the electrocatalytic oxygen reductive reaction (ORR) activities of Pt and

Pt-Ni alloy catalyst thin film coated on Cr and Ni base nanorod arrays, respectively, and also

ORR of Pt-Ni alloy nanorods. Cr and Ni nanorods were used as low cost, high surface area

metallic supports for the conformal Pt and Pt-Ni alloy thin film, respectively. Nanorods were

grown on glassy carbon electrodes using a magnetron sputtering glancing angle deposition

(GLAD) technique and conformal coating of catalyst thin film on the base nanorods were

achieved using a small angle deposition (SAD) technique. Pt-Ni alloy nanorods were also grown

using GLAD. The electrocatalytic ORR activity of the nanostructured electrodes were

investigated using cyclic voltammetry (CV) and rotating disk electrodes (RDE) in a 0.1M

aqueous perchloric (HClO₄) acid solution. The electrochemical active surface area (ECSA),

surface area specific activity (SA), and mass activity (MA) values were determined and

compared to the Pt and Pt-Ni alloy catalyst results in the literature. The results from GLAD Pt-Ni

alloy nanorods exhibit higher values of ECSA compared to geometric area of the nanorods. The

MA of the Pt-Ni nanorods was found to be a factor of 2.3 to 3.5 higher than that of pure Pt

nanorods of the same dimensions and increasing with increasing Ni contents. However, the SA

enhancement was only observed for the nanorods with the highest Pt contents. In addition, both

the SAD-Pt/GLAD-Cr and GLAD-Pt-Ni alloy nanorods were found to have higher stability

against loss of ECA during potential cycling in the acidic electrolyte. Our preliminary results on

the SAD-Pt-Ni/GLAD-Ni nanorod arrays will also be presented

EN-TuP9 XPS Study of Ternary Chalcogenide Semiconductors Deposited by a Solution-based Method for Solar Cells Applications, Francisco Aguirre-Tostado, R. Garza-Hernandez, CIMAV-Monterrey, Mexico, R. Mayen-Mondragon, UNAM-Punta, Mexico, E. Martinez-Guerra, CIMAV-Monterrey, Mexico

The use of solution-based methods for semiconducting thin film deposition is of great importance for large area photovoltaics applications, enabling as well the deposition on flexible substrates. Chalcogenide semiconductor materials present p- and n-type characteristics that are attractive for photovoltaics applications. The optimization of device structure for a solar cell requires an atomistic understanding of the structure and chemical reactions taking place during deposition and post-deposition processes. In this regard, X-ray photoelectron spectroscopy (XPS) is uniquely suited for tracking chemical reactions occurring at the surface and interface of sub-nanometric layers. The chemical analysis and thermal stability for surface and interface reactions of binary and ternary chalcogenide semiconductors is presented. CuS, ZnS, SnS₂, CdS thin films and some of its combinations were deposited by the successive ionic layer absorption and reaction method (SILAR) under controlled environment next to the XPS analysis load-lock chamber. Step by step XPS analysis of the SILAR process reveals an incubation period that depends on temperature and ion concentrations. The stability of the heterostructures is discussed in terms of chemical reactivity and inter-diffusion.

EN-TuP10 Enhanced Photovoltaic Response of Pb_{0.95}La_{0.05}Zr_{0.54}Ti_{0.46}O₃ Thin Film Based Solar Cells, Vaishali Batra, G. Cabot, S. Kotru, University of Alabama

Ferroelectrics materials have generated considerable interest in the field of ferroelectric photovoltaic (FE-PV) in recent years and are still being researched as potential alternative material for future photovoltaic applications. However, the PV response from these FE-PV devices is still very low. In this work, various approaches were adopted to improve the PV response from the FE-PV devices. The ferroelectric material used for fabricating the capacitor type solar cells was Pb_{0.95}La_{0.05}Zr_{0.54}Ti_{0.46}O₃ (PLZT) in thin film form, prepared using chemical solution deposition method. In one approach, a thin layer of lead titanate (PTO) was introduced as a seed layer to control the (001)/(100) orientation and to suppress the (110) orientation of the PLZT films. Presence of seed layer was seen to show a remarkable effect on the ferroelectric and the photovoltaic properties of the devices. Another approach used was the incorporation of silver nanoparticles (SNPs) in PLZT matrix. The narrow band gap nanoparticles (NP) embedded in PLZT films enhances the optical absorption in Pt/PLZT/Pt by extending the absorption spectra from ultraviolet to a fraction of the visible light spectrum. Results showing the effect of seed layer and incorporation of NP on PLZT devices will be presented.

EN-TuP11 Influence of Orientation and Size in Crystallite on Various Properties in Al-doped ZnO Films for Solar Cell Transparent Electrode Applications, T. Minami, Toshihiro Miyata, T. Yamanaka, Kanazawa Institute of Technology, Japan

We have recently reported that impurity-doped ZnO thin films appropriate for transparent electrode applications in thin-film solar cells were related more to the content rather than the kind of impurity doped into the films as well as to the deposition method used [1]. This paper describes the influence of the orientation and size in crystallite on the resulting optical absorption and the obtainable surface texture structure and carrier mobility in Al-doped ZnO (AZO) thin films prepared with different types of magnetron sputtering deposition (MSD) methods. The AZO thin films were prepared with a thickness of 500-3500 nm on OA-10 glass substrates at a sputter Ar gas pressure of 0.2-12 Pa and a temperature of room temperature (RT)-350°C by d.c. MSD or r.f. power superimposed d.c. MSD. The surface texture formation was carried out as a result of MSD under the appropriate deposition condition or by wet-chemical etching (in a 0.1% HCl solution at 25°C). For example, when the AZO films were prepared with increasing a

sputter gas pressure from 0.4 to 12 Pa at a deposition temperature of 350°C, the films exhibited the red shift with tailing in both the absorption edge and plasma edge as the sputter pressure was increased. With increasing the sputter gas pressure, the deposited films exhibited the increase of etching rate and the decrease of etch pit size obtained from the etching, whereas the pyramid type textured surface was formed at a pressure above approximately 6 Pa. It was also found that both in the c-axis orientation and the crystallite size as well as the carrier mobility in the deposited films were decreased by increasing the sputter gas pressure. It should be noted that the sputter gas pressure dependence described above was strongly dependent on the thickness of deposited films and MSD method used. In addition, the result described above was considerably affected by after heat-treatment with rapid thermal annealing (RTA) in air. Consequently, observed sputter gas pressure dependences such as the expanded tailing of absorption coefficient, etching characteristics and decrease of mobility were mainly correlated to the degradation of crystallinity as evidenced by the c-axis orientation and the crystallite size.

[1] T. Minami, T. Miyata, and J. Nomoto, *Materials Science and Engineering*, **34**, 012001 (2012).

EN-TuP13 Surface Analytical Investigation on Organometal Triiodide Perovskite, Yongli Gao, C.G. Wang, C.C. Wang, University of Rochester, X.L. Liu, Central South University, Changsha, China, J.S. Huang, University of Nebraska Lincoln

In a little over a year, there has been an unexpected breakthrough and rapid evolution of highly efficient solid-state hybrid solar cells based on organometal trihalide perovskite materials. This technology has the potential to produce solar cells with the very highest efficiencies while retaining the very lowest cost. We have measured the electronic density of states of CH₃NH₃PbI₃ using ultraviolet photoelectron spectroscopy (UPS), inverse photoemission spectroscopy (IPES), and x-ray photoelectron spectroscopy (XPS). The valence band maximum (VBM) and conduction band minimum (CBM) positions are obtained from the UPS and IPES spectra, respectively, by linear extrapolation of the leading edges. With the Fermi level close to the VBM, the sample is slightly p-type, with the E_{VBM}=0.76 eV, E_{CBM}=-0.9 eV, and transport energy gap 1.7 eV. The ionization potential (IP) of 6.16 eV can be obtained from the sum of the UPS measured E_{VBM} and the work function of 5.40 eV. The XPS spectra reveal an obvious deficiency of N is, whereas the concentrations of I and Pb are close to the expected values. The existence of O and excessive C indicate that the surface is contaminated, and the contamination is reduced by 12-20% by thermal annealing in vacuum. The interface between CH₃NH₃PbI₃ and TiO₂ is also investigated. As CH₃NH₃PbI₃ layer thickness increases, one sees a gradual shift of the vacuum level cut-off. At the CH₃NH₃PbI₃ thickness of 8.2 nm, the shift saturates, signaling the end of the interface dipole formation. The evolution of the VB is even more gradual, and it appears to mature only at the thickest layer. Given the UPS probing depth of ~1.5 nm and the typical interface formation in other systems, the saturation of the vacuum level cut-off at 8.2 nm in CH₃NH₃PbI₃/TiO₂ is surprisingly large. It points at the possibility that the films are not truly uniform. On the other hand, the interface dipole of 0.7 eV CH₃NH₃PbI₃ and TiO₂ is important for further understanding of the energy level alignment and charge transfer across the interface.

EN-TuP14 Synthesis, Characterization and Hydrogen-Storage Performance of Nanoporous Graphene-based Adsorbents, Claus Rebholz, N. Kostoglou, University of Cyprus, V. Tzitzios, C. Tampaxis, G. Charalambopoulou, T. Steriotis, K. Giannakopoulos, National Center for Scientific Research Demokritos, Y. Li, K. Liao, K. Polychronopoulou, Khalifa University of Science, Technology & Research

In the present work, we synthesized and systematically characterized two novel graphene-based nanomaterials, a reduced graphene oxide sponge and a microwave-exfoliated graphene oxide. Their textural properties were determined by N₂ adsorption/desorption at 77 K, while additional characterization techniques were employed in order to elucidate further their structure, surface chemistry and morphology such as X-Ray Diffraction (XRD), Fourier-Transform Infrared Spectroscopy (FT-IR), Field-Emission Scanning Electron Microscopy (FE-SEM) and High-Resolution Transmission Electron Microscopy (HR-TEM). Both nanomaterials were additionally evaluated for their H₂ storage performance and were critically compared to commercially available carbons (e.g. graphene nanoplatelets, carbon nanotubes) based on systematic H₂ adsorption/desorption measurements at 77K between 0-1 bar. Maximum H₂ gravimetric capacities ~0.5 wt% and ~0.7 wt% were recorded at 77 K and 1 bar for the reduced GO sponge and the microwave-exfoliated GO, respectively. A linear relationship was found between the H₂ uptake values and the BET specific surface area of the materials included in this study.

EN-TuP15 Vacuum Deposition Of Photosystem 1 Films In P-Doped Silicon Surface To Improve The Efficiency Of Bio-Photovoltaic Cells, *CarlosFelipeRezende Facchini, L.T. Manera, P. Mazzafera, R.V. Ribeiro, E. Kiyota*, University of Campinas, Brazil

The high efficiency which some organisms perform photosynthesis and its abundance around the globe, coupled with high world energy demand in the coming years and the low competitiveness of current photovoltaic devices in comparison with other forms of energy, inspired us to build a Bio-photovoltaic device composed of a heavily p-doped silicon substrates and a tandem of protein complex called Photosystem 1 (PS1) found in the thylakoid of leaves.

The process extraction of PS1 complexes from spinach essentially consists of two general steps: the extraction of thylakoid membranes from the spinach leaves and the isolation and purification of PS1 complexes from the thylakoids.

For the deposition of PS1 films onto silicon substrates we use a simple and straightforward method. The procedure entails depositing a volume (100 μ L) of an aqueous PS1 suspension on to a silicon surface modified with 3-aminopropyl-triethoxysilane (APTS) and applying a negative pressure (~70 mTorr) to remove the solvent from the PS1 solution via vacuum deposition process. The thermodynamic driving force for the formation of these films arises from hydrophobic interactions between neighboring protein complexes in the film and by tuning the silicon Fermi energy by doping. This promotes the alignment of silicon bands with redox active sites of PS1, which leads to the formation of dense and resilient films.

Iterative depositions were similarly performed and for two deposition steps, a thickness of ~600nm was achieved, thereby increasing the efficiency of the bio-hybrid cell.

These results represent significant progress toward affordable, biologically-inspired renewable energy conversion platforms.

EN-TuP16 Cross Sectional Mapping of CdTe PV Devices with Scanning Capacitance Microscopy, *Gilad Zorn, B.A. Korevaar, J.R. Cournoyer, K. Dovidenko*, GE Global Research Center

Scanning capacitance microscopy (SCM) is a powerful method for mapping dopant variation in semi-conductor and PV devices. In SCM a conducting AFM tip is used to scan the surface in contact mode. The tip and sample surface form a metal-insulator-semiconductor structure. Simultaneous with the topography data collection, an AC bias is applied to the sample while the tip is grounded. The resulting oscillation of carriers near the tip, leads to a modulated capacitance (dC/dV), which is measured by a capacitance-sensing circuit. The capacitance measured by the SCM sensor varies as the carriers move towards (accumulation) and away from (depletion) the probe. When the sample is fully depleted the measured capacitance is that of the oxide plus the depletion layer. When carriers are accumulated at the surface, the measured capacitance is that of the oxide layer. The magnitude of the change in capacitance (dC) for a given change in voltage (dV) depends on the carrier concentration. For heavily doped materials the carriers do not move far. Hence, the measured capacitance variation between accumulation and depletion is small. The opposite is true for lightly doped semiconductors which yield a large capacitance change. The sign of the measured dC/dV signal changes between n-type and p-type. In p-type semiconductors, as the sample voltage becomes more negative relative to the tip, the width of the surface depletion layer will increase. Hence, the total capacitance will decrease. If the sample voltage is positive, accumulation will occur, and the capacitance measured will be that of the oxide layer only. For n-type samples the effects are opposite.

This work describes SCM cross-sectional mapping of CdTe devices, focusing on the role of the various processing steps during the device fabrication. These steps include CdTe deposition, CdCl₂-treatment, and a copper-step. Generally it is accepted within the CdTe community that as deposited CdTe is lightly doped and could be both n-type or p-type depending on the deposition temperature and process. The effect of the CdCl₂ treatment is typically presented as a way to create so-called A-centers, which dope the CdTe p-type. The final copper-step then fills the A-centers and creates Cu on Cd-sites, which further dopes the CdTe p-type to levels in the range of 5x10¹³ to 5x10¹⁴ cm⁻³. Here SCM is used to demonstrate the role of the various processing steps with regards to carrier density. SCM dopant map could clearly distinguish n and p-type CdTe as well as the p-n transition across the interface. It was found that the doping distribution across the CdTe layer depends on the type of the copper treatment.

Energy Frontiers Focus Topic

Room: 315 - Session EN+AS+EM+SE-WeM

Thin Film Photovoltaics

Moderator: Rachel Morrish, Colorado School of Mines

8:20am EN+AS+EM+SE-WeM2 **Epitaxy and Nanochemistry of CdS on Cu(In,Ga)Se₂ for Photovoltaic Devices**, *X. He*, University of Illinois at Urbana Champaign, *H. Tellez, J. Druce*, Kyushu University, Japan, *K. Demirkan, Miasole, P. Ercius*, Lawrence Berkeley National Laboratory, *V. Lordi*, Lawrence Livermore National Laboratory, *J. Kilner*, Imperial College London, UK, *T. Ishihara*, Kyushu University, Japan, *Angus Rockett*, University of Illinois at Urbana Champaign

Cu(In,Ga)Se₂ (CIGS) photovoltaics are very promising candidates for high-performance energy generation from sunlight. They typically include a heterojunction between CdS and CIGS. The nature of that heterojunction is critical to the performance of the devices. We present experimental results on the nanochemistry of CIGS and CIGS/CdS heterojunctions and the nanostructure of the junctions. In particular we present low energy ion scattering (LEIS) results on epitaxial single crystal CIGS and CIGS/CdS heterojunctions formed by chemical bath deposition of CdS. Also shown are results of high-resolution transmission electron microscopy (TEM) studies of the CIGS/CdS heterojunction where the junction is formed by physical vapor deposition. LEIS has single-atomic-layer chemical sensitivity that provides a unique ability to distinguish the nanochemical nature of CIGS surfaces and heterojunctions. TEM provides both nanostructural information and the possibility to determine the chemistry of the junction on the nanoscale by energy dispersive spectroscopy and energy filtered imaging. Complete epitaxy of the CdS throughout its ~50 nm thickness is observed in the physical-vapor-deposited CdS. Domains of cubic zincblende and hexagonal wurtzite structure CdS have been observed. Twins in the CIGS grains were found to propagate into and often through the CdS layer, resulting in a twin or grain boundary in the CdS. The CdS epitaxial relationship and the effect of surface steps on the CIGS surface are shown. The nanochemical analysis results show significant penetration of Cu into the CdS layer, although no alteration in the CdS nanostructure is observed. The other elements show an abrupt nanochemical junction. LEIS results show the presence of segregated layers on the CIGS surface and further refine the nature of the nanochemical intermixing across the interface.

8:40am EN+AS+EM+SE-WeM3 **Microstructure Development in Cu₂ZnSn(S_xSe_{1-x})₄ Thin Films During Annealing of Colloidal Nanocrystal Coatings**, *B.D. Chernomordik, M. Ketkar, K. Hunter, A.E. Béland, Eray Aydil*, University of Minnesota

A potentially high-throughput and inexpensive method for making Cu₂ZnSn(S_xSe_{1-x})₄ (CZTSSe) thin film absorber layers for solar cells is annealing of coatings cast from colloidal dispersions of CZTS nanocrystals (NCs). The nanocrystal coatings can be annealed in sulfur or selenium atmosphere to make CZTS or CZTSSe, respectively. During annealing, the nanocrystal films can transform into polycrystalline thin films with micrometer size grains. Understanding the roles of key annealing parameters in the development of microstructure in CZTSSe thin films is critical for achieving inexpensive and high-efficiency CZTSSe solar cells. In this presentation, we will discuss the effects of parameters such as selenium vapor pressure, annealing temperature, substrate, and heating ramp-rate on the microstructure development in CZTSSe films and contrast the results with films annealed in sulfur. By using a closed system, rather than a flow furnace, we can quantify and systematically control selenium pressure. Annealing films at high selenium pressure (450 Torr) leads to the formation of a layer of 2-5 μm size CZTSSe grains on top of a nanocrystalline layer that is rich in carbon. This segregation of carbon at the CZTSSe-substrate interface is commonly ascribed to the immediate formation of a capping/blocking layer of CZTSSe grains, which trap the carbon, originating from the ligands on NC surfaces, beneath these grains. However, we found that a continuous layer of CZTSSe grains is not necessary to observe carbon segregation to the film-substrate interface. In contrast, films annealed with sulfur do not show such distinct carbon-rich layers and most of the carbon volatilizes from the film during annealing. Increasing the heating ramp-rate to the annealing temperature eliminates the formation of the carbon-rich layer and results in grains that are approximately 500 nm. We will discuss the results of a series of experiments which led us to conclude that Se condensation during annealing may play a key role in grain growth and carbon segregation.

9:00am EN+AS+EM+SE-WeM4 **Effect of Chemical Wet Cleaning on Surface Composition and Work Function of Thin Film CZTS,Se**, *Kasra Sardashti*, University of California at San Diego, *E.A. Chagarov, T. Kaufman-Osborn*, University of California, San Diego, *S.W. Park*, University of California San Diego, *R. Haight, W. Wang, D.B. Mitzi*, IBM T.J. Watson Research Center, *A.C. Kummel*, University of California at San Diego

Polycrystalline Copper-tin-zinc-sulfide/selenide (CZTS,Se) compounds have received wide research interest due to their potential as inexpensive absorber materials composed earth-abundant elements. Photovoltaic devices fabricated on CZTS,Se has reached the highest (or record) conversion efficiency of the 12.6 %. One of the key parameters to further boost the conversion efficiency is to control the concentration of recombination sites at the surface, in the grain boundaries, and in the bulk. Surface states formed on the sample surface as a result of carbon and oxygen contamination can act as non-radiative recombination sites which limit the ultimate cell efficiency. Therefore, a surface-cleaning method which can effectively reduce the amount of surface oxygen and carbon is necessary for CZTS,Se processing. In this work, 2 μm thick CZTS,Se films were prepared by spin coating hydrazine-based precursor solutions onto Mo-coated soda lime glass substrates in a nitrogen-filled glove box. To clean the CZTS,Se surfaces, three different wet cleaning recipes were used: a) NH₄OH only; b) HCl followed by NH₄OH; 3) H₂O₂ followed by NH₄OH. The effect of the wet cleaning on the surface composition including carbon and oxygen content has been studied via X-ray photoelectron spectroscopy (XPS) and femtosecond ultraviolet photoelectron spectroscopy (fs-UPS). Spatial variation of work function over the surface upon surface cleaning was measured via Kelvin Probe Force Microscopy (KPFM). The stability of the clean surface against reoxidation in ambient was modeled by density functional theory (DFT). The H₂O₂/NH₄OH recipe showed the best result reducing the amount of surface O and C down to 5% and 20%, respectively. This is due to the oxidizing effect of H₂O₂ which converted the carbonaceous surfaces contaminants into oxides which were later removed by NH₄OH. DFT calculations are consistent with a group VI surface being stable against oxidation by ambient moisture. KPFM measurements showed strongly non-homogeneous surfaces after both NH₄OH-only and H₂O₂/NH₄OH clean. Areas with work function different from CZTS could be the binary chalcogenides formed during the growth and were covered by the native oxide. NH₄OH etch successfully removed the covering oxide and made those phases visible to KPFM.

9:20am EN+AS+EM+SE-WeM5 **Phase Transformation, Surface States, and Electronic Structures of Pyrite Thin Films Under *In Situ* Heating and Oxygen Gas Exposure**, *Yu Liu, N. Berry, Y.N. Zhang*, University of California Irvine, *C.-C. Chen*, Argonne National Laboratory, *H. Bluhm, Z. Liu*, Lawrence Berkeley National Laboratory, *R.Q. Wu, M. Law, J.C. Hemminger*, University of California Irvine

Iron pyrite (cubic FeS₂) with its exceptional optical absorption and suitable band gap is a promising earth-abundant semiconductor for thin film solar cells. Using ambient pressure synchrotron x-ray spectroscopies, we report the nanoscale depth profiles of surface and electronic structures for phase-pure pyrite thin films under *in situ* heating and oxygen gas exposure. Polarized x-ray absorption spectra show that the absorption edge of Fe L₂-edge shifts closer to the Fermi surface with increasing temperature. The XAS line shapes of Fe and S L-edge provide the information of ligand crystal field environment and the phases of the FeS₂ particles. We also report the non-destructive photoemission depth distributions of sulfur defects, vacancies, impurities and oxide as a function of temperature and oxygen dose. Valence band spectra indicate a band gap narrowing related to the creation of surface states at elevated temperature. An irreversible phase transition from pyrite (FeS₂) to pyrrhotites (Fe_{1-x}S) occurs above 430 °C. In addition, our results under *in situ* oxygen gas exposure suggest that the surface monosulfide species is oxidized first, and the reduction in the total density of states near the Fermi surface is caused by oxide layers of sulfate like and iron oxide products on the top ~2 nm.

9:40am EN+AS+EM+SE-WeM6 **Improvement of SnS-based Photovoltaic Devices via Reverse Engineering of the V_{oc} and Study of Optimal n-Type Material**, *Rona Banai, N.J. Tanen, J.J. Cordell, J.R. Nasr, R.E. Urena, H. Lee, J.R.S. Brownson, M.W. Horn*, Penn State University

Tin (II) Monosulfide (SnS) has theoretical promise as a new material for thin film photovoltaics (PV). Despite a full decade of rigorous research to develop SnS-based devices, improvement beyond single-digit percent efficiencies seems unattainable. Engineering this material into a usable device is crucial for future development. Our group has been investigating

the optical and structural properties of magnetron sputtered SnS_x thin films [1,2,3]. This work will investigate the properties that govern open-circuit voltage, including band gap, series resistance, carrier concentration and built-in potential. Some of these parameters are directly related to the junction material paired with SnS. Several partner materials will be presented with p-SnS including, but not limited to highly doped n-ZnO and n-SnS. Current work is underway to produce n-type SnS as well which would have potential to produce a homojunction.

The optoelectronic properties of SnS make it a suitable material for PV. Its high absorption coefficient, greater than 10⁴ cm⁻¹, and band gap near 1.3 eV are well matched with the solar spectrum. SnS also has a carrier concentration greater than 10¹⁵ cm⁻³ and potential to be both n-type and p-type. Our group is able to produce dense SnS thin films with optimal electronic properties. Sputtering the material gives great control over the material properties and recent work optimizing post-deposition heat treatment has shown great promise for improving the material.

Tin sulfide thin films were sputtered on glass and oxidized silicon substrates at varying substrate-to-target distances, substrate temperature, target power, and chamber pressure. The sputter target was a 3" SnS₂ with 99.999% purity (LTS Research Laboratories, Inc.). These sulfur-rich samples were then annealed under medium vacuum (<2x10⁻⁶ Torr) in the deposition chamber at 400°C to produce a uniform α-SnS, which is most likely to be p-type. Producing n-type SnS is possible via annealing of the films in a methanol/SnCl₄ solution. Production of homojunction SnS-based thin film devices is not found in the literature. Our work aims to produce these devices for the first time and compare them to a well-known partner material such as ZnO.

- [1] R. E. Banai, et al., in *Proceedings of 2012 38th IEEE Photovoltaics Specialists Conference*, Austin, 2012, pp. 164-169.
- [2] R. E. Banai, et al., *IEEE Journal of Photovoltaics*, vol. 3, no. 3, pp. 1084-1089, 2013.
- [3] R. E. Banai, et al., in *Proceedings of 2013 39th IEEE Photovoltaic Specialists Conference*, Tampa, 2013, pp. 2562-2566.

11:00am **EN+AS+EM+SE-WeM10 Advanced Contacts for High Efficiency CdTe Solar Cells**, *D. Meysing, J.J. Li, J. Beach, T.R. Ohno*, Colorado School of Mines, *M.O. Reese, T.M. Barnes*, National Renewable Energy Laboratory, *Colin Wolden*, Colorado School of Mines

Record CdTe device efficiency has recently surpassed 20%, and it is the leading thin film photovoltaic technology in terms of commercial installation with current manufacturing capacity exceeding 1 GW/year. However, with a Shockley-Queisser limit of ~33% there remains substantial room for additional improvements in efficiency. The quality of both the front and back contacts has substantial influence on CdTe solar cells device efficiency, impacting the current and voltage respectively. This talk will focus on recent work directed at understanding the materials science of both the front and back contact interfaces and optimizing their performance.

Cadmium sulfide is the most commonly employed window layer in the front contact, and its properties can greatly affect cell performance through optical absorption and the quality of the CdS-CdTe junction. In this work, we develop reactive sputtering as an alternative to chemical bath deposition (CBD) for the production of oxygenated cadmium sulfide (CdS:O) to enable high efficiency CdTe solar cells. The intrinsic properties of CdS:O as well as their impact on device performance were studied by varying the oxygen content in the Ar sputtering ambient over the range of 0–10%. XRD, RBS, XPS, and spectrophotometry were used to measure the crystal structure, composition, bonding, and optical properties, respectively. The variation in properties is unsurprisingly non-linear, and optimal performance is attributed to a compromise between optical transmission, which improve monotonically with oxygen content, and band alignment which sharply attenuates device performance beyond a critical threshold.

It is notoriously difficult to make a good ohmic contact to CdTe using conventional metals, because this requires a work function of greater than 5.7 eV. Copper-doped zinc telluride (ZnTe:Cu) is one of the most commonly employed buffer layers to mitigate this issue. ZnTe was identified due to its valence band alignment and compatibility with CdTe. Copper has both positive and deleterious effects and it is critical to precisely control both its amount and spatial distribution in order to obtain high efficiency. We have developed a back contacting procedure that employs rapid thermal processing (RTP) to deliver precise control over the activation and distribution of Cu. The RTP process is coupled with atom probe tomography and advanced optoelectronic characterization to improve our understanding of the structure-property-performance relationships in this system. The advances achieved here using commercially scalable processes are combined to produce devices with V_{oc} > 850 mV and efficiencies exceeding 16%.

11:20am **EN+AS+EM+SE-WeM11 Structural Variations and their Effects on the Fundamental Bandgap of ZnSnN₂**, *Nathaniel Feldberg*, University at Buffalo-SUNY, *Y. Yang*, University of Michigan, *W.M. Linhart, T.D. Veal*, University of Liverpool, UK, *P.A. Stampe, R.J. Kennedy*, Florida A&M University, *D.O. Scanlon*, University College London, UK, *L.F.J. Piper*, Binghamton University, *N. Senabulya, R. Clarke*, University of Michigan, *R.J. Reeves*, University of Canterbury, New Zealand, *S. Durbin*, Western Michigan University

In recent years Zn-IV-N₂ compounds have seen increased interest as potential earth abundant element semiconductors for photovoltaic and solid state lighting applications. Several reports of successful growth for the Ge and Si containing compounds are extant as well as more recent publications on the Sn containing member of the family. This material offers a possible alternative to indium containing materials which have experienced large price fluctuations due to limited domestic supply, lack of recycling and heightened demand. Our films were grown by plasma assisted molecular beam epitaxy on (111)-yttria stabilized zirconia. In the case of an ordered lattice, density functional theory (DFT) predicts an orthorhombic structure; however, the disordered lattice is predicted to be pseudo-hexagonal. Reflection high energy electron diffraction patterns for these films indicate single crystal structure with hexagonal symmetry, consistent with X-ray diffraction measurements. Hall effect indicates carrier concentrations in the 3-10x10²¹ cm⁻³ range for which we would expect a significant Burstein-Moss shift. Contrary to expectations, optical measurements of absorption onset occur at higher energy in films with lower carrier concentrations. As in ZnSnP₂, the bandgap is expected to narrow with the introduction of disorder for this material; this narrowing behavior is consistent with observed variations in absorption spectra. Of practical interest is the possibility of a material with a tunable bandgap without the need for traditional alloying. Zn-Sn-N₂ is expected to have a bandgap varying from 1.1 to 2 eV controlled by the continuous degree of order in the cation sublattice. Although hard X-ray diffraction measurements of these films do not show any variation from a hexagonal structure, Hall measurements of carrier concentrations compared with absorption data indicates that our samples vary their absorption onset, not as would be expected from Burstein-Moss Shift, but in a manner consistent with a variation in the lattice order. DFT calculations indicate that there is a variation in the Density of States between the ordered and disordered films. Films which were consistent with increased order absorption are also consistent with an increased order density of states measured by HAXPES.

This project is supported by NSF grant DMR1244887 (Program Director Charles Ying), and EPSRC grant EP/G004447/2.

11:40am **EN+AS+EM+SE-WeM12 Inhomogeneity of p-n Junction and Grain Structure of Thin Film CdTe Solar Cells Studied by Electron Beams**, *Heayoung Yoon, P. Haney*, NIST, *P. Koirala*, University of Toledo, *J.I. Basham, Y. Yoon*, NIST, *R.W. Collins*, University of Toledo, *N.B. Zhitenev*, NIST

Thin film CdTe solar cells are a promising photovoltaic (PV) technology in today's market due to their high optical absorption and inexpensive fabrication processes. However, the current module efficiency is well below the theoretically estimated maximum efficiency (13% vs. 30%). Recent studies have suggested that inhomogeneity of the PV materials is mainly responsible for the low power conversion efficiency. In this work, we investigate the variation of local PV properties of CdTe solar cells, focusing on grain bulk, grain boundaries, and n-CdS / p-CdTe junctions. The window (~120 nm thick CdS) and absorber (~2.2 μm thick CdTe) layers were sputtered on a TCO (transparent conductive oxide) coated glass substrate followed by CdCl₂ treatment. The back contact metals (3 nm Cu / 30 nm Au) were deposited and annealed, creating 256 devices in a 15 cm by 15 cm solar panel. Following light and dark current-voltage measurements, we performed local characterizations using electron beams for high (> 13%) and low efficiency (< 6%) devices within the panel. Electron beam induced current (EBIC) was used to measure the local carrier collection efficiency with a spatial resolution of ~20 nm exciting carriers either from the top surface or the cross-sections of the devices. Cross-sectional EBIC data reveals that the peak of efficiency is in the middle of CdTe layer in the low efficiency devices, while the carrier collection is maximal near the p-n junction in the high efficiency devices. The EBIC contrasts at grains/grain boundaries in these devices are also compared. The measured local electronic properties are correlated to microstructural morphology (Transmission Electron Microscopy), orientation (Electron Back Scattered Diffraction), and chemical composition (Energy Dispersive X-ray spectroscopy). We perform 2D model drift-diffusion simulations to determine the magnitude of downward band-bending near grain boundaries (with typical magnitude of 0.2 eV). We will discuss the impact of carrier generation rate (high level injection vs. low level injection) in EBIC analysis.

12:00pm **EN+AS+EM+SE-WeM13 Micro-Structural Activation Mechanisms in Thin Film CdTe Photovoltaic Devices**, *John Walls, A. Abbas, J.W. Bowers, P.M. Kaminski*, Loughborough University, UK, *K. Barth, W. Sampath*, Colorado State University

Thin Film CdTe photovoltaics is a commercially successful second generation technology now used extensively in solar energy generation at the utility scale. Although the cadmium chloride treatment is a process that is essential to produce high efficiency devices, the precise mechanisms involved in the re-crystallization and associated improvement in electronic properties have not been fully understood. In this paper we report on the application of advanced micro-structural characterization techniques to study the effect of the cadmium chloride treatment on the physical properties of the cadmium telluride solar cell deposited by both close space sublimation (CSS) and magnetron sputtering and relate these observations to device performance. In particular, High Resolution Transmission Electron Microscopy (HRTEM) reveals that the untreated material contains high densities of planar defects which are predominantly stacking faults and that the optimized cadmium chloride treatment removes these completely with only twins remaining. Parallel theoretical studies using Density Functional Theory (DFT) shows that certain types of stacking fault are responsible for the poor performance of the untreated material. Extending the treatment time or increasing the annealing temperature above $\sim 400^\circ\text{C}$ improves the microstructure but results in lower efficiency devices. Composition –depth profiling using XPS and SIMS reveals that this deterioration in performance is linked with chlorine build up at the CdS/CdTe junction. These experiments and parallel theoretical studies have improved our understanding of the mechanisms at work in the cadmium chloride assisted re-crystallization of CdTe and could lead to further increases in device efficiency

Surface Science

Room: 309 - Session SS+AS+EN-WeM

Dynamic Processes of Single Atoms and Molecules at Surfaces

Moderator: Arthur Utz, Tufts University, Andrew Gellman, Carnegie Mellon University

8:00am **SS+AS+EN-WeM1 Construction and Manipulation of Individual Functional Molecules: from Reversible Conductance Transition to Reversible Spin Control**, *Hong-Jun Gao*, Chinese Academy of Science, China **INVITED**

Control over charge and spin states at the single molecule level is crucial not only for a fundamental understanding of charge and spin interactions but also represents a prerequisite for development of molecular electronics and spintronics. While charge manipulation has been demonstrated by gas adsorption and atomic manipulation, the reversible control of a single spin of an atom or a molecule has been challenging. In this talk, I will present a demonstration about a robust and reversible spin control of single magnetic metal-phthalocyanine molecule via attachment and detachment of a hydrogen atom, with manifestation of switching of Kondo resonance. Low-temperature atomically resolved scanning tunneling microscopy was employed. Using density functional theory calculations, the spin control mechanism was revealed, by which the reduction of spin density is driven by charge redistribution within magnetic 3d orbitals rather than a change of the total number of electrons. This process allows spin manipulation at the single molecule level, even within a close-packed molecular array, without concern of molecular spin exchange interaction. This work opens up a new opportunity for quantum information recording and storage at the ultimate molecular limit.

References:

1. L.W. Liu, K. Yang, Y.H. Jiang et al., Scientific Report 3, 1210 (2013).
2. L. Gao et al., Phys. Rev. Lett. 99, 106402 (2007).

*In collaboration with Liwei Liu, Kai Yang, Yuhang Jiang, Boqun Song, Wende Xiao, Linfei Li, Haitao Zhou, Yeliang Wang, and Shixuan Du, Institute of Physics, Chinese Academy of Sciences, Beijing 100190, China

8:40am **SS+AS+EN-WeM3 Single Molecule Origins of Electronic Disorder: Random Conformations of α -NPD Molecules on Au(111)**, *Daniel Dougherty, J. Wang, J. Wang*, North Carolina State University

Disorder is an important aspect of modeling organic and polymeric electronic materials. Proper accounting of the effects of disorder both in active layers and at interfaces with contacts determine the detailed current-voltage characteristics in organic thin film devices [1]. Our study seeks to visualize and statistically quantify the disorder in α -NPD films at the single

molecule scale. This molecule is a common hole transport material in organic LEDs and has been found to exhibit strong disorder in thin film diode geometries [2]. We used scanning tunneling microscopy and spectroscopy to observe numerous surface structures of α -NPD on the (111) surface of Au. These structures are distinguished by different lateral order as well as different local molecular conformations. Random molecular conformations on the surface lead to an statistical distribution of hole transport states that is consistent with the distribution inferred from device analysis. *This work was funded by an NSF CAREER award through DMR-1056861. [1]Tessler et al., Adv. Mater. 21, 2741 (2009) [2] van Mensfoort et al., J. Appl. Phys. 107, 113710 (2010)

9:00am **SS+AS+EN-WeM4 Pt-Cu Single Atom Alloys for the Selective Partial Hydrogenation of Butadiene**, *Felicia Lucci, M. Marcinkowski, E.C.H. Sykes*, Tufts University

Butene is a common feedstock for polymerization reactions; however, butadiene is a minority impurity that poisons the polymerization catalyst. The selective hydrogenation of butadiene to butene serves to increase the purity of the feedstock without reducing the overall concentration of butene. Therefore, catalysts that selectively hydrogenate butadiene to butene and prevent the hydrogenation of butene to butane are of great interest. Using scanning tunneling microscopy (STM) and temperature programmed desorption/reaction (TPD/R), we show that Pt-Cu single atom alloys catalyze hydrogenation of butadiene to butene with 100% selectivity. The addition of small amounts of Pt ($\sim 1\%$) into Cu reduces the barrier for H_2 dissociation, allowing for the low temperature dissociation of H_2 . H atoms spill-over onto the Cu sites increasing the concentration of weakly bound H atoms available for the hydrogenation reaction. The weakly bound H atoms readily hydrogenate butadiene to butene. TPR of co-adsorbed H and butadiene shows the exclusive desorption of reactively formed butene, where the reaction extent is limited by the availability of H on the surface. While the individual, isolated Pt atoms in the Cu terrace activate molecular H_2 , they do not induce the decomposition of butadiene as observed on Pt(111) surfaces. The ability to control geometries of atomic ensembles and hence the extent of hydrogenation reactions using *single atom alloys* allows for the production of new and efficient catalysts.

9:20am **SS+AS+EN-WeM5 Toward a Dynamical Understanding of Chemistry at Metal Surfaces**, *Alec Wodtke*, Max Planck Institute for Biophysical Chemistry **INVITED**

One of our most fundamental scientific challenges is to develop predictive theories of chemistry rigorously grounded in the laws of physics. In 1929, Dirac identified the problem famously in a comment about the importance of quantum mechanics to chemistry... "*The underlying physical laws necessary for the mathematical theory of... the whole of chemistry are thus completely known, and the difficulty is only that the exact application of these laws leads to equations much too complicated to be soluble.*" Despite electrifying advances in computational power, Dirac is still right. The theory of chemistry requires approximate methods for practical computations.

For the theory of surface chemistry, three central approximations are made, involving the use of: 1) classical mechanics for describing nuclear motion, 2) density functionals for calculating electronic states and the Born-Oppenheimer approximation to separate electronic and nuclear degrees of freedom.

The growing importance of computational surface chemistry motivates us to design rigorous experimental tests of these assumptions. Many fundamental questions arise. Can we trust the Born-Oppenheimer approximation for calculating potential energy surfaces for reactions at metal surfaces? Can we characterize and overcome the weaknesses of density functional theory, for example by developing new wave-function based methods for the solid-state? For all of these reasons, it is important to carefully design experimental tests of the capabilities of modern computational surface chemistry.

Using modern molecular beams methods in state-to-state scattering experiments, we obtain a wealth of observational data characterizing the interactions of molecules with metal surfaces. Emphasizing quantitative comparison to first principles theories, we find that energy conversion can occur by unexpected mechanisms, where the electronically adiabatic approximation separating the time scales of electronic and nuclear motion is found to be invalid. The simplicity of the systems under study provides opportunities for developing new theories that go beyond the Born-Oppenheimer approximation. One important outcome of this is the realization that Born-Oppenheimer breakdown can be induced by simple electron transfer events that are common in surface chemistry.

11:00am **SS+AS+EN-WeM10 Steric Effect in O₂ Chemisorption on Al(111)**, *Mitsunori Kurahashi, Y. Yamauchi*, National Institute for Materials Science (NIMS), Japan

O₂ adsorption on Al(111) has been investigated intensively as the most representative system of surface oxidation. The dynamical process happening on the surface, however, remained unclear. An STM study by Brune et al.[1] has proposed that adsorbed O-atoms are atomic and are well separated each other. Initially, this has been ascribed to the transient mobility driven by the O₂ chemisorption energy ("hot-atom" mechanism)[1], but this mechanism has been found to be unlikely. The abstraction mechanism, in which one O-atom is bound to the surface while the other is ejected, has been proposed alternatively based on the resonance enhanced multi-photon ionization measurement.[2] It is however not evident whether or not the abstraction process is the dominant event at low translational energies (E₀). In addition, the STM study by Schmid et al.[3] has suggested that the adsorbates consist of two O-atoms locating at nearby sites. This cannot be explained by the abstraction mechanism.

In this study, we focused attention to the alignment dependence in the O₂ sticking to clarify the reaction mechanism. A single spin-rotational state-selected [(J,M)=(2,2)] O₂ beam, for which we can specify both the molecular alignment and spin direction relative to the magnetic field, was adsorbed on an Al(111) surface. The results show that O₂ molecules parallel to the surface have much higher sticking probabilities than those perpendicular to the surface at E₀ < 0.2 eV. The E₀ dependence of the sticking probability indicates that the dissociation barrier at the perpendicular geometry is about 0.1 eV higher than at the parallel geometry. The present results reveal that the abstraction process, which occurs at the perpendicular geometry, is a minor event at low E₀. [4]

[1] Brune et al., Phys. Rev. Lett., 68, 624 (1992). [2] Komrowski et al., Phys. Rev. Lett., 87, 246103 (2001). [3] Schmid et al., Surf. Sci., 478, L355 (2001). [4] Kurahashi et al., Phys. Rev. Lett., 110, 246102 (2013)

11:20am **SS+AS+EN-WeM11 Surface Temperature Effects in Methane Dissociation on Ni and Ir Surfaces**, *Arthur Utz, E. Peterson, E. Dombrowski, E. High, E. Nicotera*, Tufts University

Recent transition state and quantum dynamics calculations have suggested an important role for surface atom motion in promoting methane dissociation on transition metals including Ni, Pt, and Ir. Here, we describe state-resolved gas-surface scattering measurement of methane dissociation on Ni(111), Ir(111), and Ir(110)-(1x2). Infrared laser excitation prepares methane in a single excited rotational and vibrational state with a precisely defined internal energy. A supersonic molecular beam provides tight control over the translational energy of the methane molecules. The methane molecules, with their well-defined energy, accentuate the role of surface temperature, and the resulting thermal motion of surface atoms, on reactivity.

The presentation will focus on recent experimental results. On the Ir(110)-(1x2) surface, we observe both precursor-mediated and direct reaction channels for the vibrationally excited (v₃, v=1) molecules at surface temperatures of 300K or higher. For v=0 molecules, a precursor-mediated pathway appears for surface temperatures above 500K, but not for temperatures of 500K or lower. The abrupt disappearance of the precursor-mediated reaction path correlates with a surface reconstruction to (331) facets that was previously reported to occur at 500K. We will report on measurements that extend the temperature range for the vibrationally excited (v₃, v=1) molecules to temperatures between 100 and 300K on the Ir(110) surface. We will also report on more recent studies that explore the surface temperature dependence of more highly vibrationally excited methane molecules.

11:40am **SS+AS+EN-WeM12 Activation of C₁-C₉ Alkanes on Pt(111): Importance of Dynamics, van der Waals Interactions, and Gas-Surface Energy Transfer**, *Jason Navin, S.B. Donald, G. Cushing, I.A. Harrison*, University of Virginia

A variety of dissociative sticking coefficients (DSCs) were measured for alkanes varying in size from methane to nonane on Pt(111) using an effusive molecular beam technique. Thermal equilibrium (T_g = T_s) and non-equilibrium (T_g ≠ T_s) DSC measurements provided information about the gas-surface reactivity and energy transfer. Angle-resolved DSCs, S(700 K; 9), measured for methane, ethane, and propane on Pt(111) were used to define thermal DSCs, S(T), and discern dynamical behavior. Methane and ethane DSCs were sharply peaked around the surface normal and were found to have similar dynamical biases away from statistical behavior. Precursor-mediated microcanonical trapping (PMMT) models were used to both analyze and predict DSCs over a wide range of experimental conditions and experiments. It was found that the activation energy for dissociative chemisorption of an alkane scales linearly with its molecular desorption energy from the physisorption well in front of the surface. The molecular desorption energy should be proportional to the van der Waals

stabilization energy for the products of dissociative chemisorption. The gas-surface energy transfer increased as the alkane size increased from C₁ to C₉. For alkanes larger than C₄, the gas-surface energy transfer was apparently sufficient to fully thermalize the impinging molecule to the temperature of the surface before reaction such that, S(T_g=300K, T_s) = S(T).

12:00pm **SS+AS+EN-WeM13 Shining light on an Important Intermediate Step in Photocatalysis: Probing Polarons in ZnO using Infrared Reflection Absorption Spectroscopy**, *Fabian Bebensee, H. Sezen*, Karlsruhe Institute of Technology, Germany, *A. Nefedov, C. Wöll*, Karlsruhe Institute of Technology

ZnO is a wide-bandgap metal oxide exhibiting various highly desirable physico-chemical properties, among them high photocatalytic activity. As such, it has been widely studied employing virtually all available techniques over the past 50 years.^[1] In the context of photoexcitations, primarily excitons have been studied extensively including their very recently reported ultrafast formation dynamics.^[2] In photocatalysis, dissociation of excitons into free electrons and holes takes place and therefore the binding energies of the polaronic states become crucial for the subsequent steps on the way to finally transferring an electron or hole onto an adsorbed molecule. Despite their importance in photochemistry (see recent work on TiO₂^[3]), very little work has been devoted to these trap states in ZnO. Here, we report a novel approach to study polarons in ZnO single crystal substrates: the polaron traps are populated via UV-light irradiation and then probed using infrared reflection absorption spectroscopy (IRRAS). Upon irradiation, a number of previously unobserved, well-defined and sharp absorption bands appear in the IR-spectra. Among these new features is an absorption-edge like feature that we assign to excitations of electrons from the conduction band into hole polaronic trap states. From their time-dependent intensity, we infer a (temperature-dependent) life time of 25 seconds at 75 K. The implications of these findings for ZnO photochemistry will be discussed.

[1] C. Klingshirn, *physica status solidi (b)* **2007**, 244, 3027-3073.

[2] J.-C. Deinert, D. Wegkamp, M. Meyer, C. Richter, M. Wolf, J. Stähler, *Physical Review Letters* **2014**, 113, 057602.

[3] H. Sezen, M. Buchholz, A. Nefedov, C. Natzeck, S. Heissler, C. Di Valentin, C. Wöll, *Sci Rep-Uk* **2014**, 4, 3808.

Wednesday Afternoon, November 12, 2014

Electronic Materials and Processing

Room: 311 - Session EM+EN+TF-WeA

Thin Films and Materials for Energy Storage

Moderator: Christopher Hinkle, University of Texas at Dallas

2:20pm **EM+EN+TF-WeA1 Investigation of Composite Dielectric Materials for Energy Storage, Kimberly Cook-Chennault, U. Sundar, W. Du,** Rutgers, the State University of New Jersey

Electrical energy storage plays a key role in electronics, stationary power systems, hybrid electric vehicles and pulse power applications. Traditionally, bulk ceramic dielectric oxides are used for these applications, though they suffer from inherently low breakdown field strength, which limits the available energy density and increases the dielectric loss. On the other hand, polymers have high break down field strengths, low dielectric losses and can be readily processed into thin films, but suffer from relatively low dielectric permittivity, and thus low energy densities. As a result, contemporary materials have become a limiting factor to the realization of miniaturized devices, due to Moore's Second law, in terms of size, cost and parasitic impedances. Realization of micrometer to sub-micrometer scale commercial and industrial devices such as, high density DRAM (dynamic access memory), non-volatile memory (NRAM) and capacitors, require advanced materials that can both accumulate and deliver vast amounts of energy nearly instantaneously with minimal dielectric losses. This work focuses on examination of piezoelectric-epoxy based composites for dielectric materials, and explores the interrelationship processing plays on realized electrical and dielectric properties. Materials under investigation include lead-zirconate-titanate, and barium titanate – epoxy composites.

2:40pm **EM+EN+TF-WeA2 Preparation and Characterization of ZnO Nano Rods, P. Thamaraiselvan,** Selvam Arts and Science College, India, **M. Saroja, M. Venkatchalam, P. Gowthaman,** Erode Arts and Science College, India, **S. Ravikumar,** Sengunthar Arts and Science College, India, **S. Shankar,** Erode Arts and Science College, India

ZnO nano rods were prepared using chemical bath deposition technique. ZnO seed layer thin films were deposited on glass substrates by dip coating method. Subsequently, ZnO seed-coated glass substrates were immersed in aqueous solution of zinc nitrate and hexamethylenetetramine (HMT) at three different growth time of 3, 4 and 5 hours at low temperature of 90°C. 0.02 mol of Zinc nitrate and 0.2 mol of Hexamethylenetetramine (HMT) on 1:10 molar concentration were used for the growth of Zinc oxide nano rods. The structure and surface morphology of the ZnO nano rod were studied using X-ray diffraction Scanning Electron Microscopy (SEM), respectively.

3:00pm **EM+EN+TF-WeA3 Rational Design of Energy Storage Materials from Earth Abundant Elements, Kyeongjae Cho,** UT Dallas
INVITED

As a part of global scale renewable energy technology solutions, large scale energy storage system (ESS) would be critical in mediating the gaps between cycles of energy demands and intermittent solar and wind energy generations. Furthermore, electric vehicles (EV) require significantly larger energy storage capacity compared to the batteries used electronic device applications. There are significant challenges in extending the current Li ion battery (LIB) technology (based on graphite anode, organic liquid electrolyte, and Co oxide cathode) to EV and ESS applications. Many different approaches are currently investigated to overcome the capacity, safety and cost issues of LIB in EV and ESS applications, and new battery technology researches include Si anode, Na and Mg batteries, metal-air batteries, over-lithiated-oxide (OLO) [1] and silicate cathodes [2] for LIB. OLO and silicate cathode materials provide two times larger charge storage capacity (~300 mAh/g) compare to current commercial LiCoO₂ (LCO) or Li(Ni,Co,Mn)O₂ (NCM) cathodes. Both Li₂MnO₃ and Li₂FeSiO₄ are based on earth abundant transition metals of Mn and Fe so that a successful development of these cathode materials would improve cathode capacity and cost problems. In order to achieve the short term goal of OLO and silicate cathode development and the long term goal of EV and ESS material development, we have applied the rational material design and development framework developed for pollution control technology in which Pt catalysts are replaced by PdAu alloy and Mn-mullite catalysts. [3-5] In this talk, we will discuss the current status of OLO and silicate cathode material research based on the integrated material design-synthesis-characterization framework.

This work was supported by Samsung GRO project.

1. R. C. Longo et al., "Phase stability of Li-Mn-O oxides as cathode materials for Li-ion Batteries: insights from ab initio calculations" (submitted)

2. R. C. Longo, K. Xiong and K. Cho, "Multicomponent Silicate Cathode Materials for Rechargeable Li-ion Batteries: An ab initio study," Journal of the Electrochemical Society 160, A60 (2013).

3. X. Hao et al., "Experimental and Theoretical Study of CO Oxidation on PdAu Catalysts with NO Pulse Effects," Top. Catal. 52, 1946 (2009).

4. B. Shan et al., "First-principles-based embedded atom method for PdAu nanoparticles," Phys. Rev. B 80, 035404 (2009).

5. W. Wang, G. McCool, N. Kapur, G. Yuan, B. Shan, M. Nguyen, U. M. Graham, B. H. Davis, G. Jacobs, K. Cho, X. Hao, "Mixed-Phase Oxide Catalyst Based on Mn-Mullite (Sm, Gd)Mn₂O₅ for NO Oxidation in Diesel Exhaust," Science 337, 832-835 (2012).

4:20pm **EM+EN+TF-WeA7 Transferring Environmentally Sensitive Battery Materials between GloveBox and UHV Surface Analysis Chamber: Composition Study of Model Battery Interfaces and their Controlled Oxidation, Hugo Celio,** University of Texas at Austin

Environmentally sensitive battery materials prepared in an inert environment (e.g., Argon filled glovebox containing trace levels of water and oxygen at ~1 part-per-million) are often difficult to transfer to an ultra-high vacuum (UHV) chamber for surface analysis. While minimizing additional oxidant(s) exposure, three challenging factors arise from transferring environmentally sensitive materials: 1) Engineering a pump-down load-lock to transition from atmospheric pressure to UHV regime, 2) developing a method to generate a set of figures of merit (FOMs) that allows a user to evaluate transfer reliability, and 3) evaluating of the amount of material that subsequently undergoes, due to reaction with trace ppm levels of oxidants in the Argon gas, oxidation during transfer. To target these issues a novel transfer load-lock/capsule was built and directly coupled to a UHV surface analysis chamber, equipped with X-ray photoelectron spectrometer (XPS). This new load-lock/capsule has lead to a new capability to study the composition of model battery materials (e.g., silicon anode and metal oxide cathode) at the solid electrolyte interfacial (SEI) layer, including their controlled oxidation post-transfer.

4:40pm **EM+EN+TF-WeA8 Development of Thin Film Si-C Based High Temperature Supercapacitor Devices, J.P. Alper, C.-H. Chang, C. Carraro, Roya Maboudian,** University of California at Berkeley

On-chip integrated energy storage and delivery at high power is an important aspect in realizing the full potential of microsystems technology such as remote mobile sensor platforms. One promising high power device which has garnered much attention is the supercapacitor. Energy is stored in SC's at the electrode-electrolyte interface, making the high specific surface area of thin films of 1-d materials particularly attractive for application to these devices. However many operations such as in the chemical process industries which could benefit from remote sensor deployment reach temperatures beyond current electrode and electrolyte material constraints. Here we report on the use of bottom-up chemical vapor deposition based silicon carbide (SiC) nanowires and top-down chemically etched SiNWs passivated with an ultrathin carbon sheath as thin film micro-SC electrodes. The electrochemical performance of the two nanowire types in high temperature compatible electrolytes such as ionic liquids and yttria stabilized zirconia (YSZ) are presented. The materials are stable during cycling and achieve specific capacitance values comparable to or better than previously reported carbon electrodes. Operation at temperatures above those attainable with standard electrode-electrolyte systems is also demonstrated. Current challenges for the methods presented and strategies for overcoming them are discussed.

5:00pm **EM+EN+TF-WeA9 Rate Capability of Silicon Carbon Nanotube Anodes for Lithium Ion Batteries, Lawrence Barrett, R. Fan, R.C. Davis, K. Hinton, R.R. Vanfleet,** Brigham Young University

Research has shown stable high capacity lithium ion battery anodes can be made from silicon deposited on carbon nanotubes (CNTs). However, rate capability remains a challenge. We have explored two potential limiting factors: diffusion from the top of the forest down and diffusion into the silicon coating. To probe top down diffusion, we compared a uniform CNT forest to a forest with an array 10 um holes spaced 10 um apart to allow channels for faster top down diffusion and found rate capability was unaffected, indicating top down diffusion is not a limiting factor. We also probed diffusion through the silicon coating by changing the thickness and morphology of the coating.

5:20pm **EM+EN+TF-WeA10 Characterization and Optimization of Interface Engineering on Li Metal Anode Using Atomic Layer Deposition and *In Situ* Electrochemical AFM**, *Chuan-Fu Lin, A.C. Kozen, A.J. Pearce, M. Noked, M.A. Schroeder, S.B. Lee, G.W. Rubloff*, University of Maryland, College Park

Rechargeable Li-metal anode batteries could be considered the holy grail of energy storage systems because Li offers extremely high theoretical specific capacity (3860 mAh/g), low density (0.59 g/cm³), and the lowest negative electrochemical potential (-3.040 V vs. standard hydrogen electrode). However, Li is thermodynamically unstable with organic solvents, inviting serious capacity degradation as well as safety concerns such as Li dendrite growth. The prognosis for Li anodes would be profoundly enhanced for next generation batteries if suitable passivation schemes could be developed to protect Li anodes without significantly reducing ion transport between Li and electrolyte.

In our laboratory, we use atomic layer deposition (ALD) to precisely deposit very thin layer of aluminum oxide (Al₂O₃) on Li foils, using glove box and UHV environments to avoid air exposure while depositing passivation layers on the Li metal surface. We then characterize the surface morphology of the passivated Li by AFM at varying stages of electrochemical reaction and as a function of time and film thickness. We observed the growth of defects on ALD-passivated Li metal surface, decorated by AFM structures indicative of localized electrochemical reactions. The resulting defect density decreased as the film thickness increased.

For thinner ALD protection layers, EC-AFM showed bubble-like structures decorating the steps and boundaries of ALD/Li metal surface in electrochemical system, suggesting mechanisms associated with volatile products. While thin ALD layers suppress charge transfer processes which lead to electrolyte decomposition and formation of solid electrolyte interphase (SEI) [1-2], defects in the ALD passivation layer may cause localized SEI formation, which in turn involves volatile products (e.g., C₂H₄, CO). Alternatively, trace H₂O in the propylene carbonate electrolyte may react with Li metal through pinholes in the ALD layer, leading to LiOH and volatile H₂ products. We are working to differentiate between these by applying in-situ mass spectroscopy to monitor the gas formation in the cell as a function of controlled water content and ALD film thickness. The identification of passivation layer degradation mechanisms and the development of robust approaches to metal anode protection have profound benefit to a variety of beyond-Li-ion batteries.

References:

1. Kevin Leung, *J. Phys. Chem. C*, 2012, 117, 1539-1547.
2. Kevin Leung et al., *JACS*, 2011, 133, 14741-14754.

5:40pm **EM+EN+TF-WeA11 The Road to Next-Generation Energy Storage is Paved with Zinc**, *Joseph Parker, C.N. Chervin*, Naval Research Laboratory, *I.R. Pala*, National Research Council postdoc working at Naval Research Laboratory, *E.S. Nelson*, Pathways Student working at Naval Research Laboratory, *J.W. Long, D.R. Rolison*, Naval Research Laboratory. While Li-ion batteries presently dominate the energy-storage landscape, zinc-based batteries offer a compelling alternative due to the earth-abundance of zinc, innate safety and cost advantages that arise from using aqueous electrolytes, and device-realized specific energy that is comparable to or higher than Li-ion. Yet the performance of present-day Zn-based batteries is hindered by suboptimal Zn utilization (typically <60% of theoretical capacity) and poor rechargeability—a consequence of the complex dissolution/precipitation processes that accompany Zn/Zn²⁺ cycling and the ad hoc construction of conventional powdered-bed Zn anodes. We address these limitations by designing and fabricating highly conductive, porous, and 3D-wired Zn “sponge” electrodes from emulsion-cast, consolidated Zn powders that are thermally treated to produce rugged monolithic forms. With this 3D Zn architecture, we achieve >90% Zn utilization when discharged in primary Zn–air cells with retention of the 3D framework of the Zn sponge and uniform deposition of charge/discharge products at the surfaces of the Zn sponge, as verified by scanning electron microscopy and impedance spectroscopy. We further show that the structural characteristics of the Zn sponge promote greater rechargeability when cycled in prototype Ag–Zn and Ni–Zn cells. Our results demonstrate that all Zn-based chemistries can now be reformulated for next-generation rechargeable batteries.

Energy Frontiers Focus Topic

Room: 315 - Session EN+AS+EM-WeA

Organic-Inorganic Interfaces for Energy

Moderator: Ramana Chintalapalle, University of Texas at El Paso

2:20pm **EN+AS+EM-WeA1 Towards Efficient Solution Processed Organic Photovoltaic Devices**, *Elsa Reichmanis*, Georgia Institute of Technology **INVITED**

Solution-processed π -conjugated semiconductors exhibit potential in the development of low-cost, light-weight and large-area flexible plastic optoelectronics, particularly photovoltaics (OPVs). However, one drawback to current OPVs is their limited efficiency. We have explored the use of donor-acceptor (D-A) hybridization to tailor HOMO/LUMO energy levels and thus the band gap. Materials exhibiting high charge carrier mobility and strong low-energy absorption profiles have been synthesized and characterized. Coupled with materials structure, the performance of devices fabricated using polymeric semiconductors depends critically upon alignment of the polymer chains at the nano- through meso- and macro-scales. Significant structure-process-property relationships that allow for enhancement of long-range order will be discussed. For instance, a lyotropic liquid crystalline (LC) phase has been observed in poly-(3-hexylthiophene) (P3HT) via solvent-evaporation induced self-assembly. The lessons learned through these studies may allow for simple, controllable, and cost-effective methodologies for achieving high performance flexible plastic electronic devices.

3:00pm **EN+AS+EM-WeA3 Understanding Carrier Dynamics in Cu₂ZnSn(S,Se)₄ Using Time-Resolved Terahertz Spectroscopy**, *G.W. Guglietta*, Drexel University, *K. Roy Choudhury, J.V. Caspar*, DuPont Central Research and Development, *Jason Baxter*, Drexel University

We have used time-resolved terahertz spectroscopy (TRTS) to measure lifetimes and determine recombination mechanisms in Cu₂ZnSn(S,Se)₄ (CZTSSe) thin films fabricated from nanocrystal inks. TRTS probes photoconductivity on femtosecond to nanosecond time scales that are relevant for recombination in thin film photovoltaics. Terahertz frequencies (0.2-2.5 THz) correspond to typical scattering rates in semiconductors, enabling determination of carrier density and mobility. Ultrafast time resolution permits tracking the evolution of carrier density to determine recombination mechanisms. By manipulating the photoexcitation wavelength and fluence, we can tailor the generation profile of photoexcited carriers to distinguish between surface, Shockley-Read-Hall (SRH), and Auger recombination mechanisms and determine rate constants.

TRTS experiments and modeling were used to understand the role of recombination mechanisms and their contribution to CZTSSe photovoltaic performance. TRTS photoconductivity shows an instrument-limited onset within 1 ps of an ultrafast pump pulse, followed by a slow decay over nanoseconds. Photoconductivity decay kinetics were fit with a bi-exponential model with two time constants and a weight fraction. The short time constant is typically ~200 ps and roughly corresponds to diffusion to and recombination at the surface. The long time constant is typically ~2 ns and is attributed to SRH recombination. Assignment of these mechanisms is supported by the dependence of kinetics upon excitation fluence and wavelength. Normalized kinetics are independent of fluence over a range of 40x, indicating that no Auger recombination is occurring. Without Auger recombination, we can distinguish between surface and SRH rates by tuning the pump wavelength. As the excitation wavelength is shifted towards the blue, carriers are generated nearer to the front surface and the photoconductivity kinetics are sensitive to the surface recombination velocity. With blue excitation, we see that a larger fraction, ~0.5, of carriers recombine with a short time constant. With redder excitation wavelengths, the carriers are generated more evenly throughout the film and the kinetics are dominated by SRH recombination with the long time constant having a majority of the weight fraction, ~0.8. TRTS provides a pathway to determine performance-limiting recombination mechanisms and measure key parameters like SRH lifetime and surface recombination velocity, helping to direct the design of efficient thin film photovoltaics.

3:20pm **EN+AS+EM-WeA4 Comparative Study of the Doping Effects of Titanium and Nitrogen into Tungsten Oxide (WO₃) Thin Films for Photovoltaic Device Applications**, *Mirella Vargas, C.V. Ramana*, The University of Texas at El Paso

Tungsten oxide (WO₃) is a technologically important n-type semi-conductor that is extensively studied in the fields of electronic and opto-electronic devices. Due to its unique properties such as a high work function and high-coloration efficiency, WO₃ is attractive for electrochromic and memory

devices including large area information displays, smart-windows, and optical heat-mirrors. Low-dimensional structures of WO₃ coupled with an ideal band gap ($E_g \sim 2.8$ eV) have been employed as materials for the photocatalyst driven by visible light irradiation in dye-sensitized solar cells. In addition, WO₃ has also become a strong contender to replace indium-doped tin oxide or ITO thin films in transparent electrode applications. The present work is focused on WO₃ thin films characterized as promising transparent conducting oxide (TCO) materials by investigating doping effects on the structural, chemical, and optical properties. The incorporation of titanium (Ti) was achievable by depositing the films through co-sputtering of W and Ti metal targets. The sputtering powers to the W and Ti were kept constant at 100 W and 50 W, respectively, while varying the growth temperature (T_g) in the range of 25-500 °C. While all the samples are optically transparent, the structural quality of Ti-doped WO₃ films is dependent on T_g . Ti-doped WO₃ films grown at $T_g < 400$ °C were amorphous. A temperature of 400 °C is critical to promote the structural order and formation of nanocrystalline films in the monoclinic phase. The optical constants and their dispersion profiles determined from spectroscopic ellipsometry indicate that there is no significant inter-diffusion at the film-substrate interface for W-Ti oxide film growth of ~40 nm. The index refraction (n) at $\lambda = 550$ nm vary in the range of 2.15-2.40 with a gradual increase in growth temperature. Nitrogen (N₂) incorporation was made through a post-deposition anneal in an ammonia environment on WO₃ films. The un-doped WO₃ films grown by variable growth temperature will be annealed at high temperatures for various rates to accommodate a strong N₂ incorporation. The tungsten oxynitride films will be characterized by various analytical techniques to compare the doping effects of Ti and N₂ on the structural, electronic, and optical properties of WO₃ thin films.

5:00pm **EN+AS+EM-WeA9 Engineering Exciton Recombination in Organic Light-Emitting Devices**, *Russell Holmes*, University of Minnesota **INVITED**

While capable of realizing very high peak efficiency, many organic light-emitting devices (OLEDs) suffer a significant reduction in efficiency under large injected current densities. This efficiency roll-off can limit device brightness and potentially compromise operational stability. Much previous work has identified the key contributing factors to the efficiency roll-off in phosphorescent OLEDs as triplet-triplet annihilation and triplet-polaron quenching. Here, the parameters associated with these quenching processes are independently measured, and the impact of the exciton recombination zone width on the quenching processes in various OLED architectures is examined directly. In high efficiency devices employing a graded-emissive layer (G-EML) architecture the roll-off is due to both triplet-triplet annihilation and triplet-polaron quenching, while in devices which employ a double-emissive layer (D-EML) architecture, the roll-off is dominated by triplet-triplet annihilation. Overall, the roll-off in G-EML devices is found to be much less severe than in the D-EML device. This result is well accounted for by the larger exciton recombination zone that is experimentally measured in G-EML devices, serving to reduce exciton density-driven loss pathways. Indeed, a predictive model of the device efficiency based on the quantitatively measured quenching parameters shows the role a large exciton recombination zone plays in mitigating the roll-off.

5:40pm **EN+AS+EM-WeA11 Interface Engineering to Control Magnetic Field Effects of Organic-based Devices by using a Self-Assembled Monolayer**, *Hyuk-Jae Jang*, NIST & WFU, *S.J. Pookpanratana*, NIST, *A.N. Brigeman*, Wake Forest University, *R.J. Kline*, NIST, *J.I. Basham*, NIST & PSU, *D.J. Gundlach*, *C.A. Hacker*, *O.A. Kirillova*, NIST, *O.D. Jurchescu*, Wake Forest University, *C.A. Richter*, NIST

Magnetic field effects (MFEs) in non-magnetic organic semiconductors provide a non-contact approach to control electronic and optoelectronic properties of organic-based devices by using a sub-tesla magnetic field and thus they have been of great interest to industry as well as academia around the world.^{1,2} However, there is no consensus on the physical mechanism(s) causing the MFEs in organic semiconductors even though a variety of fundamental models have been proposed to explain the effects.³ Studies on many different organic semiconductors and organic-based structures have shown that the magnitude and even the sign of the MFEs can vary by changing the measurement and fabrication conditions such as bias voltage, film thickness, and temperature. Therefore, it is suggested that there can be multiple origins inducing the MFEs and the outcome may result from a competition between different MFE mechanisms.³

In this presentation, we report a novel method of manipulating the MFEs on electrical resistance of organic semiconductors, namely organic magnetoresistance in Alq₃ (tris-(8-hydroxyquinoline) aluminum) – based devices by simply adding a molecular self-assembled monolayer (SAM) between a metal electrode and an organic semiconductor. SAMs have been known for their versatile use in various technological applications.³

Particularly, SAMs can alter the physical property of an inorganic solid surface and thus modify the interface between an electrode and an organic thin film when a SAM is inserted between them.³ We show for the first time that the interfacial modification by simply inserting a fluorinated SAM (heptadecafluoro-1-decanethiol [CF₃(CF₂)₇(CH₂)₂SH] or F-SAM) in organic-based devices changes the sign of organic magnetoresistance due to the change in relative strength of different MFE mechanisms coexisting in organic-based devices. In addition, we utilize different MFE mechanisms coexisting in organic-based devices by adding a thin TPD (N,N'-Bis(3-methylphenyl)-N,N'-diphenylbenzidine) layer to create a system whose organic magnetoresistance can be tuned by an external bias voltage.

References

1. J. Kalinowski, M. Cocchi, D. Virgili, P. Di Marco, and V. Fattori, *Chem. Phys. Lett.* vol. 380, pp. 710-715, 2003.
2. W. Wagemans, P. Janssen, A. J. Schellekens, F. L. Bloom, P. A. Bobbert, and B. Koopmans, *SPIN* vol. 1, pp. 93-108, 2011.
3. J. C. Love, L. A. Estroff, J. K. Kriebel, R. G. Nuzzo, and G. M. Whitesides, *Chem. Rev.* vol. 105, pp. 1103-1169, 2005.

6:00pm **EN+AS+EM-WeA12 Study on the Correlation between Electrode-Active Layer Interfaces and Performance of Polymer Solar Cells**, *Huanxin Ju*, *J.F. Zhu*, University of Science and Technology of China

The PSCs were fabricated with different cathodes (Ca/Al and Al) as the electron-collection layers and with PCDTBT (poly[N-9'-hepta-decanyl-2,7-carbazole-alt-5,5-(4',7'-di-2-thienyl-2',1',3'-benzothiadiazole)]) and PC70BM ([6,6]-phenyl-C71-butyric acid methyl ester) as the active layers. The Ca/Al interlayer significantly improves the open circuit voltage (VOC), short circuit current (JSC), fill factor (FF) so as to improve the PCE in comparison with Al as the cathode. In order to understand how the electrodes affect the device performance, the Ca/PCDTBT and Al/PCDTBT interfaces were investigated by transient photovoltage (TPV), charge extraction (CE) and synchrotron radiation photoemission spectroscopy (SRPES). The TPV and CE measurements were used to determine the charge carrier lifetime and density. Charge carrier recombination rate constant was found to be much smaller in the device with Ca/Al cathode as compared to that with Al cathode. Energy band diagrams and interfacial chemical reactions were characterized using high-resolution SRPES. The results indicate that the Ca interlayer can induce the stronger dipole moment, which facilitates electrons collection and drives holes away at the cathode/polymer interface. The device performance was improved because of the lower recombination.

Thin Film

Room: 307 - Session TF+EM+EN-WeA

Thin Film and Nanostructured Coatings for Light Trapping, Extraction, and Plasmonic Applications

Moderator: Tansel Karabacak, University of Arkansas at Little Rock

2:20pm **TF+EM+EN-WeA1 Enhanced Light Trapping by Glancing Angle Deposited Semiconducting and Metallic Nanostructure Arrays**, *Hilal Cansizoglu*, *R. Abdulrahman*, *M.F. Cansizoglu*, University of Arkansas at Little Rock, *M. Finckenor*, NASA Marshall Space Flight Center, *T. Karabacak*, University of Arkansas at Little Rock

Management of light trapping in nano materials has recently got attention owing to altering optical properties of materials commonly used in potential applications such as photovoltaics and photonics. Trapping the light inside the semiconducting nanostructure coating can increase optical absorption capacity of the material dramatically. Meanwhile, metallic nanostructures can serve as individual back reflectors if the light is achieved to be trapped among metallic nanostructures, which results in enhanced optical absorption of the possible surrounding absorber material around metallic structures. In this study, we examine light trapping in arrays of zig-zags, springs, screws, tilted rods, and tapered vertical rods of indium sulfide (In₂S₃) and aluminum (Al) as the model semiconducting and metallic materials, respectively. Nanostructures of different shapes were produced by glancing angle deposition (GLAD) technique. We investigated the effect of size and shape of the arrays on light trapping properties using ultraviolet-visible-near-infrared (UV-VIS-NIR) spectroscopy and finite difference time domain (FDTD) simulations. Optical characterization results show that light trapping by GLAD nanostructures can strongly depend on their shapes. Under normal incidence of light, 3D geometries of semiconducting nanostructures such as springs, screws, and tapered vertical rods can

provide an enhanced optical absorption compared to zigzags, and tilted rods. In addition, total reflectance measurements reveal that reflectance is inversely proportional to metallic nanorod length in the wavelength range of 200-1800 nm. Meanwhile, FDTD optical modelling indicates an enhanced diffuse light scattering and light trapping through uniform distribution of diffracted light within the 3D In_2S_3 nanostructure geometries such as springs, screws and vertical rods. On the other hand, zigzags and tilted rods show light absorption at relatively low level similar to the experimental results. In addition, simulations reveal that average reflectance of Al nanorods can drop down to as low as ~50%, which is significantly lower than the ~90% reflectance of conventional flat Al film at similar wavelengths. Our results demonstrate that GLAD nanostructures can provide efficient light trapping through the control of their shapes and size.

2:40pm TF+EM+EN-WeA2 Enhanced Photoresponsivity of Conformal TiO_2/Ag Nanorod Arrays Fabricated via (Successful) Glancing Angle and Atomic Layer Deposition, Ali Haider, N. Biyikli, A.K. Okyay, Bilkent University, Turkey, T. Karabacak, H. Cansizoglu, University of Arkansas at Little Rock, B. Teckcan, Bilkent University, Turkey, M.F. Cansizoglu, University of Arkansas at Little Rock

Improved charge carrier collection and optical absorption are two main techniques to enhance the photocurrent of a nanostructured photodetector. In a nanostructured photodiode, longer carrier life time and shorter transit time of the photo-generated carriers provides efficient charge carrier collection while the nanostructured device architecture contributes towards trapping the light by diffuse light scattering and enhancing optical absorption. However, efficient charge carrier collection is limited by the random and non-uniform nano-network. For nanostructured Schottky photodetectors, uniform nanostructured geometries with larger aspect ratio can enhance the interface of the Schottky junction which in turn decreases the transit time of generated carriers. In addition, most of the nanofabrication methods that can produce uniform nanostructure geometries are limited to certain materials. Therefore, it is an overwhelming demand to develop innovative low-cost nanostructured photodetector fabrication methodologies which enables the use of a variety of semiconductor alloy families with uniform and optimized geometries for improving photoresponsivity performance. In this work, we demonstrate a proof-of-concept nanostructured Schottky photodiode fabrication method combining glancing angle deposition (GLAD) and atomic layer deposition (ALD) to fabricate metal-semiconductor radial junction nanorod arrays, which offers significantly enhanced photoresponse compared to conventional planar counterpart. Firstly, silver (Ag) nanorod (NR) arrays were deposited on Ag thin film/Si templates by utilizing glancing angle deposition (GLAD) technique. A conformal and thin titanium dioxide (TiO_2) coating was deposited on silver nanorods via ALD. ALD emerge as highly attractive deposition technique for coating of nanorods due to its remarkable conformality and uniformity on the densely packed NR structures. Moreover, ALD also facilitates the ultra-precise control of deposited film thickness in the sub-nm scale. Following the growth of TiO_2 on Ag NRs, aluminum (Al) metallic top contacts were deposited by thermal evaporation to complete the fabrication of NR-based Schottky photodiodes. Due to the improved charge carrier collection and optical absorption, the resulting nanostructured detector exhibits a more-than two orders of magnitude photoresponsivity enhancement factor (3.8×10^2) under 3V reverse bias when compared to the corresponding thin film counterpart device with the same TiO_2 thickness. Our preliminary structural, optical, electrical, and photoresponse characterization results are presented.

3:00pm TF+EM+EN-WeA3 Nanostructured Photonic Materials for Light-Trapping and Photon Management in Solar Energy Conversion, Koray Aydin, Northwestern University INVITED

Nanophotonics, the emerging field of photon-material interactions at the nanoscale, poses many challenges and opportunities for researchers both in the basic and applied sciences. In this talk, I will describe our efforts in designing, realizing and characterizing nanostructured photonic materials including metals, transparent conductive oxides and inorganic semiconductors. By shaping materials at the nanoscale, one can drastically increase absorption in and/or scattering from nanostructures that could provide significant performance enhancements in solar energy conversion processes including photovoltaics and photocatalysis. First, I will discuss our research efforts on realizing broadband plasmonics absorbers enabled by nanophotonic light-trapping approaches in metal-insulator-metal resonators. By using reflective metals and transparent dielectrics, we have achieved significant absorption enhancement in the metallic parts opening routes for spectrally and spatially selective light-absorbing devices that could find use in thermophotovoltaics and hot-electron collection devices. Then, I will describe light-trapping in nanostructured inorganic silicon ultrathin films which results in drastic absorption enhancement over the entire solar spectrum and over the wide range of incident angles. This approach does not involve any plasmonic components and based solely on

localized and delocalized resonances in semiconductor nanostructures. This novel resonant light absorption phenomenon in semiconductors could find use in photocatalytic and photovoltaic applications of inorganic semiconductors. Finally, I will talk about our results on nanostructured transparent conductive oxide contacts, which is capable of light trapping over broad range of wavelengths. Nanostructured TCO contacts could benefit both organic and inorganic photovoltaic materials, offering significant absorption and short circuit enhancements.

4:20pm TF+EM+EN-WeA7 Porous Solid Phase Microextraction (SPME) Fibers by Oblique Angle Deposition, Anubhav Diwan, B. Singh, Brigham Young University, M. Kaykhaii, Sistan & Baluchestan University, Iran (Islamic Republic of), B. Paul, P. Nesterenko, University of Tasmania, Australia, M.R. Linford, Brigham Young University

Solid phase microextraction (SPME) is a solvent-free technique used for extracting organic compounds from matrices such as air or wastewater. It involves a fiber coated with a liquid or solid stationary phase that extracts target compounds directly from a solution or from the head space above a solution or material. Solid stationary phases provide faster extraction than liquid phases, but exhibit lower capacities. Porous solid phases have been able to overcome these issues by providing large surface areas for analyte adsorption. Commercial SPME fibers are rather expensive, swell in many solvents, and often extract limited numbers of compounds (show limited selectivity). Herein, we discuss the preparation of porous SPME fibers by oblique angle deposition (OAD) of sputtered silicon or other materials onto a fiber. OAD involves deposition of materials onto substrates placed at steep angles with respect to the direction of the incoming species, creating porous structures. The resulting nanoporous coatings can be modified with different functional groups to enhance selectivity of the phase towards target compounds. If normalized for thickness, our fibers show ca. three times the capacity of a commercial, 7 μm PDMS fiber. To confirm their morphologies, new OAD-based fibers have been characterized by scanning electron microscopy (SEM). Various silane coatings can be applied to our fibers, which will offer a range of selectivities. These coatings, e.g., a C18 silane, have been characterized on model planar substrates by X-ray photoelectron spectroscopy (XPS) and contact angle goniometry (wetting).

4:40pm TF+EM+EN-WeA8 Chiral Patchy Particle Arrays: A Simple Fabrication Method to Achieve Plasmonic Circular Dichroism in the Visible Region, George Larsen, Y. He, W. Ingram, Y.P. Zhao, University of Georgia, Athens

An object is said to be "chiral" if it cannot be made superimposable upon its mirror image solely by rotations and translations. That is, chiral objects do not exhibit reflective symmetry. By combining self-assembled colloid monolayers and glancing angle deposition (GLAD), we can create chiral patchy particle thin films that exhibit plasmonic activity in the visible region. Due to their chirality, these patchy particle films exhibit circular dichroism, i.e., they absorb right- and left-circular polarized light to different degrees. Interestingly, we find that the GLAD method relaxes requirements on the template quality, allowing for the production strongly chiral films from polycrystalline colloidal monolayers with randomly oriented domains. It is determined that the rotation direction during GLAD breaks the racemic symmetry of the templates by creating a chiral distribution of material which enhances the chirality of one set of enantiomers relative to the other. Microscopic analysis and geometric chirality calculations confirm that the optical chirality of the bulk film results from incomplete cancellations of even stronger local chiralities. By improving the quality of the colloidal monolayers and intentionally creating a chiral material distribution, we seek to use these chiral patchy particle arrays as plasmonic biosensors that are sensitive to the handedness of the target molecule.

5:00pm TF+EM+EN-WeA9 Tunable Three-Dimensional Helically Stacked Plasmonic Layers on Nanosphere Monolayers, Yizhuo He*, G.K. Larsen, W. Ingram, Y.P. Zhao, University of Georgia, Athens

Chiral metamaterials are artificial materials designed to interact with left- and right-handed circularly polarized light in different ways. Such a unique optical property enables applications such as negative refractive index, circular polarization, enantiomer sensing, etc. Practical applications usually require the fabrication of large-area chiral metamaterials on substrates with tunable chiroptical properties, especially in visible to near infrared wavelength region. We report a simple and scalable method to fabricate three-dimensional chiral metamaterial combining glancing angle deposition and self-assembled colloidal monolayers. Ag and SiO_2 are deposited alternately on colloidal monolayers. By controlling the azimuthal rotation of substrates between depositions, Ag and SiO_2 layers can be helically stacked in left-handed and right-handed fashions to form continuous

*** TFD James Harper Award Finalist**

helices. These helically stacked plasmonic layers (HSPLs) exhibit localized surface plasmon resonances (LSPR) and strong chiroptical responses in visible to infrared region, which is also confirmed by finite-difference time-domain simulations. The most important feature of HSPLs is the great tunability of chiroptical spectra. By increasing the nanosphere diameter from 200 nm to 500 nm, the HSPL structure can be scaled up and thus the LSPR peak redshifts from 520 nm to 1000 nm. Since the chiroptical response originates from the strong interaction of metal layers with light, i.e. LSPR, the chiroptical spectra also redshifts accordingly without a significant change in magnitude. With such flexibility in the design, HSPLs may act as tunable chiral metamaterials, as well as serve as different building blocks for chiral assemblies.

5:20pm **TF+EM+EN-WeA10 Co-deposition of Mixed-Valent Oxides of Molybdenum and Germanium ($\text{Mo}_x\text{Ge}_y\text{O}_z$): A Route to Tailored Optical Absorption**, *Neil Murphy*, Air Force Research Laboratory, *L. Sun*, General Dynamics Information Technology, *J.G. Jones*, Air Force Research Laboratory, *J.T. Grant*, General Dynamics Information Technology

Mixed-valent oxides of molybdenum and germanium were deposited simultaneously using reactive magnetron co-deposition within an oxygen-argon environment. The films' stoichiometry, optical and physical properties were varied through changes in oxygen partial pressure induced by systematic variation of the potential applied to the molybdenum cathode. The oxygen partial pressure was determined from the drop in pressure as measured by a capacitance manometer, assuming constant argon partial pressure. To facilitate deposition, a constant power of 100 W DC was applied to the germanium cathode, while power was applied to the molybdenum target using a modulated pulse power supply. Modulated pulse power magnetron sputtering was used due to its ability to generate high target power densities, allowing for rapid reduction of oxygen on the surface of the "oxygen poisoned" molybdenum cathode, as well as for its highly metallic plasma resulting in increased oxygen-gettering capability. Changes in the modulated pulse power supply's capacitor bank charge, stepped from settings of 300 to 380 V, resulted in films ranging from mixtures of transparent GeO_2 (Ge^{4+}) and MoO_3 (Mo^{6+}) to the introduction of various absorptive ionic species including Mo^{5+} , Mo^{4+} , Ge^{2+} and Ge^0 , as determined from X-ray photoelectron spectroscopy. The presence of each of the aforementioned ions results in characteristic changes in the films' band energies and optical absorption, measured using UV-VIS-NIR optical spectroscopy. As deposited $\text{Mo}_x\text{Ge}_y\text{O}_z$ thin films grown using this method have been shown to have band gaps that are able to be tailored between 2.8 eV and 0.6 eV, spanning useful ranges for devices operating in the visible and near-infrared.

5:40pm **TF+EM+EN-WeA11 Permanent Optical Tape and Solid State Data Storage Devices**, *Hao Wang*, *R. Gates*, *N. Madaan*, *J. Bagley*, *A. Diwan*, *A. Pearson*, *S. Jamieson*, *K. Laughlin*, Brigham Young University, *Y. Liu*, Lehigh University, *B. Lunt*, *M. Asplund*, Brigham Young University, *V. Shutthanandan*, Pacific Northwest National Laboratory, *R.C. Davis*, *M.R. Linford*, Brigham Young University

Recently we have prepared novel write–once–read–many (WORM) optical stacks on Mylar for archival data storage in an optical tape format.¹ Here, a nanoscale, co-sputtered bismuth–tellurium–selenium (BTS) alloy was employed as the write layer with carbon protective layers on both the top and bottom of the BTS film. We have successfully written information (matrix of marks) on the C/BTS/C optical stack using a 532 nm laser. Both the optical stack structure (film thickness) and writing conditions (laser power and laser spot size) have been optimized. Films were characterized by X-ray diffraction, X-ray photoelectron spectroscopy, time-of-flight secondary ion mass spectrometry, scanning electron microscopy, spectroscopic ellipsometry, and atomic force microscopy.^{2,3}

We have also recently developed novel WORM solid-state memory elements. These consisted of nanoscale, bowtie-like sputtered carbon films to which a voltage (ca. 10 V) is applied. These fuses have been successfully blown, and the carbon fuse shape, thickness of the carbon layer, and writing voltage have been optimized. Other aspects of the device are currently being optimized.

References

- [1] Wang, H.; Lunt, B.M.; Gates, R.J.; Asplund, M.C.; Shutthanandan, V.; Davis, R.C.; Linford, M.R. Carbon/ternary alloy/carbon optical stack on Mylar as an optical data storage medium to potentially replace magnetic tape, *ACS Appl. Mater. Interfaces*, **2013**, 5, 8407-8413.
- [2] Wang, H.; Diwan, A.; Lunt, B.M.; Davis, R.C.; Linford, M.R. XPS and SIMS characterization of a BiTeSe write layer for permanent optical tape storage, *Proceedings of ISOM 2013*, ISOM 2013 International Conference, Incheon, South Korea, 2013.
- [3] Wang, H.; Lunt, B.M.; Davis, R.C.; Linford, M.R. Simulation of laser writing on Bi-Te-Se alloy/carbon/Mylar permanent optical storage tape, ISOM 2013 International Conference, Incheon, South Korea, 2013.

Spectroscopic Ellipsometry Focus Topic

Room: 304 - Session EL+AS+EM+EN+SS-ThM

Spectroscopic Ellipsometry for Photovoltaics and Instrument Development

Moderator: Mariadriana Creatore, Eindhoven University of Technology, Netherlands, Tino Hofmann, University of Nebraska-Lincoln

8:00am **EL+AS+EM+EN+SS-ThM1 Spectroscopic Ellipsometry Characterization in the Photovoltaic Device Configuration, Nikolas Podraza, University of Toledo** **INVITED**

Thin film large area photovoltaics (PV) are a maturing field, yet challenges remain in manufacturing and fundamental research. Even the simplest thin film PV devices consist of multiple layers of doped or undoped semiconductors, transparent conducting front contacts, and metal back contacts. Characteristics of each layer, along with the interfaces between layers, all have an impact upon device performance. Within each layer, the material may evolve with thickness or exhibit spatial non-uniformity. Furthermore, studies of each thin film material can be difficult, as fundamental property measurements on special substrates may not accurately represent the characteristics of the material in the final device configuration. Spectroscopic ellipsometry (SE) data, collected over the infrared to ultraviolet, is sensitive to layer thicknesses, interface formation, and surface roughness as well as the optical response of each component in the form of the complex dielectric function spectra ($\epsilon = \epsilon_1 + i\epsilon_2$) for samples deposited on arbitrary reflective substrates. Variations in ϵ for a given layer can be linked to order (amorphous vs. crystalline, grain size, crystal phase), composition, and characteristics of opto-electronic response (band gap, dc electrical properties). In situ real time SE (RTSE) is now often applied to study the growth evolution of component materials within device configurations for hydrogenated silicon (Si:H), cadmium telluride (CdTe), and copper indium gallium diselenide (CIGS) PV. This utilization of RTSE provides a means of monitoring layer characteristics as materials are being processed in the device structure and generates appropriate structural models for analysis of similar samples when only ex situ SE measurements are available. Appropriate structural models derived from RTSE have been applied to analyze ellipsometric spectra collected over 6 inch x 6 inch rigid substrates and assess the spatial uniformity in characteristics of each layer in the sample. These maps of optically derived material properties can be compared to electrical device performance (efficiency, open circuit voltage, short circuit current, fill factor) and used to guide PV optimization principles. The optical (ϵ) and structural (layer thickness) information gained from SE is input into quantum efficiency simulations for comparison with experimental PV device measurements. These comparisons are used to assess both opto-electronic performance of devices and validity of models used in SE data analysis as well as further guide device development by identifying sources of optical and electrical losses.

8:40am **EL+AS+EM+EN+SS-ThM3 Application of Pseudo-Bulk Approach in Ellipsometric Studies of Polycrystalline Photovoltaic Thin Films, Sukgeun Choi, National Renewable Energy Laboratory, J. Li, University of Toledo, I. Repins, National Renewable Energy Laboratory**

Fundamental band gap is one of the key properties of semiconducting materials, which directly influences the functionality and performance of many photonic and photovoltaic (PV) devices. Photoluminescence (PL) and optical absorption spectroscopies are widely used to determine the band-gap energy E_g . For polycrystalline thin-film PV materials, however, it is often challenging to unambiguously interpret PL data owing to the presence of multiple peaks associated with various types of defect structures. To estimate E_g from optical absorption spectrum, on the other hand, a straight segment of the absorption coefficient curve needs to be chosen. But this selecting procedure is somewhat arbitrary, which leads to an inaccurate E_g value.

Spectroscopic ellipsometry (SE) accurately determines material's optical function spectra over a wide spectral range. For semiconductor thin-film structures, a multilayer analysis is generally used to extract the optical information from SE data. Although mainly surface overlayer artifacts need to be corrected for SE data well-above the band gap in the analysis, several contributions should be considered for those near (and below) the band gap, such as the optical characteristic of substrate, presence of interfacial layers, and finite thickness of film in addition to the artifacts from surface overlayers. As a result, the obtained optical function spectrum and E_g value become somewhat model dependent with an increased uncertainty.

To reduce complications in mathematical modeling of SE data and improve the accuracy of resulting near-band-gap optical function spectrum, we introduce the *pseudo-bulk* approach, where SE measurements are performed on thin films grown on macroscopically roughened substrate surface. The essence of this approach is in suppressing the reflection of probing light from the film/substrate interface and below. Thus, no thickness fringes appear in the SE data, despite the thin-film nature of sample, and the band-gap onset can be clearly observed with a post-growth chemo-mechanical polishing of the film surface. We apply the *pseudo-bulk* approach to study near-band-gap optical properties of $\text{Cu}_2\text{ZnSnSe}_4$ and related PV absorber materials. We present a non-monotonic temperature-dependence of E_g for $\text{Cu}_2\text{ZnSnSe}_4$ and the clear band-gap onset of Cu_2SnSe_3 at around 0.45 eV for the first time. SE results are explained by the results from the electronic structure calculations. The applicability and limit of this approach are also discussed.

9:00am **EL+AS+EM+EN+SS-ThM4 Real-Time and Through-the-Glass Mapping Spectroscopic Ellipsometry for Analysis and Optimization of CdS:O Window Layers of CdTe Superstrate Solar Cells, Xinxuan Tan, R.W. Collins, P. Koirala, J. Li, N.J. Podraza, University of Toledo**

In-situ real-time spectroscopic ellipsometry (RT-SE) has been applied for the analysis of CdS:O films sputter deposited on c-Si substrates from a CdS target using different flow ratios of $\text{O}_2/(\text{Ar}+\text{O}_2)$ from 0 to 0.05. RT-SE studies of the CdS:O layers from the film side provide the complex dielectric function spectra of each the layers over a spectral range of 0.75 to 6.5 eV and its dependence on oxygen content in the material as deduced by energy dispersive X-ray spectroscopy (EDS). Ex-situ infrared ellipsometry of these samples enables extension of the dielectric function data to ~ 0.04 eV and provides information on free carrier conduction and chemical bonding in the material. In similar RT-SE studies, data acquired during the growth of CdS:O/CdTe layers on transparent conducting oxide (TCO) coated glass superstrates have been analyzed to determine the structural evolution of the layers in the configuration used for CdTe solar cells, with the CdS:O serving as an n-type window layer for the p-type CdTe absorber. The results of this analysis assist in the development of a realistic optical model for the multilayer structure of the solar cell. Using this optical model ex-situ through-the-glass spectroscopic ellipsometry (TG-SE) has been implemented toward the analysis of glass/(TCO-stack)/CdS:O/CdTe solar cells in the superstrate configuration.

For the solar cells, CdS:O layers with different oxygen contents were deposited on 15 cm x 15 cm TCO coated glass superstrates. A 16 x 16 array of dot cells each with an area of 0.125 cm² was fabricated on the superstrate in order to optimize efficiency improvements through combinatorial methods. Because the as-deposited superstrate/film-structure undergoes additional processing steps during device fabrication, three sets of TG-SE mapping data were acquired on (i) as-deposited, (ii) CdCl₂-treated (an activation step), and (iii) back-contact coated device structures. With an optical database that has been established for both as-deposited and CdCl₂ treated CdS:O, CdTe, and back contact materials, each of the TG-SE mapping data sets were analyzed based on an optical model deduced from RT-SE studies of the CdS:O and CdS:O/CdTe depositions. Thickness and compositional non-uniformity observed over the area by mapped by TG-SE enables correlations between solar cell performance and basic property parameters of the component layers including layer thicknesses and compositions. The resulting correlations provide a pathway to expedite solar cell optimization.

9:20am **EL+AS+EM+EN+SS-ThM5 Combined Optical Emission Spectroscopy and Spectroscopic Ellipsometry Collected During Thin Film Deposition, Anna Barnes, M.M. Junda, N.J. Podraza, University of Toledo**

Plasma processes are commonly used to deposit thin film layers for a variety of optical, electronic, and coating applications. Two common processes widely used in the fabrication of thin films are physical vapor deposition (sputtering) and plasma enhanced chemical vapor deposition (PECVD). Non-contacting optical probes, such as spectroscopic ellipsometry (SE) and optical emission spectroscopy (OES), are particularly attractive techniques to study these deposition processes in situ during film growth. Connecting studies involving SE and OES offers the ability to observe and interpret the growth of thin films from plasma over time using variant parameters, though in different ways. Real time SE (RTSE) provides a means of monitoring the deposited material itself, while OES can be used to track variations in the plasma employed for the deposition. Tracking the time dependence of both film and plasma properties is desirable as variations in material properties resulting from changes in plasma conditions may impact the final device performance. In this particular

study, we look at the growth evolution of semiconductor, transparent conducting oxide (TCO), and metal contact layers commonly used in thin film photovoltaic devices. Case studies involve undoped, n-type, and p-type hydrogenated amorphous silicon prepared by PECVD, as well as zinc oxide, indium tin oxide, and silver prepared by magnetron sputtering on either smooth test substrates (glass, crystal silicon wafers) or in the full device configuration. Variations in thin film structure (bulk layer thickness, surface roughness) and optical properties in the form of the complex dielectric function spectra ($\epsilon = \epsilon_1 + i\epsilon_2$) are obtained as a function of time by RTSE. Results from RTSE (ϵ , structure) are interpreted to determine order (grain size, amorphous vs. nanocrystalline), electronic transitions (band gap, free carrier absorption characteristics), and morphology evolution as appropriate for the given material layer. OES indicates the presence and relative strength of plasma emission peaks, which correspond to the species present in the plasma and their relative concentrations. Analysis of RTSE and OES data collected simultaneously is sought to identify links present between these plasma and film characteristics.

9:40am **EL+AS+EM+EN+SS-ThM6 Optical Insights into Graphene Functionalized by Atoms, Biomolecules and Metal Nanoparticles, Maria Losurdo, M. Giangregorio, G.V. Bianco, P. Capezzuto, G. Bruno, CNR-IMIP, Italy**

New opportunities for energy production and storage, catalysis, biosensing, drug delivering and plasmonics are offered by graphene-based materials. In order to make all these applications viable technologies, it is mandatory to functionalize graphene for modulating reproducibly its properties and for better understanding the surface and interfacial electronic phenomena in graphene hybrids.

To this aim, this contribution discusses the optical properties measured by spectroscopic ellipsometry in the 0.6-6.5 eV of graphene functionalized by:

- (1) the covalent attachment of hydrogen, nitrogen, oxygen, and fluorine atoms, which strongly affect the optical properties of graphene through a partial sp²-to-sp³ conversion of carbon.
- (2) the non-covalent interaction with organic molecules such as porphyrins that interact with graphene through p-systems.
- (3) a variety of metals nanoparticles, like Au, Ag, Ga, to create a versatile graphene-based platform for plasmonics in frequency range from the terahertz to the visible.
- (4) plasmonic nanoparticles and subsequent proteins to create an electro-optical sensing graphene platform.

The graphene is grown by chemical vapor deposition (CVD) and transferred to glass substrates with coverage higher than 98%. This assures large area graphene samples that can easily accommodate the ellipsometric probing light spot avoiding uncontrolled effects due to undefined substrate/graphene boundaries. With the availability of high quality samples, effect of thickness and anisotropy, which have been debated for a while, are clarified.

Data on the real time monitoring of graphene optical properties by spectroscopic ellipsometry that allows for an unprecedented control over the degree of functionalization will also be presented.

The perspective of this work is twofold. From the fundamental point of view, in the investigated spectral range, the band structure of graphene has saddle van Hove-like singularities at the M points of the Brillouin zone, with possible excitonic effects. Focusing on the analysis of these singularities, many-body effects for all the graphene-derivates mentioned above are described.

From the technological point of view, it will be shown how the optical measurements can serve to clarify and explain the occurrence and stability of the doping of graphene by the various heteroatoms and molecules, the electron transfer between graphene and metals and molecules, and finally the sensitivity of the graphene-platform in sensing gases and biomolecules.

Spectroscopic ellipsometry data of functionalized graphene are corroborated by Raman spectroscopy, microscopies and electrical characterizations.

11:00am **EL+AS+EM+EN+SS-ThM10 Enhanced Sensitivity to Surface-Normal Dielectric Function of Uniaxial-Anisotropic Materials via Attenuated Total Reflection Ellipsometry, Thomas Tiwald, J.A. Woollam Co., Inc., J. VanDerslice, Z. Xiao, J.S. Huang, University of Nebraska Lincoln**

It is often difficult to determine the surface-normal dielectric functions of anisotropic materials, because of lack of sensitivity to optical properties out of the surface plane[1][2]. The primary cause is the large angle of refraction that occurs as the light enters from low index medium like air. In these circumstances, the penetrating light beam bends strongly towards surface normal, resulting in electric fields that are oriented primarily in the surface plane. This is a particular problem for absorbing films, since most of the light collected by the detector is reflected from the ambient/film interface. We use a total internal reflection method to enhance ellipsometric

sensitivity to optical properties of uniaxial absorbing materials in the out-of-plane direction. This non-destructive technique is illustrated using a P3HT poly(3-hexylthiophene) film on fused silica, and the results are compared to the standard air/film/substrate method.

[1] D.E. Aspnes. *J. Opt. Soc. Am.*, **70**, 10, 1275 (1980).

[2] G. E. Jellison Jr. and J. S. Baba, *J. Opt. Soc. Am. A23*, 2 468 (2006).

11:20am **EL+AS+EM+EN+SS-ThM11 Infrared to Ultraviolet Optical Properties of Gadolinium Gallium Garnet (Gd₃Ga₅O₁₂) and Bismuth Germanate (Bi₄Ge₃O₁₂) Single Crystals, Kiran Ghimire, H. Haneef, N.J. Podraza, University of Toledo**

The optical properties of commercially available oxide single crystals gadolinium gallium garnet (Gd₃Ga₅O₁₂) and bismuth germanate (Bi₄Ge₃O₁₂) have been studied over a maximum spectral range of 0.034 to 6.5 eV by multiple spectroscopic ellipsometry and transmittance measurements, via a multichannel ellipsometer from the near infrared to ultraviolet, a Fourier transform infrared (FTIR) ellipsometer, and a spectrophotometer. Spectroscopic measurements from each instrument and over the respective spectral ranges have been analyzed differently yet yield optical properties over the full measured range. Near infrared to ultraviolet ellipsometric spectra are analyzed using a divided spectral range procedure whereby information below and above the band gap are fit to models with separate physically realistic parameterizations of the complex dielectric function spectra ($\epsilon = \epsilon_1 + i\epsilon_2$) that share the same structural parameters—surface roughness thickness in these cases. The surface roughness thicknesses are then fixed and direct numerical inversion is used to determine ϵ over the continuous spectral range. Analysis of transmittance and FTIR ellipsometric spectra also relies upon fixing surface roughness from near infrared to ultraviolet spectroscopic ellipsometry analysis and either direct numerical inversion or parametric models to determine ϵ . In the vicinity of the band gap, the absorption coefficient (α) obtained from ϵ is then combined with low values of ϵ obtained from transmittance below the absorption edge, where ellipsometry lacks sensitivity. The combined α from transmission and ellipsometry is used to determine the band gap of the materials. Unlike Gd₃Ga₅O₁₂, the band gap of the Bi₄Ge₃O₁₂ is sufficiently within the measured spectral range so critical point analysis has been performed on Bi₄Ge₃O₁₂ by extending the measured spectral range up to 6.5 eV, where the material was found to have additional critical points. FTIR ellipsometric spectra are analyzed with a parametric model combining Gaussian and Lorentzian broadened resonance features to represent modes attributed to chemical bonding and lattice vibrations. The results of these analysis procedures yield ϵ from the infrared to ultraviolet, from which information on the band gap, electronic transitions, and vibrational modes are obtained.

11:40am **EL+AS+EM+EN+SS-ThM12 Cu surface reactions in hydrochloric solution probed on the atomic scale by polarization optical methods and STM, Christoph Cobet, Gh. Barati, V. Solokha, K. Hingerl, Johannes Kepler University, Austria**

Electrochemical reactions on metal electrodes have been in the focus of many scientific studies and Cu is probably the most investigated example. Mainly, the interest on Cu is motivated by questions concerning e.g. the corrosion behavior or the optimization of electro-polishing procedures. Classical electrochemical approaches contain usually a description of the occurring reaction products and concentrations. However, it is evident that a fundamental understanding also requires knowledge about the microscopic occurrence of the metal-electrolyte interface. Desirable is a fundamental knowledge as it is obtained already for surfaces in UHV. But unfortunately, most of the classical surface sensitive techniques cannot be applied in liquid environments. Thus it is not surprising that many fundamental issues in electrochemical reactions are still unsolved.

In our work we combine reflection anisotropy spectroscopy, spectroscopic ellipsometry, and a homemade electrochemical scanning tunneling microscope to study Cu single crystals in hydrochloric solutions. With these methods we enabled monitoring of the local appearance as well as the dynamics of interface transformations/reactions on the atomic scale. In particular it was possible to explain for the (110) surface in more detail the correlation of Faraday-current and structural transformation. Here, the Cl adsorption minimizes the surface energy by a formation of monoatomic steps parallel to the [001] direction which finally ends in a faceting of the surface. It turns out that characteristic redox peaks in cyclic voltammograms correlate with the stabilization of certain arrangements of these steps. The structures are formed first by Cu dissolution and at higher anodic potentials by rearrangement of Cu atoms in the surface. It is remarkable that the latter process compares nicely with oxide/chloride induced surface transformations which are observed in UHV. The comparison with the UHV results in turn is used to achieve a more comprehensive model for the processes in electrochemical environment.

Thursday Afternoon, November 13, 2014

Atom Probe Tomography Focus Topic

Room: 301 - Session AP+AS+EN+NS+SS-ThA

APT and FIM Analysis of Catalysts and Nanomaterials

Moderator: David Diercks, Colorado School of Mines,
David Larson, CAMECA Instruments Inc.

2:20pm AP+AS+EN+NS+SS-ThA1 *In Situ Study of Gas - Solid Reactions via Environmental APT*, *Krishna Rajan*, Iowa State University
INVITED

In this presentation we describe the design and examples of applications of the use of an environmental cell integrated into a LEAP atom probe. The use of such a cell helps to open up the field of in-situ gas-solid reactions by permitting one to study surface and near surface reactions which are closer to ambient conditions than is possible in traditional surfaces science studies. The implications for this experimental approach in the context of the study of catalysts and nanomaterials are discussed.

3:00pm AP+AS+EN+NS+SS-ThA3 **Propagation of Chemical Waves: A Field Emission Microscopy Study**, *Cédric Barroo*, *Y. De Decker*, *N. Kruse*, *T. Visart de Bocarmé*, Université Libre de Bruxelles, Belgium

The catalytic hydrogenation of NO₂ over platinum field emitter tips has been investigated by means of field emission techniques. Field emission microscopy (FEM), as well as field ion microscopy (FIM), has been proved to be an efficient method to study the dynamics of catalytic reactions occurring at the surface of a nanosized metal tip, which represents a good model of a single catalytic nanoparticle. These studies are performed during the ongoing reaction which is imaged in real time and space. Nanoscale resolution allows for a local indication of the instantaneous surface composition.

The presence of adsorbates modifies the value of the local work function. These variations are expressed by modulations of the brightness of field emission patterns. A qualitative investigation of the local surface composition is then possible as function of time.

The microscope is run as an open nanoreactor, ensuring that the system is kept far from thermodynamic equilibrium. Under these conditions, chemical reactions can induce time and space symmetry breaking of the composition of a system, for which periodic oscillations and target patterns are well-known examples.

Self-sustained periodic oscillations have been reported for the NO₂ reduction. By increasing the time resolution of the system, it is now possible to study the emergence of these oscillations and to observe the propagation of chemical waves at the nanoscale, on a single facet of a nanocrystal. The velocity of wave propagation is estimated to be in the μm/s range, which is in accordance with previous studies of catalytic reaction at the mesoscale.

3:20pm AP+AS+EN+NS+SS-ThA4 **3D Nanoscale Chemical/Structure Analysis in Mineral Carbon Sequestration Study using Atom Probe Tomography**, *Jia Liu*, *D.E. Perea*, *R.J. Colby*, *L. Kovarik*, *B. Arey*, *O. Qafoku*, *A. Felmy*, Pacific Northwest National Laboratory

Mineral carbon sequestration is one of the important means to store CO₂ in order to mitigate the environmental concern regarding ever-growing anthropogenic CO₂ emissions. Olivines, X₂SiO₄ where X = Mg and Fe, hold promise as potential media to sequester carbon due to its broad availability in basalt deposits and reactivity to form stable metal carbonates. Site-specific reactivity of olivine with supercritical CO₂ is of great interest in understanding the fundamental elementary reaction mechanisms, where the presence of impurities within the bulk mineral may affect reaction kinetics. A combination of atom probe tomography (APT) and scanning transmission electron microscopy (STEM) is being used to map the complex composition and nanoscale structure across various site-specific regions. APT analysis of unreacted natural fayalite indicates the presence of 2-3-nm-thick hydrated iron oxide layers. In addition, Na impurities were found to concentrate within the hydrated layers while Mg and Mn were depleted from these regions. With the ability of APT to detect the chemical/structural heterogeneity at nanometer-scale, we find that APT will provide a means to correlate with ongoing experimental reaction studies and also provide guidance into models of the heterogeneous phase formation and reaction rates at precisely defined interfaces within minerals.

4:00pm AP+AS+EN+NS+SS-ThA6 **Catalyst Nanomaterials Analysis via Atom Probe Tomography**, *P.A.J. Bagot*, Oxford University, UK, *Q. Yang*, University of Oxford, UK, *K. Kruska*, Pacific Northwest National Laboratory, *D. Haley*, University of Oxford, UK, *E. Marceau*, *X. Carrier*, Université Pierre et Marie Curie, France, **Michael Moody**, University of Oxford, UK
INVITED

Heterogeneous catalytic materials play an increasingly critical, yet largely unnoticed, role underpinning countless modern technologies. Their active components are generally transition group metals, each of which offers different catalytic properties in terms of selectivity, yield and stability under demanding operating conditions. The need to develop more efficient catalysts that meet industrial demands and comply with environmental legislation targets requires better understanding how different catalysts may alter at the atomic scale in terms of structure or surface composition under their respective operating environments. Further, many catalysts take the form of nanoparticles, the performance of which can be strongly correlated to size, shape, chemistry and structure. However, discerning the nature of nanoparticles scale poses significant challenges to conventional microscopy.

Recently, atom probe tomography (APT) techniques have been developed to provide unique insight into the behaviour of catalyst alloys subject to conditions like those experienced in service [1–3]. This study is aimed at more accurate and insightful analyses comprising unique 3D atomistic descriptions of the evolving alloy nanostructure which can then be correlated to catalyst performance. Here, APT results are presented for characterization of oxidation-induced segregation in a Pt-Pd-Rh gauze and Fe-Ni alloy catalysts. Progress in the development of new approaches for the analysis of nanoparticles via APT is also presented.

[1] T. Li et al., Atomic engineering of platinum alloy surfaces. *Ultramicroscopy* 132, 205 (2013).

[2] T. Li et al., Atomic Imaging of Carbon-Supported Pt, Pt/Co, and Ir@Pt Nanocatalysts by Atom-Probe Tomography. *ACS Catalysis* 4, 695 (2014).

[3] P. Felfer et al, Long-Chain Terminal Alcohols through Catalytic CO Hydrogenation. *Journal of the American Chemical Society* 135, 7114 (2013).

Friday Morning, November 14, 2014

Electronic Materials and Processing

Room: 311 - Session EM+EN-FrM

Nitrides for LED and PV Device Applications

Moderator: Nikolaus Dietz, Georgia State University

9:00am **EM+EN-FrM3 The Capricious Effect of Heating on the Surface Photovoltage in Si-doped GaN**, Joy McNamara, K.L. Phumisithikul, A.A. Baski, M.A. Reshchikov, Virginia Commonwealth University

Surface photovoltage (SPV) studies on gallium nitride (GaN) thin films have recently revealed much information, including the band bending at the surface, the effect of polarity on the surface potential, the role of the surface oxide layer, and many other surface related behaviors. By using the Kelvin probe method, the surface potential of GaN can be measured in respect to a vibrating metal probe. To investigate the SPV behavior of both n- and p-type GaN, several experimental conditions have been varied, such as ambient or temperature. It is expected from a thermionic model that the surface band bending decreases immediately under ultraviolet (UV) illumination with the intensity used in these measurements. This results in the production of an immediate increase in the SPV signal as measured by the Kelvin probe. In recent studies on GaN thin films grown by metal organic chemical vapor deposition (MOCVD) and doped with silicon (concentration of $\sim 10^{19} \text{ cm}^{-3}$), we observed an effect of heating on the transient SPV behavior due to the history of sample preparation. For the first group of samples, a very fast rise of the SPV signal by 0.7 eV was observed at room temperature under UV illumination in vacuum, after the samples were initially exposed to air. However, after heating these samples to 600 K in vacuum before taking measurements at room temperature, the fast SPV component decreased to 0.2 eV, while a slow, logarithmic-in-time increase was observed for longer times of UV exposure, with a maximum SPV signal of only 0.4 eV after 30 min. For the second group of samples, the heating in vacuum caused the magnitude of the initial fast SPV in vacuum to be much smaller (0.7 eV after air exposure and 0.3 eV after heating), but without a slow, logarithmic-in-time increase. The SPV behavior could be reversed by UV illumination in air at room temperature. Interestingly, similar SPV behavior has also been observed in ZnO films. The reversible heating effect is preliminarily explained by assuming that the presence of an oxide layer either inhibits or allows the transfer of UV-induced charge carriers between the bulk and surface states, depending on the conditions of the measurement.

9:20am **EM+EN-FrM4 Atomic Layer Deposition of III-Nitride Alloys using Hollow-Cathode Plasma Source for Post-CMOS Processing and 3D Integration**, C. Ozgit-Akgun, A. Haider, AliKamal Okyay, N. Biyikli, Bilkent University, Turkey

Plasma-assisted atomic layer deposition (PA-ALD) is a cyclic, low-temperature thin film deposition method, in which the substrate surface is exposed to sequential pulses of precursor molecules and plasma species separated by evacuation and/or purging periods. When compared to other techniques, ALD stands out with its self-limiting growth mechanism, which enables the deposition of highly uniform and conformal thin films with sub-angstrom thickness control. These features make PA-ALD a promising and alternative technique for the low-temperature deposition of III-nitrides and their alloys in post-CMOS processing and 3D integration technology.

In our previous reports on the PA-ALD of polycrystalline wurtzite AlN thin films at temperatures ranging from 100-500 °C using trimethylaluminum as the Al precursor, films deposited at temperatures within the ALD window (100–200 °C for both NH_3 and N_2/H_2 processes) were C-free and had relatively low O concentrations ($<3 \text{ at.}\%$). Our initial efforts for depositing GaN thin films, however, resulted in amorphous thin films with high O concentrations ($\sim 20 \text{ at.}\%$). Following experiments revealed the source of this O contamination as the quartz tube of the inductively coupled RF-plasma source itself. In view of these circumstances, the choice of N-containing plasma gas (N_2 , N_2/H_2 or NH_3) determined the severity of O incorporation into the deposited AlN and GaN thin films. As an effort to completely avoid this contamination problem, we integrated a stainless steel hollow-cathode plasma (HCP) source to the ALD system, and thereby reported on hollow cathode PA-ALD (HCPA-ALD) of nanocrystalline AlN and GaN thin films with low impurity concentrations at 200 °C using trimethylmetal precursors. Within the scope of the same study, $\text{Al}_x\text{Ga}_{1-x}\text{N}$ thin films were also deposited via digital alloying, where alloy composition was determined by the relative number of AlN and GaN subcycles in the main HCPA-ALD cycle.

In this presentation, we will review our recent efforts on the development of low-temperature HCPA-ALD processes for III-nitride alloys including GaN, InN, $\text{In}_x\text{Ga}_{1-x}\text{N}$, and $\text{In}_x\text{Al}_{1-x}\text{N}$ thin films. In-detail materials characterization results including structural, optical and electrical properties as well as potential device architectures for post-CMOS processing and 3D integration will be presented and discussed.

9:40am **EM+EN-FrM5 Development of Nitride Nanorod Light-emitting Diode Array**, C.G. Tu, C.H. Liao, Y.F. Yao, C.Y. Su, H.S. Chen, W.H. Chen, C. Hsieh, H.T. Chen, Y.W. Kiang, Chih-Chung Yang, National Taiwan University, Taiwan, Republic of China **INVITED**

With the nano-imprint lithography and the pulsed growth mode of metalorganic chemical vapor deposition, a regularly-patterned, c-axis nitride nanorod (NR) light-emitting diode (LED) array of uniform geometry with m-plane core-shell InGaN/GaN quantum wells (QWs) is formed. To grow an NR with uniform cross-sectional size, in the pulsed growth mode, the sources of groups III and V are switched on and off alternatively with fixed supply durations. By growing a p-i-n core-shell structure, an InGaN/GaN QW NR LED array can be fabricated by depositing a conformal layer of GaZnO on the NRs for serving as the transparent conductor. The electrical property of such an LED array is comparable with that of a conventional planar LED. Besides, by varying the supply duration of group III source (TMGa) in the pulsed growth process, the NR cross section can be tapered for growing another section of NR of a different cross-sectional size. Based on this growth technique, a multiple-section GaN NR of changing cross-sectional size can be obtained. When InGaN/GaN QWs are deposited on the sidewalls of the NR, the indium contents and QW thicknesses are different in different sections of different cross-sectional sizes due to different strain relaxation conditions. In this situation, the emission wavelengths of the QWs from different sections are different, leading to the multiple-color emission of such an NR array. Such an emission behavior can be used for fabricating a phosphor-free white-light LED.

10:40am **EM+EN-FrM8 Trends in Production Scale MOCVD Equipment for Nitride Semiconductors**, Alexander Gurary, Veeco Instruments, Inc. **INVITED**

Metalorganic Chemical Vapor Deposition (MOCVD) is a technology of choice for large scale production of GaN based LED and Power Electronic devices. For the last 20 years MOCVD equipment evolved from small R&D oriented deposition systems (three 50 mm wafers per run) to large industrial cluster type systems (two hundred sixteen 50 mm wafers per run) with very sophisticated in-situ devices and process control. Evolution of the production scale MOCVD equipment is driven by one major goal – Cost of Ownership (CoO) reduction. Industry is achieving this goal utilizing several trends:

Migration from R&D to production requirements. GaN MOCVD systems started as an R&D tool. Further development of these systems is the path from universality and flexibility typical for R&D tools to stability and simplicity required for production environment.

Increasing batch size. This is the most obvious way to improve CoO as the cost to manufacture system with two times more wafers per run is less than the factor of two. All major MOCVD equipment companies follow this trend and release new larger batch systems every 3-5 years. One of the most important questions for scaling up is the limit of this trend.

Move from the single reactor system to the cluster and increase level of automation. Majority of modern MOCVD systems migrated from the single reactor to the cluster type multi-reactor design with central loading module and wafer carrier transfer robot.

Increasing role of the in-situ devices for wafer parameters measurement and control. Evolution of in-situ devices for production system includes the following sequence: thermocouple - conventional pyrometer – reflectometer - emissivity compensated pyrometer - deflectometer (wafer bow measurements). There is also a trend for more sophisticated control methods that move from PID to predictive and model based algorithms.

Increased wafer carrier complexity. The wafer carrier is a unique component of MOCVD system that to a large degree defines system yield. Complexity of the wafer carriers is constantly increasing with the goal to improve deposition uniformity. Wafer carriers are a subject of majority MOCVD equipment patents.

Increased role of process modeling. Troubleshooting and process optimization in production environment exclude “trial and error” approach and require good computational models for flow dynamic and process chemistry that are fine-tuned based on experimental data.

In this presentation we will describe above trends in detail and make an attempt to predict next steps in the development of the equipment for large scale production of GaN based materials.

11:20am EM+EN-FrM10 Growth of GaN on Sapphire, Si (111), and Ge/Si (111) using a Pulsed Electron Beam Deposition (PED) Process, Nazmul Arefin, University of Oklahoma, M.H. Kane, Texas A&M University, K. Hossain, Amethyst Research Inc, B.N. Pritchett, Oklahoma Geological Survey, M.B. Johnson, P.J. McCann, University of Oklahoma

This presentation will describe results recently obtained with pulsed electron beam deposition (PED) of GaN on sapphire, silicon (111), and 2 nm germanium coated silicon (111) substrates. The PED technique is potentially useful for growth of III-nitrides at lower substrate temperatures, a capability that can allow use of new buffer layer materials, introduction of chemically dissimilar lattice-matched materials, and help solve wafer bowing and cracking problems during growth. The introduction of this technique could lead to improvements in device quality and fabrication of vertical LED structures. In this study, GaN was deposited on sapphire at a substrate temperature of 750°C, and on silicon (111) and Ge/Si (111) at 600°C in a UHP N₂ (15 mTorr) environment (without any surface pre-treatment such as pre-nitridation). A high power electron gun pulse (Neocera, Inc) was used to ablate the GaN target (1" dia. x 0.250" thick, 99.99% pure) stationed at 5 cm vertical distance from the substrate. The electron pulses were generated at 15KV, 0.3 J/pulse at 1 Hz for initial few nm of growth, and then increase to a 3 Hz pulse rate. Scanning Electron Microscopy (SEM), X-ray Diffraction (XRD), Rutherford backscattering, and optical absorption characterization were performed. SEM imaging confirms a rough surface morphology with the presence of 30 nm to 300 nm scaled GaN crystallites (for the GaN/Sapphire sample) while smaller but more coalesced crystallites of 30-50 nm size is observed for GaN/Si (111) and GaN/Ge/Si (111) samples. The average film thickness is 350 nm for the samples, yielding a growth rate of 0.16 angstrom/pulse. From SEM, it appeared that high aspect ratio filament structures have grown over the crystallites. XRD θ -2 θ scans from $2\theta = 0^\circ$ to $2\theta = 70^\circ$ on the GaN on sapphire showed only two other peaks, besides the peaks from the sapphire, near $2\theta = 34.6^\circ$. The peaks near $2\theta = 34.6^\circ$ consist of a stronger peak at 34.668° and a much weaker peak at 36.903° . These peaks correspond to the (0002) and (10-11) orientations for GaN, respectively. XRD θ -2 θ scans from $2\theta = 0^\circ$ to $2\theta = 70^\circ$ on the GaN on Si (111) and GaN on Ge/Si (111) samples show presence of only polar GaN (0002) peak at 34.7° besides the Si (111) peak at $2\theta = 28.5^\circ$. The XRD results clearly show that the deposited GaN material is not polycrystalline. Optical absorption spectroscopy over a 1.2 eV to 6.2 eV spectral range, for the GaN/Sapphire sample, showed an abrupt absorption edge at 3.4 eV, a clear indication of interband transitions in binary GaN. These results confirm that our PED-grown GaN is highly *c*-axis oriented and suitable for the initial growth of GaN on various substrate materials.

11:40am EM+EN-FrM11 Growth Template Impact on the Properties of InN Epilayers Grown by High-Pressure CVD, Sampath Gamage, M.K.I. Senevirathna, Georgia State University, H. Babar, I.T. Ferguson, University of North Carolina at Charlotte, R. Collazo, North Carolina State University, N. Dietz, Georgia State University

The unique optical and electrical properties of InN and related ternary InGaN alloys make the material system attractive for various optoelectronic device applications, including but not limited to high-speed electronics, photovoltaic solar cells, or light emitting devices. Even though progress has been made in establishing the base properties of the binaries InN and GaN, the growth of high-quality InN and indium-rich ternary InGaN epilayers and heterostructures is an open challenge. In previous work, we demonstrated the stabilization of InN and InGaN epilayers utilizing superatmospheric MOCVD (also denoted as HPCVD) to suppress the decomposition at higher growth temperatures.

In this contribution, we explored the influence of the growth templates (e.g. sapphire substrates, micrometer-scale patterned AlN/sapphire templates, and/or patterned GaN/AlN/sapphire) on the properties of bulk InN epilayers, keeping the reactor pressure constant at 8bar (15bar) as well as the III/V precursor ratio. The growth temperature was optimized in the range of 800°C to 900°C based on Raman E₂(high) mode evolution. The various templates are assumed to introduce different strain fields during the initial nucleation process, affecting the extended defect generation and propagation processes. To assess this effect on the bulk properties of thick InN epilayers, Raman spectroscopy [e.g. E₂(high) and A₁(LO) mode analysis], XRD rocking and ω -2 θ scans and photoluminescence (PL) spectroscopy were performed to analyze the crystallinity as well as the extended defect and point defect densities in these layers. The free carrier concentrations in these epilayers and the mobility was determined by FTIR spectra analysis as well as Raman A₁(LO) fitting.

Authors Index

Bold page numbers indicate the presenter

— A —

Abbas, A.: EN+AS+EM+SE-WeM13, 24
Abdulrahman, R.: TF+EM+EN-WeA1, 28
Agarwal, S.: TF+EN+PS-TuA11, 17
Aguirre-Tostado, F.S.: EN-TuP9, 20
Aihara, T.: EN+EM+MN+NS+TR-MoA11, 7; EN-TuP2, 19
Alper, J.P.: EM+EN+TF-WeA8, 26
Anand, B.: EN+EM+MN+NS+TR-MoA3, 6
Ando, A.: SE+EM+EN+PS+TF-MoM3, 1
Arefin, N.: EM+EN-FrM10, 35
Arey, B.: AP+AS+EN+NS+SS-ThA4, 33
Asplund, M.: TF+EM+EN-WeA11, 30
Atwater, H.: NS+EN-MoA1, 7
Avanesian, T.: EN+AS+EM+SE-TuM3, 11
Aydil, E.S.: EN+AS+EM+SE-WeM3, 22
Aydin, K.: TF+EM+EN-WeA3, 29

— B —

Babar, H.: EM+EN-FrM11, 35
Bagley, J.: TF+EM+EN-WeA11, 30
Bagot, P.A.J.: AP+AS+EN+NS+SS-ThA6, 33
Baimpos, T.: SS+EN-MoA4, 9
Banaï, R.E.: EN+AS+EM+SE-WeM6, 22
Barati, Gh.: EL+AS+EM+EN+SS-ThM12, 32
Barclay, M.S.: SS+AS+EN-MoM11, 4
Bardeen, C.J.: SS+AS+EN-MoM1, 2
Barnes, A.: EL+AS+EM+EN+SS-ThM5, 31
Barnes, T.M.: EN+AS+EM+SE-WeM10, 23
Barrett, L.: EM+EN+TF-WeA9, 26
Barroo, C.: AP+AS+EN+NS+SS-ThA3, 33
Barth, K.: EN+AS+EM+SE-WeM13, 24
Bartis, E.A.J.: SE+EM+EN+PS+TF-MoM2, 1
Bartynski, R.A.: EN+EM+NS-TuA4, 14
Basham, J.I.: EN+AS+EM+SE-WeM12, 23; EN+AS+EM-WeA11, 28
Baski, A.A.: EM+EN-FrM3, 34
Batra, V.: EN-TuP10, 20
Baxter, J.B.: EN+AS+EM-WeA3, 27
Beach, J.: EN+AS+EM+SE-WeM10, 23
Bebensee, F.: SS+AS+EN-WeM13, 25
Begum, M.: EN-TuP8, 19
Béland, A.E.: EN+AS+EM+SE-WeM3, 22
Berry, N.: EN+AS+EM+SE-WeM5, 22
Bertel, E.: SS+AS+EN-MoM3, 2
Besland, M.-P.: EN-TuP5, 19
Bianco, G.V.: EL+AS+EM+EN+SS-ThM6, 32
Biyikli, N.: EM+EN-FrM4, 34; TF+EM+EN-WeA2, 29
Bluhm, H.: EN+AS+EM+SE-WeM5, 22
Bongers, W.A.: EN-TuP6, 19
Bonnell, D.A.: NS+EN-MoA10, 8; SS+AS+EN-TuM1, 12
Bourke, P.: SE+EM+EN+PS+TF-MoM6, 1
Bowen, K.H.: SS+EN-MoA6, 9
Bowers, J.W.: EN+AS+EM+SE-WeM13, 24
Brannaka, J.A.: SS+AS+EN-MoM11, 4
Brigeman, A.N.: EN+AS+EM-WeA11, 28
Brown, T.M.: TF+EN+PS-TuA12, 18
Browning, J.: EN+EM+MN+NS+TR-MoA9, 6
Brownson, J.R.S.: EN+AS+EM+SE-WeM6, 22
Bruno, G.: EL+AS+EM+EN+SS-ThM6, 32
Bumueller, D.: SS+EN-MoA6, 9
Bux, S.: EN+AS+EM+SE-TuM13, 12

— C —

Cabot, G.: EN-TuP10, 20
Cansizoglu, H.: TF+EM+EN-WeA1, 28; TF+EM+EN-WeA2, 29
Cansizoglu, M.F.: EN-TuP8, 19; TF+EM+EN-WeA1, 28; TF+EM+EN-WeA2, 29
Cao, L.: EN+AS+EM+SE-TuM6, 11
Capezzuto, P.: EL+AS+EM+EN+SS-ThM6, 32
Carraro, C.: EM+EN+TF-WeA8, 26
Carrier, X.: AP+AS+EN+NS+SS-ThA6, 33
Cartas, W.: SS+AS+EN-TuM2, 12

Caspar, J.V.: EN+AS+EM-WeA3, 27
Cavanagh, A.S.: TF+EN+PS-TuA8, 17
Celio, H.C.: EM+EN+TF-WeA7, 26
Chabal, Y.J.: EN+EM+MN+NS+TR-MoA3, 6
Chagarov, E.A.: EN+AS+EM+SE-WeM4, 22
Chang, C.-H.: EM+EN+TF-WeA8, 26
Chang, J.P.: TF+EN+PS-TuA2, 16
Charalambopoulou, G.: EN-TuP14, 20
Chaukulkar, R.P.: TF+EN+PS-TuA11, 17
Chen, C.-C.: EN+AS+EM+SE-WeM5, 22
Chen, D.A.: SS+EN-MoA3, 8
Chen, H.S.: EM+EN-FrM5, 34
Chen, H.T.: EM+EN-FrM5, 34
Chen, W.H.: EM+EN-FrM5, 34
Chen, X.: SS+EN-MoA8, 9; TF+EN+PS-TuA7, 17
Chernomordik, B.D.: EN+AS+EM+SE-WeM3, 22
Chervin, C.N.: EM+EN+TF-WeA11, 27
Cho, J.: TF+EN+PS-TuA2, 16
Cho, K.J.: EM+EN+TF-WeA3, 26
Choi, H.K.: NS+EN-MoA4, 7
Choi, J.S.: NS+EN-MoA4, 7
Choi, S.G.: EL+AS+EM+EN+SS-ThM3, 31
Christopher, P.: EN+AS+EM+SE-TuM3, 11
Chu, S.: EN+EM+NS-TuA10, 15
Clarke, R.: EN+AS+EM+SE-WeM11, 23
Cobet, C.: EL+AS+EM+EN+SS-ThM12, 32
Cohen, H.: EN+EM+MN+NS+TR-MoA8, 6
Colby, R.J.: AP+AS+EN+NS+SS-ThA4, 33
Collazo, R.: EM+EN-FrM11, 35
Collins, R.W.: EL+AS+EM+EN+SS-ThM4, 31; EN+AS+EM+SE-WeM12, 23
Cook, B.: EN+AS+EM+SE-TuM12, 11
Cook-Chennault, K.: EM+EN+TF-WeA1, 26
Cordell, J.J.: EN+AS+EM+SE-WeM6, 22
Cordin, M.: SS+AS+EN-MoM3, 2
Coulter, K.: SE+EM+EN+PS+TF-MoM5, 1
Cournoyer, J.R.: EN-TuP16, 21
Creator, M.: TF+EN+PS-TuA12, 18
Cullen, P.J.: SE+EM+EN+PS+TF-MoM6, 1
Culver, J.: EN+EM+NS-TuA10, 15; EN+EM+NS-TuA9, 15
Cushing, G.: SS+AS+EN-WeM12, 25

— D —

Dameron, A.: TF+EN+PS-TuA11, 17
Davis, R.C.: EM+EN+TF-WeA9, 26; TF+EM+EN-WeA11, 30
De Decker, Y.: AP+AS+EN+NS+SS-ThA3, 33
Demirkan, K.: EN+AS+EM+SE-WeM2, 22
Deng, X.: SS+EN-MoA7, 9
D'Epifanio, A.: TF+EN+PS-TuA12, 18
Derouin, J.: SS+EN-MoA9, 9
Deutsch, T.G.: SS+EN-MoM9, 5
di Carlo, A.: TF+EN+PS-TuA12, 18
di Giacomo, F.: TF+EN+PS-TuA12, 18
Dietz, N.: EM+EN-FrM11, 35
Dillon, R.J.: SS+AS+EN-MoM1, 2
Dingemans, G.: TF+EN+PS-TuA9, 17
Diwan, A.: TF+EM+EN-WeA11, 30; TF+EM+EN-WeA7, 29
Dombrowski, E.: SS+AS+EN-WeM11, 25
Donald, S.B.: SS+AS+EN-WeM12, 25
Dorman, J.: EN+EM+MN+NS+TR-MoA10, 6
Doscher, H.: SS+EN-MoM9, 5
Doudin, N.: SS+AS+EN-TuM5, 13
Dougherty, D.B.: SS+AS+EN-WeM3, 24
Dovidenko, K.: EN-TuP16, 21
Druce, J.: EN+AS+EM+SE-WeM2, 22
Du, W.: EM+EN+TF-WeA1, 26
Duerrbeck, S.: SS+AS+EN-MoM3, 2
Duke, A.S.: SS+EN-MoA3, 8
Dunn, B.: TF+EN+PS-TuA2, 16
Durbin, S.: EN+AS+EM+SE-WeM11, 23

— E —

Ercius, P.: EN+AS+EM+SE-WeM2, 22
Ertekin, E.: SS+AS+EN-TuM6, 13

— F —

Facchini, C.F.R.: EN-TuP15, 21
Fairbrother, D.H.: SS+AS+EN-MoM11, 4; SS+EN-MoA6, 9
Fan, R.: EM+EN+TF-WeA9, 26
Farber, R.: SS+EN-MoA9, 9
Feldberg, N.: EN+AS+EM+SE-WeM11, 23
Felmy, A.: AP+AS+EN+NS+SS-ThA4, 33
Ferguson, I.T.: EM+EN-FrM11, 35
Finckenor, M.: TF+EM+EN-WeA1, 28
Fleurial, J.P.: EN+AS+EM+SE-TuM13, 12
Foxon, C.T.: SS+EN-MoM3, 4
Franchini, C.: SS+AS+EN-MoM3, 2
Fujii, H.: EN+EM+MN+NS+TR-MoA11, 7
Fukuyama, A.: EN+EM+MN+NS+TR-MoA11, 7; EN-TuP2, 19

— G —

Galhenage, R.P.: SS+EN-MoA3, 8
Gamage, S.: EM+EN-FrM11, 35
Gantefer, G.: SS+EN-MoA6, 9
Gao, H.-J.: SS+AS+EN-WeM1, 24
Gao, Y.: EN-TuP13, 20
Gartstein, Y.: EN+EM+MN+NS+TR-MoA3, 6
Garza-Hernandez, R.: EN-TuP9, 20
Gates, R.: TF+EM+EN-WeA11, 33
George, S.M.: SS+EN-MoM9, 5; TF+EN+PS-TuA8, 17
Gerasopoulos, K.D.: EN+EM+NS-TuA10, 15
Ghimire, K.: EL+AS+EM+EN+SS-ThM11, 32
Ghodssi, R.: EN+EM+NS-TuA10, 15; EN+EM+NS-TuA9, 15
Giannagregorio, M.: EL+AS+EM+EN+SS-ThM6, 32
Giannakopoulos, K.: EN-TuP14, 20
Gillette, E.: EN+EM+NS-TuA3, 14; TF+EN+PS-TuA7, 17
Gnerlich, M.: EN+EM+NS-TuA10, 15; EN+EM+NS-TuA9, 15
Goede, A.P.H.: EN-TuP6, 19
Gorai, P.: SS+AS+EN-TuM6, 13
Gowthaman, P.: EM+EN+TF-WeA2, 26
Grant, J.T.: TF+EM+EN-WeA10, 30
Graswinckel, M.F.: EN-TuP6, 19
Gregorczyk, K.: TF+EN+PS-TuA7, 17
Guglietta, G.W.: EN+AS+EM-WeA3, 27
Gundlach, D.J.: EN+AS+EM-WeA11, 28
Gurary, A.: EM+EN-FrM8, 34

— H —

Hacker, C.A.: EN+AS+EM-WeA11, 28
Haider, A.: EM+EN-FrM4, 34; TF+EM+EN-WeA2, 29
Haight, R.: EN+AS+EM+SE-WeM4, 22
Haile, S.M.: EN+AS+EM+SE-TuM1, 11
Haley, D.: AP+AS+EN+NS+SS-ThA6, 33
Haneef, H.: EL+AS+EM+EN+SS-ThM11, 32
Haney, P.: EN+AS+EM+SE-WeM12, 23
Hare, C.D.: TF+EN+PS-TuA8, 17
Harrison, I.A.: SS+AS+EN-MoM6, 3; SS+AS+EN-WeM12, 25
Hart, C.: SE+EM+EN+PS+TF-MoM2, 1
Hayden, B.E.: SS+EN-MoA1, 8
He, X.: EN+AS+EM+SE-WeM2, 22
He, Y.: TF+EM+EN-WeA8, 29; TF+EM+EN-WeA9, 29
Hellman, A.: EN+AS+EM+SE-TuM5, 11
Hemming, J.C.: EN+AS+EM+SE-WeM5, 22
Henderson, M.A.: SS+AS+EN-TuM13, 13; SS+EN-MoM5, 5
Herath, N.: EN+EM+MN+NS+TR-MoA9, 6
High, E.: SS+AS+EN-WeM11, 25
Hines, M.A.: SS+EN-MoA10, 10
Hingerl, K.: EL+AS+EM+EN+SS-ThM12, 32
Hinton, K.: EM+EN+TF-WeA9, 26
Holmes, R.J.: EN+AS+EM-WeA9, 28
Horn, M.W.: EN+AS+EM+SE-WeM6, 22

Hossain, K.: EM+EN-FrM10, 35
 Hou, J.: NS+EN-MoA10, 8
 Howansky, A.: EN+EM+NS-TuA4, 14
 Hsieh, C.: EM+EN-FrM5, 34
 Hu, J.J.: SE+EM+EN+PS+TF-MoM8, 2
 Huang, J.S.: EL+AS+EM+EN+SS-ThM10, 32;
 EN-TuP13, 20
 Hunter, K.: EN+AS+EM+SE-WeM3, 22
 Hur, J.: TF+EN+PS-TuA2, 16
 Hwang, E.: NS+EN-MoA4, 7

— I —
 Ikari, T.: EN+EM+MN+NS+TR-MoA11, 7; EN-TuP2, 19
 Ingólfsson, O.: SS+AS+EN-MoM11, 4
 Ingram, W.: TF+EM+EN-WeA8, 29; TF+EM+EN-WeA9, 29
 Ishidzuka, S.: SS+AS+EN-MoM10, 3
 Ishihara, T.: EN+AS+EM+SE-WeM2, 22

— J —
 Jach, T.: SS+AS+EN-TuM12, 13
 Jamieson, S.: TF+EM+EN-WeA11, 30
 Jang, H.-J.: EN+AS+EM-WeA11, 28
 Jennings, J.: EN+EM+NS-TuA11, 15
 Jing, D.: SS+EN-MoA10, 10
 Johnson, M.B.: EM+EN-FrM10, 35
 Jones, J.G.: TF+EM+EN-WeA10, 30
 Joo, J.-B.: SS+AS+EN-MoM1, 2
 Jouan, P.Y.: EN-TuP5, 19
 Ju, H.X.: EN+AS+EM-WeA12, 28
 Junda, M.M.: EL+AS+EM+EN+SS-ThM5, 31
 Jurchescu, O.D.: EN+AS+EM-WeA11, 28

— K —
 Kale, M.J.: EN+AS+EM+SE-TuM3, 11
 Kaminski, P.M.: EN+AS+EM+SE-WeM13, 24
 Kane, M.H.: EM+EN-FrM10, 35
 Kang, H.: SS+AS+EN-MoA4, 2
 Karabacak, T.: EN-TuP8, 19; TF+EM+EN-WeA1, 28; TF+EM+EN-WeA2, 29
 Kariuki, N.: EN-TuP8, 19
 Kaufman-Osborn, T.: EN+AS+EM+SE-WeM4, 22
 Kaykhaii, M.: TF+EM+EN-WeA7, 29
 Kennedy, R.J.: EN+AS+EM+SE-WeM11, 23
 Kessels, W.M.M.: TF+EN+PS-TuA10, 17; TF+EN+PS-TuA12, 18; TF+EN+PS-TuA9, 17
 Ketchum, D.: EN+EM+NS-TuA9, 15
 Ketkar, M.: EN+AS+EM+SE-WeM3, 22
 Khudhayer, W.J.: EN-TuP8, 19
 Kiang, Y.W.: EM+EN-FrM5, 34
 Killelea, D.R.: SS+EN-MoA9, 9
 Kilner, J.: EN+AS+EM+SE-WeM2, 22
 Kim, Y.: SS+AS+EN-MoM4, 2
 Kimmel, G.A.: SS+EN-MoM5, 5
 Kirillova, O.A.: EN+AS+EM-WeA11, 28
 Kiyota, E.: EN-TuP15, 21
 Kline, R.J.: EN+AS+EM-WeA11, 28
 Knoll, A.J.: SE+EM+EN+PS+TF-MoM2, 1
 Knoops, H.C.M.: TF+EN+PS-TuA9, 17
 Koel, B.: SS+EN-MoM1, 4
 Koirala, P.: EL+AS+EM+EN+SS-ThM4, 31; EN+AS+EM+SE-WeM12, 23
 Komuro, A.: SE+EM+EN+PS+TF-MoM3, 1
 Kopeck, J.: EN-TuP6, 19
 Korevaar, B.A.: EN-TuP16, 21
 Kostoglou, N.: EN-TuP14, 20
 Kotru, S.: EN-TuP10, 20
 Kovarik, L.: AP+AS+EN+NS+SS-ThA4, 33
 Kozen, A.C.: EM+EN+TF-WeA10, 27; EN+EM+NS-TuA7, 14; EN+EM+NS-TuA8, 15; TF+EN+PS-TuA1, 16; TF+EN+PS-TuA7, 17
 Krieg, U.: NS+EN-MoA6, 7
 Kronawitter, C.: SS+EN-MoM1, 4
 Krooswyk, J.: SS+AS+EN-MoM8, 3
 Kruse, N.: AP+AS+EN+NS+SS-ThA3, 33
 Kruska, K.: AP+AS+EN+NS+SS-ThA6, 33
 Kummel, A.C.: EN+AS+EM+SE-WeM4, 22
 Kuradome, H.: EN-TuP2, 19
 Kurahashi, M.: SS+AS+EN-WeM10, 25

— L —
 Lafond, A.: EN-TuP5, 19
 Lalor, J.: SE+EM+EN+PS+TF-MoM6, 1
 Larsen, G.K.: TF+EM+EN-WeA8, 29; TF+EM+EN-WeA9, 29
 Lau, J.: TF+EN+PS-TuA2, 16
 Laughlin, K.: TF+EM+EN-WeA11, 30
 Lauter, V.: EN+EM+MN+NS+TR-MoA9, 6
 Law, M.: EN+AS+EM+SE-WeM5, 22
 Lawson, A.P.: NS+EN-MoA3, 7
 Lechner, B.A.J.: SS+AS+EN-MoM3, 2; SS+AS+EN-MoM4, 2
 Lee, H.: EN+AS+EM+SE-WeM6, 22; NS+EN-MoA4, 7
 Lee, I.: SS+AS+EN-MoM1, 2
 Lee, J.: SS+EN-MoA7, 9
 Lee, S.B.: EM+EN+TF-WeA10, 27; EN+EM+NS-TuA3, 14; EN+EM+NS-TuA7, 14; EN+EM+NS-TuA8, 15; TF+EN+PS-TuA7, 17
 Lee, Y.K.: NS+EN-MoA4, 7
 Leins, M.: EN-TuP6, 19
 Lepkowski, D.L.: NS+EN-MoA11, 8
 Lewis, J.S.: EN+AS+EM+SE-TuM12, 11
 Li, J.: EL+AS+EM+EN+SS-ThM3, 31; EL+AS+EM+EN+SS-ThM4, 31
 Li, J.J.: EN+AS+EM+SE-WeM10, 23
 Li, M.: SS+AS+EN-TuM6, 13
 Li, Y.: EN-TuP14, 20
 Li, Z.: SS+EN-MoM6, 5
 Liao, C.H.: EM+EN-FrM5, 34
 Liao, K.: EN-TuP14, 20
 Lichtenstein, T.: NS+EN-MoA6, 7
 Licocchia, S.: TF+EN+PS-TuA12, 18
 Liliental-Weber, Z.: SS+EN-MoM3, 4
 Lin, C.F.: EM+EN+TF-WeA10, 27; TF+EN+PS-TuA1, 16
 Linford, M.R.: TF+EM+EN-WeA11, 30; TF+EM+EN-WeA7, 29
 Linhart, W.M.: EN+AS+EM+SE-WeM11, 23
 Liu, C.: EN+EM+NS-TuA7, 14; TF+EN+PS-TuA1, 16; TF+EN+PS-TuA7, 17
 Liu, D.-J.: EN+EM+NS-TuA1, 14
 Liu, J.: AP+AS+EN+NS+SS-ThA4, 33
 Liu, X.L.: EN-TuP13, 20
 Liu, Y.: EN+AS+EM+SE-WeM5, 22; TF+EM+EN-WeA11, 30
 Liu, Z.: EN+AS+EM+SE-WeM5, 22
 Long, J.W.: EM+EN+TF-WeA11, 27
 Lopez, T.: EN+AS+EM+SE-TuM13, 12
 Lordi, V.: EN+AS+EM+SE-WeM2, 22
 Losurdo, M.: EL+AS+EM+EN+SS-ThM6, 32
 Luan, P.: SE+EM+EN+PS+TF-MoM2, 1
 Lucci, F.R.: SS+AS+EN-WeM4, 24
 Lunt, B.: TF+EM+EN-WeA11, 30
 Lynn, K.G.: EN+EM+NS-TuA11, 15

— M —
 Ma, L.: SS+AS+EN-TuM5, 13
 Maboudian, R.: EM+EN+TF-WeA8, 26
 Macco, B.: TF+EN+PS-TuA10, 17
 Madaan, N.: TF+EM+EN-WeA11, 30
 Malko, A.: EN+EM+MN+NS+TR-MoA3, 6
 Manandhar, S.: SS+AS+EN-TuM13, 13
 Manera, L.T.: EN-TuP15, 21
 Mangolini, L.: EN+AS+EM+SE-TuM13, 12
 Marceau, E.: AP+AS+EN+NS+SS-ThA6, 33
 Marcinkowski, M.: SS+AS+EN-WeM4, 24
 Martin, R.W.: SS+EN-MoM3, 4
 Martinez-Guerra, E.: EN-TuP9, 20
 Martirez, J.M.: SS+AS+EN-TuM1, 12
 Mattsson, A.: SS+EN-MoM2, 4
 Mayen-Mondragon, R.: EN-TuP9, 20
 Mayergoz, I.D.: NS+EN-MoA3, 7
 Mazzafera, P.: EN-TuP15, 21
 McAvoy, P.C.: NS+EN-MoA3, 7
 McCann, P.J.: EM+EN-FrM10, 35
 McElwee-White, L.: SS+AS+EN-MoM11, 4
 McNamara, J.D.: EM+EN-FrM3, 34
 Menzel, A.: SS+AS+EN-MoM3, 2

Meunier, R.: EN-TuP5, 19
 Meysing, D.: EN+AS+EM+SE-WeM10, 23
 Miller, M.A.: SE+EM+EN+PS+TF-MoM5, 1
 Milosavljevic, V.: SE+EM+EN+PS+TF-MoM6, 1
 Minami, T.: EN-TuP11, 20
 Minnal, C.: EN+EM+NS-TuA11, 15
 Mitzi, D.B.: EN+AS+EM+SE-WeM4, 22
 Miyata, T.: EN-TuP11, 20
 Moody, M.P.: AP+AS+EN+NS+SS-ThA6, 33
 Morales, E.H.: SS+AS+EN-TuM1, 12
 Morris, J.R.: SS+AS+EN-MoM9, 3
 Mueller, T.: EN+AS+EM+SE-TuM6, 11
 Mullins, D.R.: SS+AS+EN-TuM3, 12
 Mundle, R.M.: NS+EN-MoA11, 8
 Muratore, C.: SE+EM+EN+PS+TF-MoM8, 2
 Murphy, N.R.: TF+EM+EN-WeA10, 30
 Musgrave, C.B.: TF+EN+PS-TuA8, 17
 Myers, D.J.: EN-TuP8, 19

— N —
 Nakano, Y.: EN+EM+MN+NS+TR-MoA11, 7; EN-TuP2, 19
 Nandasiri, M.I.: SS+AS+EN-TuM13, 13
 Narimannezhad, A.: EN+EM+NS-TuA11, 15
 Nasr, J.R.: EN+AS+EM+SE-WeM6, 22
 Navin, J.K.: SS+AS+EN-WeM12, 25
 Nefedov, A.: SS+AS+EN-WeM13, 25
 Nelson, E.S.: EM+EN+TF-WeA11, 27
 Nemeth, W.: TF+EN+PS-TuA11, 17
 Nesterenko, P.: TF+EM+EN-WeA7, 29
 Netzer, F.P.: SS+AS+EN-TuM5, 13
 Newberg, J.T.: SS+EN-MoA11, 10
 Nguyen, H.: EN+EM+MN+NS+TR-MoA3, 6
 Nicotera, E.: SS+AS+EN-WeM11, 25
 Nishimoto, K.: SS+AS+EN-MoM10, 3
 Nishioka, K.: EN+EM+MN+NS+TR-MoA11, 7; EN-TuP2, 19
 Noebels, M.: EN+EM+MN+NS+TR-MoA10, 6
 Noked, M.: EM+EN+TF-WeA10, 27; EN+EM+NS-TuA7, 14; EN+EM+NS-TuA8, 15; TF+EN+PS-TuA1, 16
 Novikov, S.V.: SS+EN-MoM3, 4

— O —
 Odom, T.W.: NS+EN-MoA8, 8
 Oehrlin, G.S.: SE+EM+EN+PS+TF-MoM2, 1
 Ogawa, S.: SS+AS+EN-MoM10, 3
 Ohno, R.: SE+EM+EN+PS+TF-MoM3, 1
 Ohno, T.R.: EN+AS+EM+SE-WeM10, 23
 Okyay, A.K.: EM+EN-FrM4, 34; TF+EM+EN-WeA2, 29
 Osgood, R.M.: SS+EN-MoM6, 5
 Österlund, L.: SS+EN-MoM2, 4
 Ozgit-Akgun, C.: EM+EN-FrM4, 34

— P —
 Pala, I.R.: EM+EN+TF-WeA11, 27
 Park, J.Y.: NS+EN-MoA4, 7
 Park, S.W.: EN+AS+EM+SE-WeM4, 22
 Parker, J.F.: EM+EN+TF-WeA11, 27
 Paul, B.: TF+EM+EN-WeA7, 29
 Pearce, A.J.: EM+EN+TF-WeA10, 27; EN+EM+NS-TuA3, 14; EN+EM+NS-TuA7, 14; EN+EM+NS-TuA8, 15; TF+EN+PS-TuA1, 16; TF+EN+PS-TuA7, 17
 Pearson, A.: TF+EM+EN-WeA11, 30
 Peng, W.: EN+EM+MN+NS+TR-MoA3, 6
 Perea, D.E.: AP+AS+EN+NS+SS-ThA4, 33
 Peterson, E.: SS+AS+EN-WeM11, 25
 Petrik, N.G.: SS+EN-MoM5, 5
 Pfadler, T.: EN+EM+MN+NS+TR-MoA10, 6
 Pfitür, H.: NS+EN-MoA6, 7
 Phumisithikul, K.L.: EM+EN-FrM3, 34
 Piper, L.F.J.: EN+AS+EM+SE-WeM11, 23
 Podraza, N.J.: EL+AS+EM+EN+SS-ThM1, 31; EL+AS+EM+EN+SS-ThM11, 32; EL+AS+EM+EN+SS-ThM4, 31; EL+AS+EM+EN+SS-ThM5, 31
 Poenitzsch, V.Z.: SE+EM+EN+PS+TF-MoM5, 1
 Polychronopoulou, K.: EN-TuP14, 20
 Pookpanratana, S.J.: EN+AS+EM-WeA11, 28

Potapenko, D.V.: SS+EN-MoM6, 5
Pradhan, A.K.: NS+EN-MoA11, 8
Pritchett, B.N.: EM+EN-FrM10, 35
Putnik, M.: EN+EM+MN+NS+TR-MoA10, 6

— Q —

Qafoku, O.: AP+AS+EN+NS+SS-ThA4, 33
Qin, H.: SS+EN-MoA8, 9
Qiu, J.: NS+EN-MoA7, 8

— R —

Rabin, O.: NS+EN-MoA3, 7
Rai, R.: SS+AS+EN-TuM2, 12
Raites, Y.: SE+EM+EN+PS+TF-MoM2, 1
Rajan, K.: AP+AS+EN+NS+SS-ThA1, 33
Raman, S.: SS+EN-MoA4, 9
Ramana, C.V.: EN+AS+EM-WeA4, 27
Rangan, S.: EN+EM+NS-TuA4, 14
Rappe, A.M.: SS+AS+EN-TuM1, 12
Ravikumar, S.: EM+EN+TF-WeA2, 26
Rebholz, C.G.: EN-TuP14, 20
Redinger, J.: SS+AS+EN-MoM3, 2
Reese, M.O.: EN+AS+EM+SE-WeM10, 23
Reeves, R.J.: EN+AS+EM+SE-WeM11, 23
Reichmanis, E.: EN+AS+EM-WeA1, 27
Ren, Y.: SS+AS+EN-MoM5, 3
Repins, I.: EL+AS+EM+EN+SS-ThM3, 31
Reshchikov, M.A.: EM+EN-FrM3, 34
Ribeiro, R.V.: EN-TuP15, 21
Ricci, M.: EN-TuP5, 19
Richter, C.A.: EN+AS+EM-WeA11, 28
Rockett, A.: EN+AS+EM+SE-WeM2, 22
Rolison, D.R.: EM+EN+TF-WeA11, 27
Romijn, I.G.: TF+EN+PS-TuA9, 17
Roy Choudhury, K.: EN+AS+EM-WeA3, 27
Rubloff, G.W.: EM+EN+TF-WeA10, 27;
EN+EM+NS-TuA3, 14; EN+EM+NS-TuA7,
14; EN+EM+NS-TuA8, 15; TF+EN+PS-TuA1,
16; TF+EN+PS-TuA7, 17
Rupich, S.: EN+EM+MN+NS+TR-MoA3, 6

— S —

Saidi, W.A.: SS+AS+EN-TuM1, 12
Salmeron, M.B.: SS+AS+EN-MoM4, 2
Sampat, S.: EN+EM+MN+NS+TR-MoA3, 6
Sampath, W.: EN+AS+EM+SE-WeM13, 24
Santiago, K.C.: NS+EN-MoA11, 8
Sardashti, K.: EN+AS+EM+SE-WeM4, 22
Sarney, W.L.: SS+EN-MoM3, 4
Saroja, M.: EM+EN+TF-WeA2, 26
Sathe, A.: SS+AS+EN-TuM2, 12
Scanlon, D.O.: EN+AS+EM+SE-WeM11, 23
Schaefer, A.: SS+AS+EN-TuM2, 12
Scheu, C.: EN+EM+MN+NS+TR-MoA10, 6
Schmidt-Mende, L.: EN+EM+MN+NS+TR-
MoA10, 6
Schroeder, M.A.: EM+EN+TF-WeA10, 27;
EN+EM+NS-TuA7, 14; EN+EM+NS-TuA8,
15; TF+EN+PS-TuA1, 16; TF+EN+PS-TuA7,
17
Schulz, A.: EN-TuP6, 19
Seebauer, E.G.: SS+AS+EN-TuM6, 13
Seegmiller, T.: TF+EN+PS-TuA2, 16
Segalman, R.: EN+AS+EM+SE-TuM10, 11
Senabulya, N.: EN+AS+EM+SE-WeM11, 23
Senevirathna, M.K.I.: EM+EN-FrM11, 35
Sezen, H.: SS+AS+EN-WeM13, 25
Shaikh, A.U.: EN-TuP8, 19

Shankar, S.: EM+EN+TF-WeA2, 26
Shrestha, B.R.: SS+EN-MoA4, 9
Shutthanandan, V.: SS+AS+EN-TuM13, 13;
TF+EM+EN-WeA11, 30
Singh, B.: TF+EM+EN-WeA7, 29
Skuzza, J.R.: NS+EN-MoA11, 8
Smit, S.: TF+EN+PS-TuA10, 17
Smith, L.: TF+EN+PS-TuA2, 16
Solokha, V.: EL+AS+EM+EN+SS-ThM12, 32
Song, A.: SS+EN-MoA10, 10
Song, Y.: SS+AS+EN-MoM6, 3
Sorescu, D.C.: SS+EN-MoA7, 9
Spencer, J.A.: SS+AS+EN-MoM11, 4
Stampe, P.A.: EN+AS+EM+SE-WeM11, 23
Steriotis, T.: EN-TuP14, 20
Stradins, P.: TF+EN+PS-TuA11, 17
Su, C.Y.: EM+EN-FrM5, 34
Sugiyama, M.: EN+EM+MN+NS+TR-MoA11, 7;
EN-TuP2, 19
Sun, L.: TF+EM+EN-WeA10, 30
Sun, X.: TF+EN+PS-TuA3, 16
Sundar, U.: EM+EN+TF-WeA1, 26
Surnev, S.: SS+AS+EN-TuM5, 13
Sutter, P.: SS+EN-MoA3, 8; SS+EN-MoA8, 9
Suzuki, H.: EN+EM+MN+NS+TR-MoA11, 7
Svensson, S.P.: SS+EN-MoM3, 4
Sykes, E.C.H.: SS+AS+EN-WeM4, 24

— T —

Takahashi, K.: SE+EM+EN+PS+TF-MoM3, 1
Takakuwa, Y.: SS+AS+EN-MoM10, 3
Tampaxis, C.: EN-TuP14, 20
Tan, X.: EL+AS+EM+EN+SS-ThM4, 31
Tanen, N.J.: EN+AS+EM+SE-WeM6, 22
Tang, G.: SE+EM+EN+PS+TF-MoM3, 1
Tang, J.: SS+AS+EN-MoM10, 3
Tang, X.: SS+EN-MoA6, 9
Taylor, D.: EN+EM+MN+NS+TR-MoA3, 6
Teckcan, B.: TF+EM+EN-WeA2, 29
Teegenkamp, C.: NS+EN-MoA6, 7
Tellez, H.: EN+AS+EM+SE-WeM2, 22
Tenney, S.A.: SS+EN-MoA3, 8
Teraoka, Y.: SS+AS+EN-MoM10, 3
Thamaraiselvan, P.: EM+EN+TF-WeA2, 26
Thevuthasan, S.A.: SS+AS+EN-TuM13, 13
Thon, S.M.: EN+EM+MN+NS+TR-MoA1, 6
Thorman, R.G.: SS+AS+EN-MoM11, 4
Thorpe, R.: EN+EM+NS-TuA4, 14
Thoulon, P.Y.: EN-TuP5, 19
Tiwald, T.: EL+AS+EM+EN+SS-ThM10, 32
Tolstaya, E.I.: EN+EM+NS-TuA9, 15
Toprasertpong, K.: EN-TuP2, 19
Trenary, M.: SS+AS+EN-MoM5, 3; SS+AS+EN-
MoM8, 3
Tu, C.G.: EM+EN-FrM5, 34
Turner, J.A.: SS+EN-MoM9, 5
Tzitzios, V.: EN-TuP14, 20

— U —

Urena, R.E.: EN+AS+EM+SE-WeM6, 22
Utz, A.L.: SS+AS+EN-WeM11, 25

— V —

Valtiner, M.: SS+EN-MoA4, 9
van de Loo, B.W.H.: TF+EN+PS-TuA9, 17
van de Sanden, M.C.M.: EN-TuP6, 19
VanDerslice, J.: EL+AS+EM+EN+SS-ThM10, 32
Vanfleet, R.R.: EM+EN+TF-WeA9, 26

Vanhemel, D.: TF+EN+PS-TuA10, 17
Vargas, M.: EN+AS+EM-WeA4, 27
Varshney, V.: SE+EM+EN+PS+TF-MoM8, 2
Veal, T.D.: EN+AS+EM+SE-WeM11, 23
Venkatachalam, M.: EM+EN+TF-WeA2, 26
Visart de Bocarmé, T.: AP+AS+EN+NS+SS-
ThA3, 33
Voevodin, A.A.: SE+EM+EN+PS+TF-MoM8, 2

— W —

Walker, M.: EN-TuP6, 19
Walls, J.M.: EN+AS+EM+SE-WeM13, 24
Walukiewicz, W.: SS+EN-MoM3, 4
Waluyo, I.: SS+AS+EN-MoM5, 3
Wang, C.C.: EN-TuP13, 20
Wang, C.G.: EN-TuP13, 20
Wang, H.: TF+EM+EN-WeA11, 30
Wang, J.: SS+AS+EN-WeM3, 24
Wang, W.: EN+AS+EM+SE-WeM4, 22
Wang, Z.L.: EN+EM+MN+NS+TR-MoA6, 6
Weaver, J.F.: SS+AS+EN-TuM2, 12
Weber, M.H.: EN+EM+NS-TuA11, 15
Wei, R.: SE+EM+EN+PS+TF-MoM5, 1
Wei, W.D.: NS+EN-MoA7, 8
Weickert, J.: EN+EM+MN+NS+TR-MoA10, 6
Welzel, S.: EN-TuP6, 19
Wisnet, A.: EN+EM+MN+NS+TR-MoA10, 6
Wodtke, A.M.: SS+AS+EN-WeM5, 24
Wolden, C.A.: EN+AS+EM+SE-WeM10, 23
Wöll, C.: SS+AS+EN-WeM13, 25
Wu, R.Q.: EN+AS+EM+SE-WeM5, 22
Wu, Y.: TF+EN+PS-TuA10, 17

— X —

Xiao, Z.: EL+AS+EM+EN+SS-ThM10, 32
Xie, K.: SS+EN-MoA3, 8
Xin, H.: EN+AS+EM+SE-TuM3, 11

— Y —

Yamanaka, T.: EN-TuP11, 20
Yamauchi, Y.: SS+AS+EN-WeM10, 25
Yan, J.: EN+AS+EM+SE-TuM3, 11
Yang, C.-C.: EM+EN-FrM5, 34
Yang, Q.: AP+AS+EN+NS+SS-ThA6, 33
Yang, Y.: EN+AS+EM+SE-WeM11, 23
Yao, Y.F.: EM+EN-FrM5, 34
Yoon, H.: EN+AS+EM+SE-WeM12, 23
Yoon, Y.: EN+AS+EM+SE-WeM12, 23
Yoshigoe, A.: SS+AS+EN-MoM10, 3
Young, J.L.: SS+EN-MoM9, 5
Young, M.J.: TF+EN+PS-TuA8, 17
Yu, K.M.: SS+EN-MoM3, 4
Yurtsever, F.M.: EN-TuP8, 19
Yurukcu, M.: EN-TuP8, 19

— Z —

Zaera, F.: SS+AS+EN-MoM1, 2
Zardetto, V.: TF+EN+PS-TuA12, 18
Zhang, Y.N.: EN+AS+EM+SE-WeM5, 22
Zhang, Y.F.: SS+AS+EN-MoM9, 3
Zhao, P.: SS+EN-MoM1, 4
Zhao, Y.P.: TF+EM+EN-WeA8, 29; TF+EM+EN-
WeA9, 29
Zhitenev, N.B.: EN+AS+EM+SE-WeM12, 23
Zhou, G.W.: SS+EN-MoA8, 9
Zhu, J.F.: EN+AS+EM-WeA12, 28
Zhu, X.: SS+AS+EN-TuM10, 13
Zorn, G.: EN-TuP16, 21